An evaluation of the silicon spectral range for determination of nutrient content of grape vines

By

Grant W.F. Anderson

B.S. Royal Military College, 2005

A thesis submitted in partial fulfillment of the

requirements for the degree of Master of Science

in the Chester F. Carlson Center for Imaging Science

of the College of Science

Rochester Institute of Technology

14 July, 2016

Signature of the Author _____

Accepted by _____

Coordinator, M.S. Degree Program Date

CHESTER F. CARLSON CENTER FOR IMAGING SCIENCE

ROCHESTER INSTITUTE OF TECHNOLOGY

COLLEGE OF SCIENCE

ROCHESTER, NEW YORK

CERTIFICATE OF APPROVAL

M.S. DEGREE THESIS

The M.S. Degree Thesis of Grant W.F. Anderson
has been examined and approved by the
thesis committee as satisfactory for the
thesis required for the
M.S. degree in Imaging Science

_____

Dr. Jan A. van Aardt, Thesis Advisor

_____

Dr. Peter Bajorski, Thesis Advisor

_____

Dr. Carl Salvaggio, Committee Member

_____

Date

An evaluation of the silicon spectral range for determination of nutrient content of grape vines

Abstract

The grape industry relies on in situ crop assessment to aid in the day-to-day and seasonal management of their crop. In the case of soil-plant chemistry interactions, there are six key nutrients of interest to viticulturists in the growing of wine grapes: nitrogen, potassium, phosphorous, magnesium, zinc, and boron. Traditional methods of determining the levels of these nutrients are through collection and chemical analysis of petiole samples from the grape vines themselves. In this study, however, we collected ground-level observations of the spectra of the grape vines using a hyperspectral spectroradiometer (0.4-2.5µm range; 1nm resampled spectral interval) at the same time that petioles samples were harvested. The data were collected for two different grape cultivars, both during bloom and veraison phenological stages to provide analytical variability, while also considering the impact of temporal/seasonal change. The data were interpolated to 1nm bandwidths, yielding a consistent 1nm spectral resolution before comparing it to the nutrient data collected. Spectral reflectance also was resampled to match the 10nm bands used by the Airborne Visible and Infrared Imaging Spectrometer (AVIRIS); this was done to assess the efficacy of nutrient modeling using a more standard, airborne system's spectral resolution. Our analysis was limited to the silicon photodiode range to increase the utility of the approach for wavelength-specific cameras (via spectral filters) in a low cost unmanned aerial vehicle (UAV) platform. Five different approaches were tested to fit the data to the nutrient data. These were: a narrow-band Normalized Difference Index (NDI) approach using a standard linear fit, step-wise linear regression (SLR) using the silicon range of wavelengths, SLR using the NDI that correlated highly with the nutrient data, SLR using the 1st derivative of the reflectance spectra, and SLR using continuum-removed spectra, applied over the red trough (560-750nm) spectral region. For 1nm reflectance data, these methods generated models for nutrient modeling using between 2-10 wavelengths, and associated coefficients of determination values ranging between R^2 = 0.74-0.86 across the six nutrients. In the case of the 10nm resampled spectral data, model fits ranged between R^2 = 0.61-0.93 across the six nutrients, using 2-18 unique wavelength bands. These results bode well for eventual non-destructive, accurate and precise assessment of vineyard nutrient status through the use of UAVs.

Acknowledgments

I would like to thank my wife Carly and our new born daughter Astrid for giving me the time and support to complete this endeavor. Your support means everything. I would also like to thank all my friends and co-workers who assisted, supported, or came out to the field and helped to collect data. Thank you to my advisors, thesis committee, and external specialists for their help in getting me through this and for their expertise.

Table of Contents

List of Figures:

List of Tables:

Table 90: Peak R^2 values for 10nm Riesling nutrient models from the bloom phenological stage at the canopy nadir view angle

Table 91: Peak R^2 values for 10nm Riesling nutrient models from the bloom phenological stage at the canopy 15^o off-nadir view angle

Table 92: Peak R^2 values for 10nm Riesling nutrient models from the veraison phenological stage at the leaf view angle

Table 93: Peak R^2 values for 10nm Riesling nutrient models from the veraison phenological stage at the canopy nadir view angle

Table 94: Peak R^2 values for 10nm Riesling nutrient models from the veraison phenological stage at the canopy 15^o off-nadir view angle

1.0 Introduction

In 2016, according to businesswire.com, the global wine market is forecast to have a value of $303.6 billion. This is a vast and lucrative business, in which any advances that reduce the cost of operations or improve the quality or volume of the grape-based products would be beneficial. A typical grower needs to monitor the nutrient content of the grape vines in order to maximize yield and to ensure that the grapes are producing the correct fruit flavors. As described by Klein *et al.* (2000), the nutritional content of vineyards is determined through two different methods, either through soil analysis or plant tissue analysis. The industry standard in New York is plant tissues analysis, specifically petiole nutrient analysis. For a petiole nutrient analysis, a number of grape leaves are removed from the various grape vines in a panel (i.e., a post-to-post section containing typically 3-5 vines). The leaf portion is then removed from the petiole (shown below in Figure 1) and discarded, while the petiole is retained for analysis. The petioles for each panel are then dried, ground up, and combined before analysis, which produces an average nutrient value for that panel.

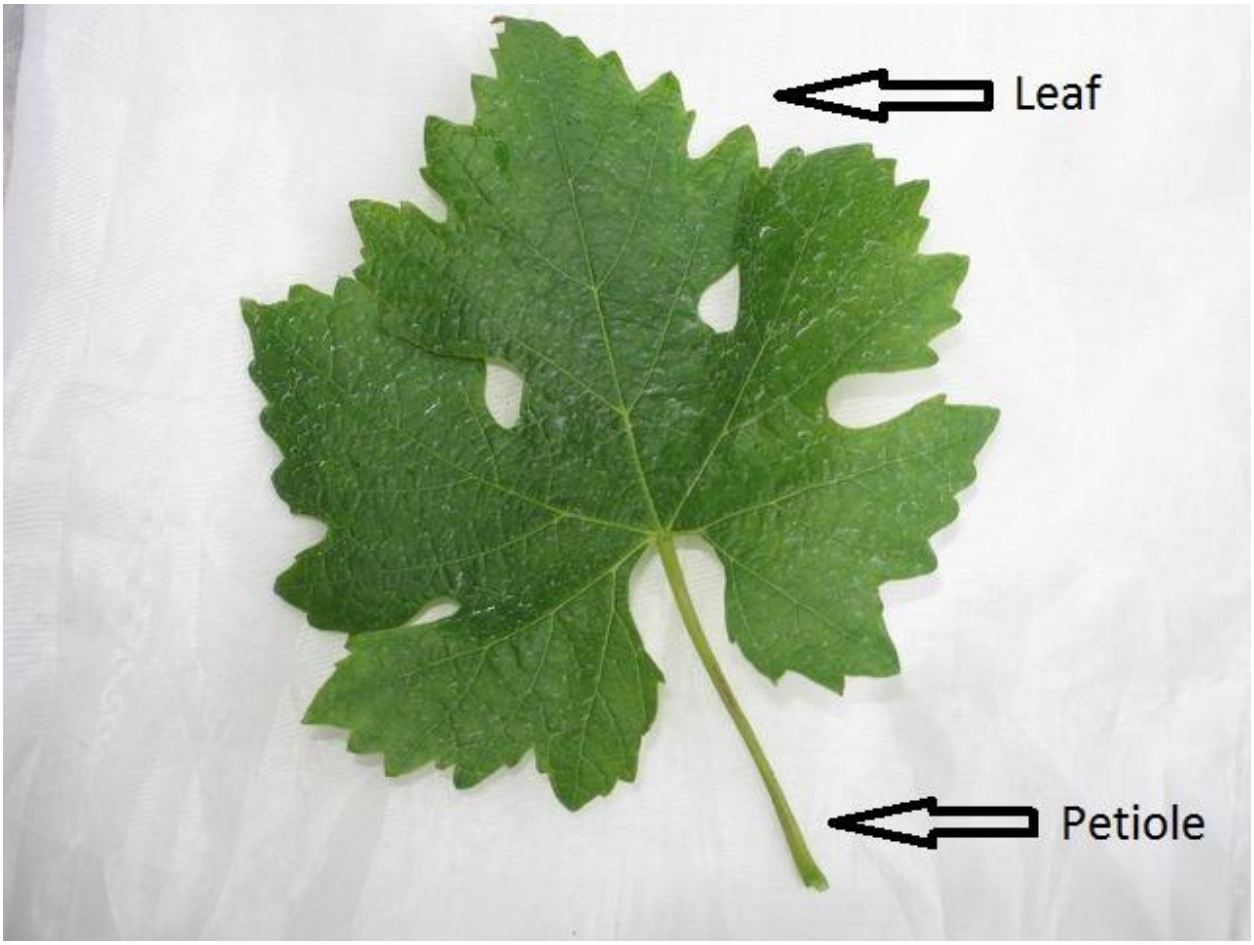

Figure 1: Description of the leaf versus petiole structures

This approach is not only time-consuming, but also costly: The Cornell Nutrient Analysis Laboratory (CNAL) charges $23/sample to conduct a routine total elemental nutrient analysis; total carbon and nitrogen analysis costs another $7/sample, resulting in a total cost of $30/sample. In this study we focused on relatively small grape blocks with 24 plant-level samples in one and 31 in the other, which yielded a total cost of $1650 for a complete nutrient analysis over the two small blocks. It is obvious that, for a commercial vineyard, the number of samples, and by extension the cost of the nutrient analyses, would be increased by at least an order of magnitude. This is exacerbated by the time required to collect the samples, prepare collected samples, and perform the laboratory analysis. For our two blocks it took an individual a full day to collect the petiole samples for a single block, followed by sample preparation and transport to the lab. Finally, CNAL documentation states that a typical suite of chemical analysis takes approximately 2-3 weeks before results can be expected.

For these reasons we were interested in finding a way to make the process of assessing the grape vine nutrient content more rapidly and more cost effective. Viticulture experts from Cornell University recommended that we focus not on all 14 elements that a routine elemental nutrient analysis and total carbon and nitrogen analysis would yield, but rather constrain our analysis to six key macronutrients and micronutrients. These were: boron (B), magnesium (Mg), nitrogen (N), phosphorus (P), potassium (K), and zinc (Zn).

Wolf (2008) provides a description of the importance of several of the macronutrients and micronutrients found in grape vines. Boron, though critical, is only required in very small amounts as a micronutrient. It is important for the normal growth and development of the plant and deficiencies can reduce the pollen fertility of the plant, subsequently reducing the yield of the vines. Magnesium is a critical component of plant chlorophyll - low levels of Mg thus can hamper the production of chlorophyll. Nitrogen, on the other hand, is critical for building many of the compounds that are essential for the growth and development of the vines; these include both amino and nucleic acids, as well as proteins and pigments, such as the green chlorophyll of the leaves. Phosphorus is aids in plant metabolism and reproduction, as well as being a fundamental element in a plant's internal energy transport. If the P level falls below the required amount, it can severely impact plant health. Potassium plays a number of regulatory roles in the plant, e.g., carbohydrate production, protein synthesis, and maintenance of water status. Though not explained in the book, from discussion with Dr. Justine Vanden Heuvel (Cornell University, pers.

comm.; 2016) it was explained that Zn is involved in fruit set (flowers becoming berries), as well as shoot elongation and pollen development.

We therefore we able to constrain our overarching study goal with our search limited to these six specific nutrients and with the aim of streamlining the nutrient analysis process using remote sensing: To identify the silicon-range wavelengths (spectral bands) that are ideally suited to modeling (assessing) the nutrient content of grape vines. We argued that, in future implementation, a number of cameras could be set to these wavelengths/spectral bands by means of spectral filters. These cameras would in turn be mounted on small-unmanned aerial vehicles (UAVs) that could be flown along the rows of grapes to map their nutrient content. In an effort minimize the cost of such a remote sensing approach; the use of silicon photodiode cameras would be preferred. This would limit the spectral range to between 400-1000nm. The quantum efficiency curve for a silicon photodiode is seen in Figure 2 (from Hamamatsu.com) below and demonstrates why the spectral range is limited.

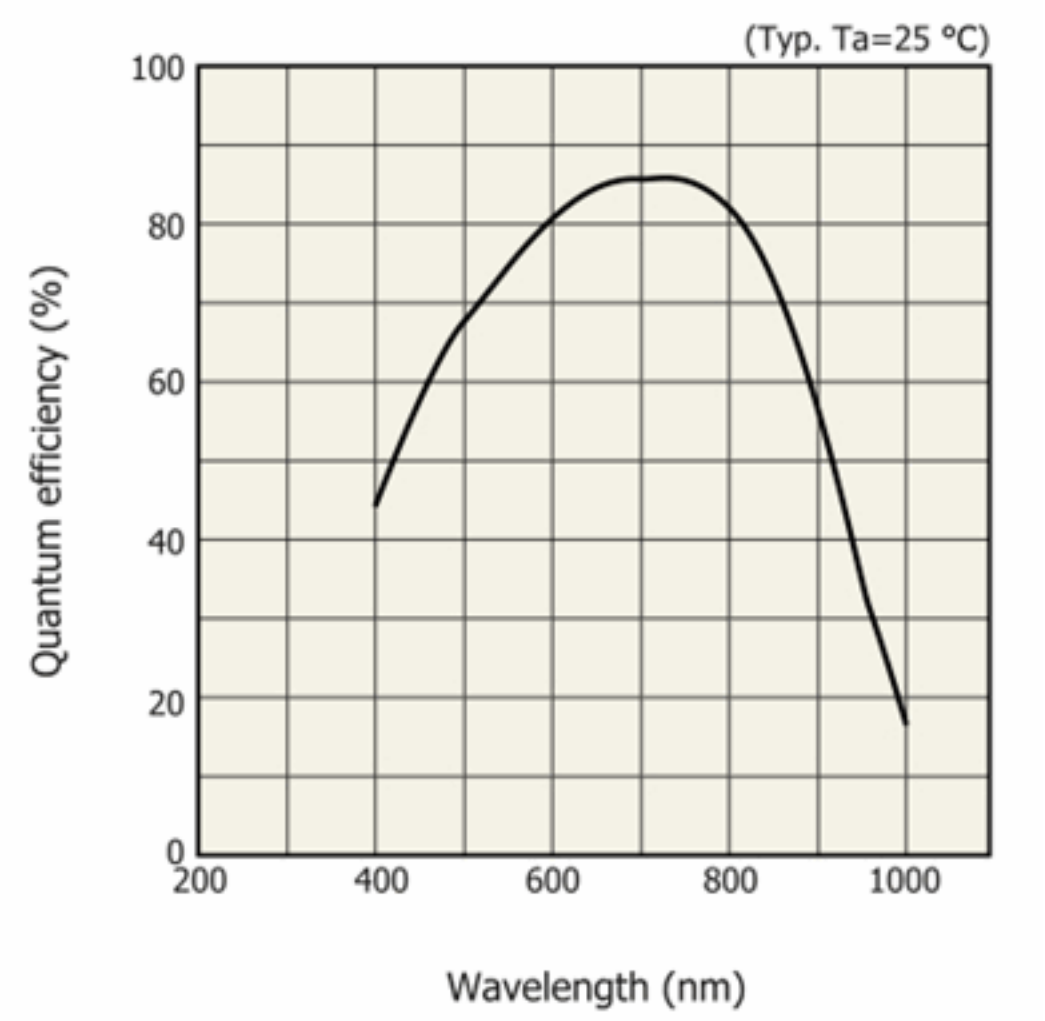

Figure 2: The quantum efficiency (QE) curve for a silicon photodiode

Finally, based on the needs of the industry, the six nutrients of interest, and the limitations of UAV-based assessment for sampling various grape cultivars, we formed our hypotheses and associated objectives.

1.1 Hypotheses and Objectives of Work

In accordance with good scientific practice, both a null- and alternate hypothesis were formed for the study.

Hypothesis: Wavelengths in the silicon range can be identified to model each of the six different nutrients of interest at an acceptable level of accuracy; this acceptable level was defined as an $R^2 \geq 0.70$.

Alternate-hypothesis: The silicon range is not conducive to accurate modeling of the six selected nutrients.

Objective: Assess the efficacy of a linear modeling approach, based on fewer than 15 independent variables, to model grape vine nutrients at an $R^2 \geq 0.70$.

A discussion of past efforts in the domain of nutrient modeling in grape vines follows next. We focused on imaging spectroscopy (hyperspectral) approaches, ideally in the silicon range, and for the six nutrients of interest.

2.0 Background and Theory

The use of remote sensing to determine the attributes of an object is not a new concept: Remote sensing has been used to visually identify objects and track them; it can determine the reflectance of an object or see how much heat it radiates; it can be used to determine the make-up of an object or scene, i.e., assess if objects are stone, or metal, live vegetation or dead. Such approaches have evolved to include not only object identification, but also object properties. Thenkabail *et al.* (1999) used wavelengths in the VNIR region of the electromagnetic spectrum (350-1050nm) to assess features like the leaf area index, height, yield, and wet biomass of crops such as cotton, potato, soybeans, corn, and sunflowers. Claudio *et al.* (2006) showed that by using a water absorption band found at 970nm, one could form an index, and between that water band index and the normalized difference vegetation index (NDVI), one could determine the water content of chaparral, a shrub-like plant group. Using wavelengths between 1100-2500nm in the shortwave-infrared (SWIR) spectrum, Ciavarella *et al.* (1998) found correlations between particular wavelengths and the K content of various vegetative samples such rice shoots, orange leaves, and the leaves and petiole from grape vines.

Ciavarella et al. (1998) were not the only group interested in using remote sensing to determine the concentration of components in grapes. Serrano (2010) discussed the use of the water index on vineyards to determine the water level of the plants and see its effects on the growth of the vines. Larrain *et al.* (2008) looked at the ripeness of grapes using NIR spectroscopy. Other researchers even imaged the grape berries themselves, e.g., Herrera *et al.* (2003) used two sets of wavelengths, between 650-1100nm and between 750-1100nm, to determine the weight percentage of soluble sugar in a solution, i.e., the Brix value of the grapes.

We were not concerned with these other features, but only with the nutrient concentrations found within the grape vines. There exists a limited body of work focused on remote sensing-based nutrient assessment in vineyards. Shao and He (2010) did examine the concentrations of N, P, and K, three of the nutrients we are interested in. Their work focused on using the SWIR and midwave-infrared (MWIR) parts of the electromagnetic spectrum to determine the nutrient concentrations in soil. Herrmann (2010) used a selection of indices, formed using the SWIR range, in order to estimate N concentrations in potatoes. The most promising study was from Ciavarella *et al.* (1998), who used SWIR data to assess K concentrations in grape leaves and petioles. However, we needed to constrain our review to studies on the selected nutrients and crop type, while also focusing on

the correct part of the EM spectra, i.e., the visible-near-infrared (VNIR) range. If we could find work on the nutrients on interest in the VNIR spectrum, we could evaluate their results against our data.

Some of the most promising work found in the VNIR range in our area of interest was that of Hunt *et al.* (2013), who worked on N assessment in maize. They created the triangle greenness index (TGI) using three wavelengths in the green, blue and red regions. From this they discovered that chlorophyll, which has a strong green response, had a close relationship to the N content of the plant. Da Silva et al. (2006) found similar results by using an index from Gitelson *et al.* (1997). They determined that the best results for N was found using the green normalized difference index and that using a green band in place of a red band, was more effective in discriminating the N content of the plant.

Our original plan was to test existing indices for grapes that work well for our six nutrients of interest. However, we were forced to create our own indices from our data, given the lack of past results for grape vines and our constrained wavelength range. Some of the existing "non-grape" indices were included as a comparison against those we created, while other forms of the spectral data manipulation were considered, beyond simple indices.

Adams *et al.* (1999) used three indices between 400-1100nm, the NDVI, the vegetation index (a ratio of IR and red bands) and their yellowness index to determine the stress levels on the plants (chlorophyll content of soybeans). Cho and Skidmore (2006) used the red edge position to estimate the foliar chlorophyll or N content of their crop. Beyond just using indices, they also took the 1st and 2nd derivatives of the reflectance spectra and found good results using these methods. These authors were not the first to consider using the derivative of the reflectance spectrum. Horler *et al.* (1983) proposed the use of the derivative of the spectra, as this could be useful in removing sources of (magnitude) variability in the data. Demetriades-Shah *et al.* (1990) went a step further: They used the 1st derivative, as it reduced the variability in the data, but they also suggested the use of the 2nd derivative. From their research they found that for canopy measurements the 2nd derivative eliminated the effects from the soil background. Grossman *et al.* (1996) proposed the use of step-wise linear regression, in conjunction with the 1st and 2nd derivatives of the spectra, to determine the N content of their vegetation targets. We therefore decided to attempt using the derivatives of our reflectance spectrum in order to reduce some of the variability in the data and obtain a better fit for our models beyond that generated by one of the indices we used. A somewhat novel analytical tool, namely continuum removal, augmented this approach.

Continuum removal was proposed by Kokaly and Clark (1999); this method involves finding the absorption bands for the nutrient of interest and calculating the depths of this absorption region relative to a linear fit regression, and evaluating how this enhanced absorption trough's features vary between samples. This approach works best on data in the SWIR region, as that is the region in which the majority of the absorption features for the nutrients in question reside. As we are focusing solely on the VNIR, we were required to find a different feature of the reflectance spectra to employ the continuum removal technique on; more details will be discussed in the Methods section. Finally, we had to identify a robust modeling approach.

In the last decade, a number of researchers have moved from using from using univariate methods to multivariate methods. As Cozzolino *et al.* (2009) describe in their work, a multivariate method addresses the system as a whole, i.e., instead of considering each variable individually, you consider the system via a more holistic method realizing that each variable acts upon the other variables - in order to model any of the variables in the most exact manner you need to model the whole. Typically this will be done in conjunction with a univariate method and the results compared. Fernandex-Novales *et al.* (2008) used both multiple linear step-wise regression (MLS) and partial least squares regression (PLS) on wavelengths between 800-1050nm to develop predictive models for sugar content found in grapes, must, and wine. From their work they found four wavelengths in the 900nm range that modeled the reducing sugar content the best. Li *et al.* (2014), on the other hand, discussed their results in using a combination of spectral indices and PLS to determine the N content in winter wheat, while Sauvage *et al.* (2002) used PLS and MLS in the VNIR-SWIR range to determine the metal content for K and Mg in white wine.

While there is solid evidence regarding the use of multivariate methods to model the nutrients in wine grapes, it was felt that a bottom-up approach would be the best start. To that end we started by generating indices for the silicon range and related those to the six nutrients in question. After that we evaluated the use of the 1st derivative and continuum removal methods and how these could further improve the nutrient models. Multivariate methods will not be addressed in this work, but will be left for a follow-on study, as was decided for analysis using the 2nd derivative. The ultimate goal is to enable a UAV camera system to collect the reflectance spectra in the more cost-effective silicon range wavelengths. It is worth noting that by using the 1st derivative method, the number of required wavelengths that would need to be collected is doubled. E.g., if the ideal model fit was created from three derivative bands, this would require collecting the spectral data for six

separate wavelengths. Thus using the 2nd derivative method would further double the number of wavelengths required and make it unfeasible to collect easily in the manner we are considering.

In a previous study (Anderson *et al.*, 2016) we examined three separate indices related to the nutrients we were interested in to assess correlations. The first that was examined was the Gitelson and Merzlyak (GM) index, from Gitelson and Merzlyak (1997). This index is created from a ratio between a red wavelength and a green wavelength, as in the equation below.

$$GM = \frac{\lambda_{750}}{\lambda_{550}} \quad (1)$$

The results from the GM index are seen below in Table 1. In short, the highest correlation value achieved for our data was 0.54. This was from the Riesling grape cultivar for Zn data, collected at the leaf level.

Table 1: Correlation coefficient results from the GM index: (a) from bloom, (b) from veraison

Gitelson and Merzlyak	Correlation	Nutrient
Cabernet Franc - Leaf	0.22	Zinc
Cabernet Franc - Nadir	0.17	Nitrogen
Cabernet Franc - 15 Deg	0.15	Zinc
Riesling- Leaf	0.39	Nitrogen
Riesling - Nadir	0.34	Potassium
Riesling - 15 Deg	0.33	Nitrogen

Gitelson and Merzlyak	Correlation	Nutrient
Cabernet Franc - Leaf	0.41	Boron
Cabernet Franc - Nadir	0.44	Zinc
Cabernet Franc - 15 Deg	0.20	Magnesium
Riesling- Leaf	**0.54**	Zinc
Riesling - Nadir	0.31	Nitrogen
Riesling - 15 Deg	0.12	Nitrogen

The next index that we attempted was the Vogelmann Index, proposed in Vogelmann et al. (1993). This index focuses on the red edge, as seen in equation 2 below, in an attempt to capture the variability in red edge position in the spectral data:

$$\mathrm{VOG} = \frac{\lambda_{740}}{\lambda_{720}} \quad (2)$$

Table 2 below shows the results from using the VOG index; in this case the values were slightly superior to those found using the GM index, with a maximum correlation value of 0.57 from the veraison phonological stage for the Riesling cultivar's Zn data, viewed at the leaf level.

Table 2: Correlation coefficient results from the VOG index: (a) from bloom, (b) from veraison

Vogelmann Index	Correlation	Nutrient
Cabernet Franc - Leaf	0.22	Zinc
Cabernet Franc - Nadir	0.01	Nitrogen
Cabernet Franc - 15 Deg	0.17	Zinc
Riesling- Leaf	0.43	Nitrogen
Riesling - Nadir	0.36	Potassium
Riesling - 15 Deg	0.38	Nitrogen

Vogelmann Index	Correlation	Nutrient
Cabernet Franc - Leaf	0.44	Boron
Cabernet Franc - Nadir	0.44	Zinc
Cabernet Franc - 15 Deg	0.19	Magnesium
Riesling- Leaf	**0.57**	Zinc
Riesling - Nadir	0.31	Nitrogen
Riesling - 15 Deg	0.13	Potassium

The third index that we compared our data against was the Green Leaf Index, from Louhaichi et al. (2001). The specific wavelengths used were selected from the eligible ranges, with the blue wavelength being chosen from the middle of that range, the green wavelength selected as the peak green, and the red wavelength being selected as the approximate wavelength corresponding to the bottom of the spectral dip in the red region:

$$\mathrm{GLI} = \frac{(2*\mathrm{G}-\mathrm{B}-\mathrm{R})}{(2*\mathrm{G}+\mathrm{B}+\mathrm{R})} \qquad (3)$$

where B = 450nm, G = 555nm, and R = 684nm.

Table 3 shows the results for the GLI index. It achieved the highest correlation value of the three indices, with a value of 0.64 for the Riesling cultivar (P) data, viewed at nadir.

Table 3: Correlation coefficient results from the GLI index: (a) from bloom, (b) from veraison

Green Leaf Index	Correlation	Nutrient
Cabernet Franc - Leaf	0.34	Phorphosus
Cabernet Franc - Nadir	0.51	Boron
Cabernet Franc - 15 Deg	0.38	Phorphosus
Riesling- Leaf	0.08	Zinc
Riesling - Nadir	0.21	Zinc
Riesling - 15 Deg	0.09	Zinc

Green Leaf Index	Correlation	Nutrient
Cabernet Franc - Leaf	0.20	Magnesium
Cabernet Franc - Nadir	0.31	Magnesium
Cabernet Franc - 15 Deg	0.22	Phosphorus
Riesling- Leaf	0.50	Phosphorus
Riesling - Nadir	**0.64**	Phosphorus
Riesling - 15 Deg	0.56	Magnesium

In conclusion, we found that the highest correlation value achieved was 0.64, with the others combinations producing correlation values as low at 0.01. These results will be compared against the indices generated later in this study to see which is more effective for our data set.

3.0 Data Collection

3.1 Location

We had access to an experimental farm located in Lansing, NY (42°34'22.1" N, 76°35'47.9" W) by partnering with Cornell University. This farm had two different grape cultivars, which we were given permission to sample: a block of Riesling (shown in blue in Figure 3 below), and a block of Cabernet Franc (shown in red in Figure 3 below). These blocks were selected for analysis as they had varying soil management treatments applied to them throughout the last several years, which theoretically should have resulted in a wide range of nutrient concentrations in the leaves. This in turn should add variability to the spectral data, which translates to a range of values across the collected spectral and nutrient data.

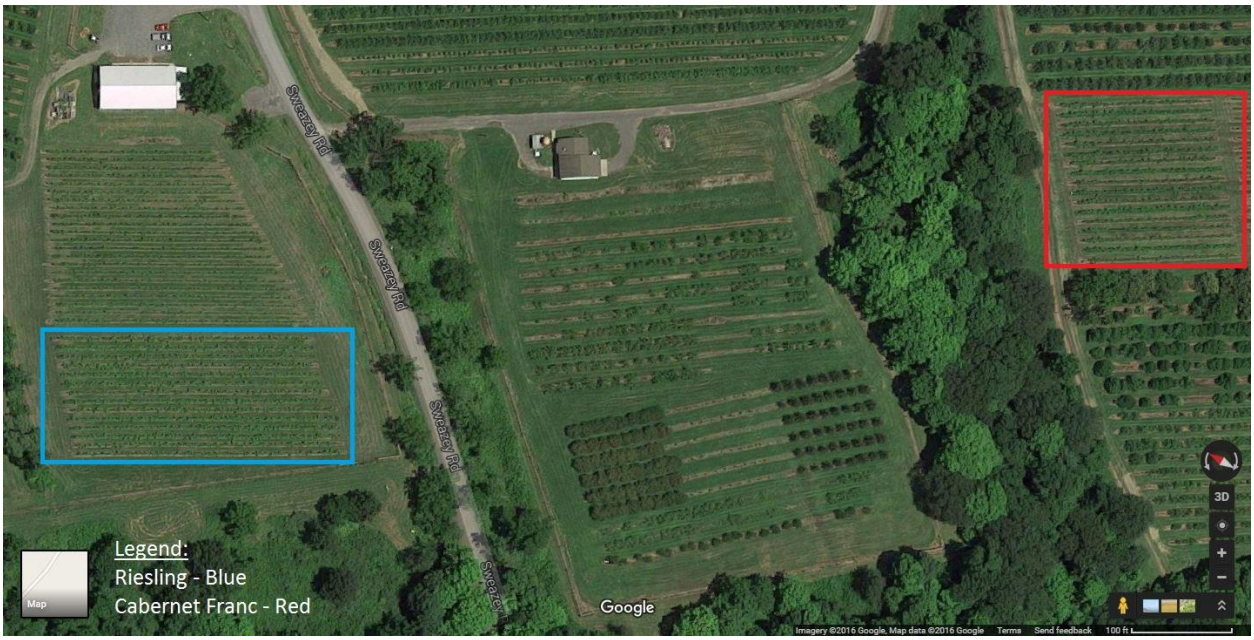

Figure 3: Study area - grape blocks in Lansing, NY

The spectral data were collected over a period of five days in June 2015 (17, 19, 20, 22, and 24 June) during the bloom phenological stage (referred to as "bloom" from now on) and again during a four-day period in August 2015 (13, 17, 19, and 22 August) during the phenological stage of veraison (referred to as "veraison" from now on). Note: Bloom is the period in which the buds on the grape vines start to open and veraison is the onset of ripening of the grapes.

3.2 Grape blocks

The data were collected in two separate grape blocks, with differing numbers of rows and panels in each. The Riesling block consisted of 14 rows, with 10 panels in each row. Rows 1 and 14 were barrier rows and so were not sampled, leaving 12 rows. The outer two panels (1 and 10) and inner two panels (5 and 6) of each row were barrier panels, leaving six viable panels in each row. This is depicted in Figure 4 below, with the barrier rows and panels shown in grey and the sampled panels numbered in white. For the nutrient analysis, two sets of three panels in each row were grouped together in a single data point, resulting in a total of 24 unique samples. The spectral data (described below) were generated by averaging the six readings (two from each panel) collected in each sample.

Riesling										
Row	Panels									
1										
2		2	3	4			7	8	9	
3		2	3	4			7	8	9	
4		2	3	4			7	8	9	
5		2	3	4			7	8	9	
6		2	3	4			7	8	9	
7		2	3	4			7	8	9	
8		2	3	4			7	8	9	
9		2	3	4			7	8	9	
10		2	3	4			7	8	9	
11		2	3	4			7	8	9	
12		2	3	4			7	8	9	
13		2	3	4			7	8	9	
14										

Figure 4: The Riesling cultivar sampling block layout; the rows and panels in each row are shown

The Cabernet Franc block consisted of 17 rows with six panels in each row. The odd numbered rows were used as barrier rows and so were not sampled. Of the six panels, the outer panels were barrier panels, leaving four viable panels each, shown in Figure 5 below. Again, the barrier rows/panels are shown in grey and the sampled panels numbered in white. For Cabernet Franc, each sampled panel was considered a data point, resulting in a total of 32 unique nutrient samples. During the collection process it was found that panel 5 from row 2 was dead, reducing the total

number of samples for this grape cultivar to 31. For each panel, the spectral data were generated by averaging the two readings taken in that panel.

Cabernet Franc						
Row	Panels					
1						
2		2	3	4	5	
3						
4		2	3	4	5	
5						
6		2	3	4	5	
7						
8		2	3	4	5	
9						
10		2	3	4	5	
11						
12		2	3	4	5	
13						
14		2	3	4	5	
15						
16		2	3	4	5	
17						

Figure 5: The Cabernet Franc cultivar sampling block layout; the rows and panels in each row are shown

3.2.1 Ground Treatments

Different ground treatments and irrigation were used on each of the blocks. A ground treatment relates to how the ground (growth medium) surrounding the grape vines is prepared and tended to throughout the growing seasons. This can vary from growing other vegetation under the vines, to the application of fertilizer, to tilling or other methods of turning the soil to deal with weeds. The reason for using ground treatments is that, depending on the treatment selected, the nutrient concentrations of the soil are affected differently. As this was an experimental farm, a number of

different ground treatments were used for a single cultivar to test treatment effects on the quality of the grapes produced.

In the Riesling block there were three different ground treatments used under the grape vines. These were included i) growing buckwheat, ii) growing chicory, and iii) the application of glyphosate (a pesticide used to kill the undergrowth). They were used in half rows, and were distributed over the block with each treatment being used for four rows total. Also in the Riesling field, half of each row was irrigated, while the other half was not. The fact that a half of each row was set up with a different irrigation and ground treatment plan, corroborates our approach to using the center two panels as barrier panels.

In the Cabernet Franc block four different ground treatments were used: i) cultivated (the earth was tilled periodically), ii) white clover, iii) glyphosate, and iv) native (left untouched). In each row, these four ground treatments were used for a different panel. Unlike the Riesling block, no irrigation was used on the Cabernet Franc vines.

We decided for our analysis that all panels would be treated the same, regardless of the ground treatment or irrigation treatment; this decision was mainly based on the limited number of data points for each of the blocks. Further analysis could be conducted in follow-on projects to assess the impact of the various ground treatments and to further refine the nutrient prediction models. We opted to focus on a broadly applicable nutrient modeling approach, i.e., an approach that would be viable across treatments.

3.3 Weather

The ideal conditions for a remote sensing collect are during mid-day on a sunny, cloud-free day. This ensures that the sun angle does not induce too many bi-directional distribution function (BRDF) artifacts, while limiting the absorption of the atmosphere and scatter from clouds on target as discussed by Schott (2007). While ideal, this is fairly impractical for time-constrained collects (matching the growing season of the vines) in upper New York State. Also, the final goal of this project is to mount a camera on a UAV to be flown over fields for private growers and ideal weather conditions cannot be guaranteed. We therefore attempted to collect data during ideal conditions, although other conditions also were accepted. The collection of the reflectance samples typically took place between 10h00-15h00 (EST), but in some cases, in order to avoid inclement weather, the collects started as early as 09h00 hours and ended as late as 16h00. The weather conditions for the collect varied from 100% sunny and cloudless, through cirrus clouds, partly cloudy, broken clouds,

fully cloudy, to overcast. The overcast conditions were avoided as much as possible, but due to the rapidly changing weather forecasts and the requirement to complete specific rows as the nutrient samples had been collected, this was sometimes unavoidable. Spectral data, however, always were calibrated to reflectance using a white reference panel, as described below.

Similar to the ground treatments, all spectral samples, regardless of the weather conditions, were treated the same. By collecting a reference sample immediately prior to collecting a target sample, any changes in atmospheric conditions can be removed (limited) and all data samples should be equivalent as far as illumination conditions are concerned.

3.4 Nutrient analysis

Members of the Cornell University viticulture program were on hand during collection days to collect samples for the nutrient analysis. The collection of samples from the grape vines were timed such that they were collected, at a maximum, within hours of the spectral samples being collected from the vines, and typically within minutes of the spectra being collected. The petioles from the vines in each panel were collected and prepared using the standard method mentioned in Wolf (2008). Along with the standard petiole nutrient analysis, a second analysis on the leaf blades was conducted in order to evaluate whether there was a significant difference in the results between the two collections methods, i.e., petioles vs. leaves. This is especially important in order to link the remote sensing at the leaf and canopy levels to the analysis performed more typically at the petiole level. To this end, instead of discarding the leaves once they have been removed from the petiole, the leaves were retained and prepared in the same way as the petioles, ands subjected to the same nutrient analysis.

3.5 Spectral data collection

The reflectance spectra of the grape vines were collected for a variety of view angles. This required the use of various field equipment to ensure that the samples were collected in as uniform a fashion as possible.

3.5.1 Spectroradiometer:

The reflectance spectra of the grapes were collected using a Spectra Vista Corporation (SVC) spectroradiometer, SVC HR-768i. This is a hand-held device with a hyperspectral sensor that ranges from 350-2500nm using three separate detector arrays that are joined at 1000nm and 1890nm (spectravista.com, 2016). The device also allows the collection of a reference sample prior to a target sample to ensure that each target sample is correctly calibrated. It also has the ability to

collect photographs of the area surrounding and inclusive of the target area and a selection of replaceable fore-optics to adjust the field of view (FOV) of the device.

3.5.1.1 Fore-optics

The SVC spectroradiometer comes with a number of fore-optics that can be attached to the device. These include, but are not limited to, a fiber optic cable with a 10^{o} FOV, a standard 4^{o} FOV fore-optic, and a standard 14^{o} FOV fore-optic. During the bloom collect for Riesling we started by using the 4^{o} FOV fore-optic for the leaf view and the 14^{o} FOV fore-optic for the canopy view. Following data review, we found that using the 4^{o} FOV fore-optic was unnecessary and the 14^{o} FOV fore-optic would be sufficient for both the leaf and canopy views. Therefore for the bloom Cabernet Franc collect, as well as for both cultivars during the veraison, the 14^{o} FOV fore-optic was used for all view angles.

3.5.2 Reference panels

During the bloom data collection, a Spectralon panel was used as the reference panel. This is the standard reference panel used for remote sensing as it has a near 100% reflectance across the 350-2500nm range, resulting in an accurate representation of the prevailing radiance conditions. However, the Spectralon panel was not available during the veraison data collection. A section of Tyvek therefore was used as the reference material in place of the traditional Spectralon approach. Janecek (2012) mentions that the spectrum for Tyvek in the silicon range, while not as strong a reflector as Spectralon (reflectance coefficient = 0.993), is still a strong reflector (reflectance coefficient = 0.97), and more importantly, is relatively flat throughout the silicon photodiode range. As we were concerned more with the relative reflectance of the grape leaves and not the absolute reflectance, the fact that Tyvek is less reflective was not an issue and did not have to be corrected for.

3.5.3 Miscellaneous equipment

3.5.3.1 Ladder

A ladder was required in order to be sufficiently high enough above the canopy to properly collect the canopy view angle samples. A standard aluminum field ladder was used for this purpose, i.e., to collect the nadir view samples. From analysis of the images collected by the SVC device during collection, we were successful in ensuring that the ladder did not fall inside the FOV of the SVC device during the sampling process. It is possible that a small amount of illumination was reflected from the ladder and onto the grape leaves, while the samples were being collected. This would be

less of a concern during the periods in which the sun was obscured by cloud. While the additional background illumination would be in the scene, due to the view angles and the surface of the ladders, the contribution is likely to be very small. This could not be calculated or removed and therefore was considered a part of the scene.

3.5.3.2 Inclinometer

An inclinometer was required in order to measure the off-nadir collection angle for the canopy. It was attached to the top of the SVC unit with Velcro. Magnets would have been preferable, but were not used for fear of damaging the SVC device. The accuracy to which the off-nadir degree was measured fell within ±5°.

3.6 Spectral data collection - view angles

The reflectance spectra were collected using the SVC spectroradiometer. Data from three different observation angles were collected in order to evaluate the differences between responses, depending on the scene content and view angle (sun and bi-directional reflectance distribution function (BRDF) impacts).

The first view angle was at nadir for the individual grape leaves and was collected by holding the SVC approximately 0.30m (+0.03m/-0.10m) from each leaf. From that distance the FOV of the sensor ≤ 0.075m in diameter, thereby ensuring that the complete FOV was filled by the leaf. The second view angle was collected for the vine canopy at nadir using a ladder beside the row of grape vines and holding the sensor approximately 1m (+0.3m/-0.3m) above the bulk of the canopy. This view angle has an FOV = 0.246m and included not only the grape leaves, but also some of the background, such as stems, ground, and ground cover surrounding the row. This view is more representative of pixel-level data collected by an airborne sensor. The third and final view angle was a collect of the canopy at 15° off-nadir, parallel to the side of the row. Like the nadir view angle, this was again collected using a ladder, with the sensor held approximately 1m (+0.3m/-0.3m) above the bulk of the canopy. Similar to the nadir view angle, this would include some of the ground cover surrounding the row of vines, but to a lesser extent, since more of the FOV would be filled by the side mass of the vine canopy. Table 4 below shows the FOV sizes, including the error based off the distances.

Table 4: Field of view for the 4° and 14° SVC fore-optics, including error range

Field of View (m)	Minus	4 Degrees	Plus	Minus	14 Degrees	Plus
Leaf View	0.014	0.021	0.024	0.049	0.074	0.086
Canopy Nadir				0.17	0.25	0.32
Canopy 15 deg off-Nadir				0.17	0.25	0.32

3.6.1 Sample averaging

Two samples were collected per panel for each view angle. This allowed for averaging of the data to reduce spurious results. The samples were collected by first taking a white reference sample using either Spectralon (during bloom) or Tyvek (during veraison), immediately followed by taking a target sample. This approach accounts for changes in illumination levels (normalization or conversion from radiance to reflectance) and continuously updates the system's gain settings, thereby avoiding signal saturation.

3.6.2 Collection path

The order that the panels were sampled was different for each of the data collections, bloom and veraison. This change in pattern was due to optimizing sampling efficiency during site visits, when the batteries for the SVC needed to be replaced, or breaks in the sampling routine due to personnel requirements or weather.

Figures 6 and 7 below denote the order in which the panel groups were sampled for the Riesling cultivar. The field team travelled either left to right or right to left through each of the panels, depending on the direction of ascension of the numbers. In the case of the leaf view, a sample was collected, after which we moved further down the panel, collected another sample, and then moved to the next panel. The samples were spread out between the four vines in the panel, with no vine having both samples collected from that single vine. For the canopy view angles, a sample was collected for one of the canopy views, followed by collection of a sample for the other canopy view angle in the same location, before we moved down the panel to the next sampling location. Again, no vine was sampled twice for the same view angle in a panel.

Riesling Bloom Leaf Collection Order

Row	Panels									
1										
2		1			2					
3		4			3					
4		5			6					
5		8			7					
6		9			10					
7		12			11					
8		13			14					
9		15			16					
10		17			18					
11		20			19					
12		21			22					
13		24			23					
14										

Riesling Bloom Canopy Collection Order

Row	Panels									
1										
2		1			2					
3		4			3					
4		5			6					
5		8			7					
6		9			10					
7		12			11					
8		13			14					
9		**16**			**15**					
10		17			18					
11		20			19					
12		21			22					
13		24			23					
14										

Figure 6: Riesling cultivar - bloom collection order: (a) leaf view, (b) canopy views

Riesling Veraison Leaf Collection Order

Row	Panels									
1										
2		1			2					
3		4			3					
4		5			6					
5		8			7					
6		9			10					
7		12			11					
8		13			14					
9		15			16					
10		17			18					
11		20			19					
12		21			22					
13		24			23					
14										

Riesling Veraison Canopy Collection Order

Row	Panels									
1										
2		1			2					
3		4			3					
4		5			6					
5		8			7					
6		9			10					
7		12			11					
8		13			14					
9		**16**			**15**					
10		17			18					
11		20			19					
12		21			22					
13		24			23					
14										

Figure 7: Riesling cultivar - veraison collection order: (a) leaf view, (b) canopy views

Figures 8 and 9 below show the order in which the Cabernet Franc was sampled; the same sampling principles, described above for the Riesling cultivar, were used for the Cabernet Franc panels. The panel marked in red was dead and thus was unusable for analysis, as described above.

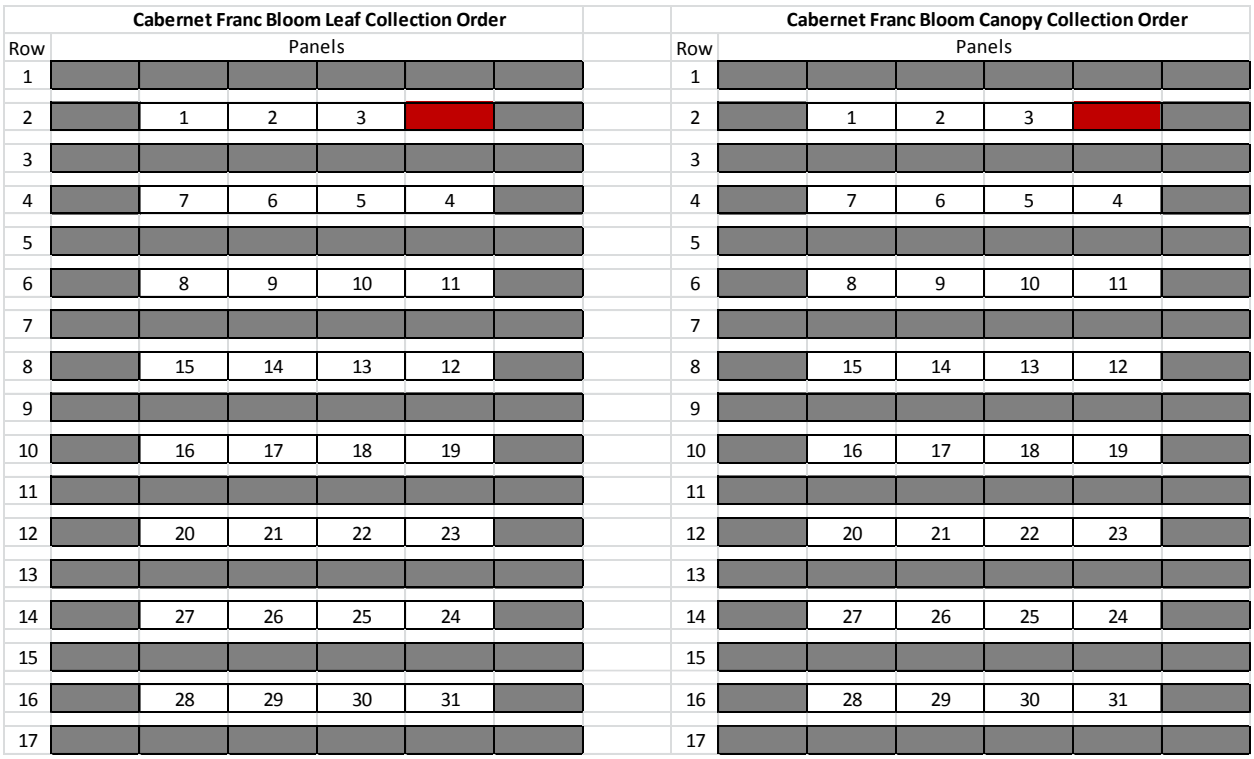

Figure 8: Cabernet Franc cultivar - bloom collection order: (a) leaf view, (b) canopy views

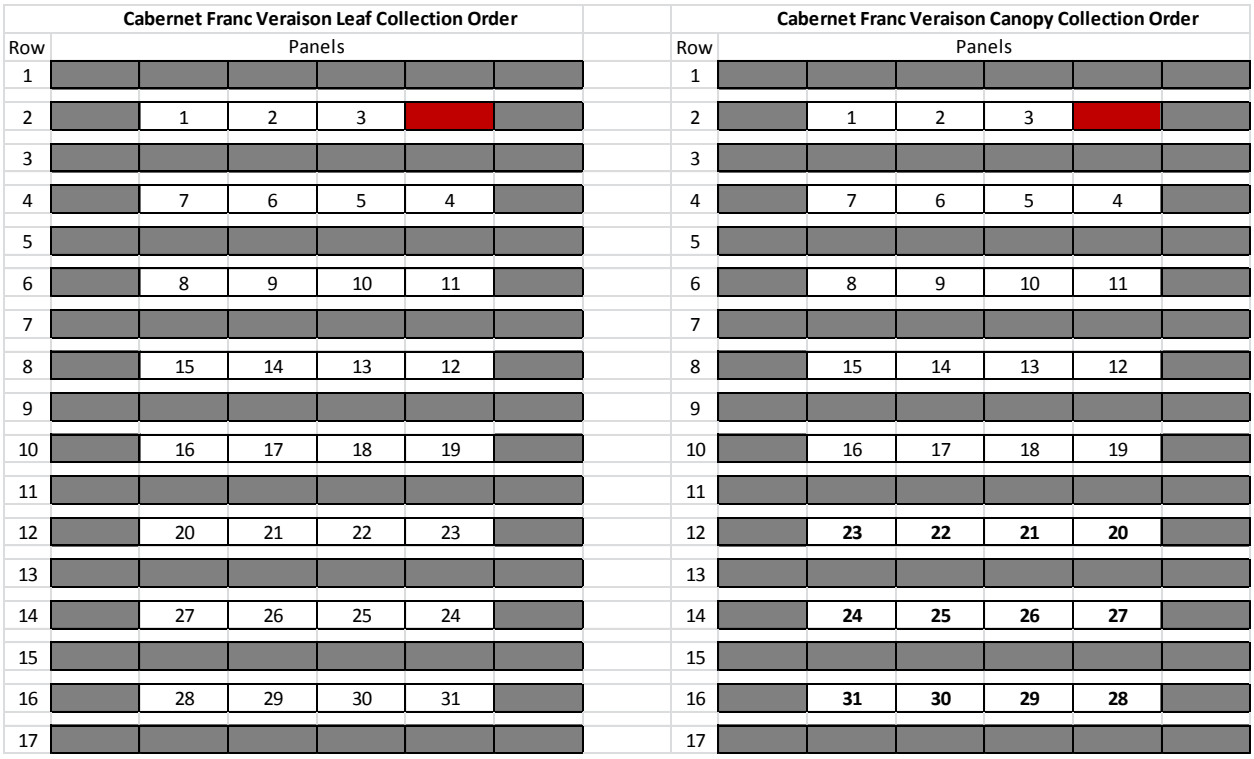

Figure 9: Cabernet Franc cultivar - veraison collection order: (a) leaf view, (b) canopy views

It was critical to document the order in which the spectral samples were collected, since nutrient samples were labeled in a different order by the Cornell University field team. The nutrient samples were collected in ascending order, from left to right down each row, starting at the top of the block and working down to the bottom. Therefore, in order to match the spectral and nutrient analysis data, we had to rearrange the spectral data to match the order in which the nutrient data were collected.

4.0 Data Analysis Methods

The spectral data were analyzed against the nutrient data at two different spectral resolutions. The first was at a consistent 1nm resolution, i.e., the native, resampled resolution from the SVC spectroradiometer, while the second was at a nominal 10nm resolution, thereby matching a more typical airborne imaging spectrometer (AVIRIS, in this case).

4.1 1 Data analysis methods – 1nm data

4.1.1 Data Preparation – 1nm data

Spectral data were read into MATLAB using the FSF post-processing toolbox. The spectroradiometer did not have regularly spaced sampling intervals, so the data were interpolated to consistent 1nm spacing across the full range of the SVC unit. The data were then averaged to match that of the cultivar nutrient sampling approach. For Cabernet Franc that consisted of averaging the two samples taken for each view angle in each panel, while for the Riesling, that involved averaging the six samples taken between the three panels that were lumped together in the nutrient sampling. Next we limited the data to our range of interest, in this case from 400-1000nm. Figures 10-13 below show the interpolated and limited reflectance spectra collected for each of the blocks, during both bloom and veraison.

The plot of the reflectance data, seen in Figure 10(c), collected at 15° off-nadir in the Cabernet Franc block during bloom, shows an anomalous spectral sample when compared to the other samples. Although no logical cause could be identified for this anomaly, it was removed during data analysis, leaving 30 samples for that view angle. Riesling data (seen in Figure 11), also collected during bloom, did not exhibit any outlier spectral samples.

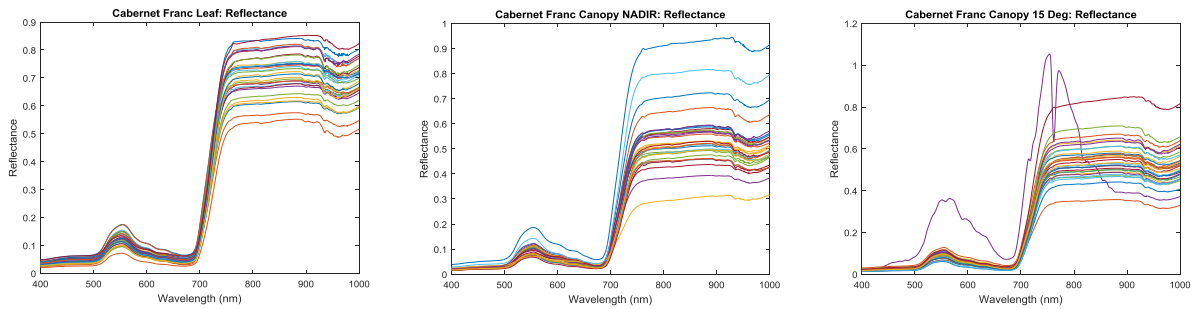

Figure 10: Reflectance for the Cabernet Franc grape cultivar for the different view angles during bloom (a) leaf view, (b) canopy nadir view, and (c) canopy 15° off-nadir view

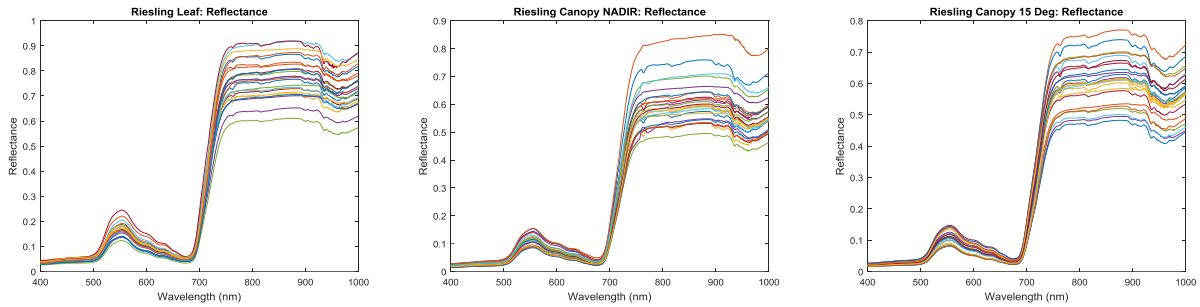

Figure 11: Reflectance for the Riesling grape cultivar for the different view angles during bloom (a) leaf view, (b) canopy nadir view, and (c) canopy 15° off-nadir view

We speculate that this anomaly in the Cabernet Franc data was caused by either atmospheric changes between white reference and sample collection, or by an off-target pointing instrument, thus resulting in spurious data. As the combined data were not downloaded and reviewed in the field, the anomalous band was not found until later and so it was impossible to repeat the sample collection. The spectra were typically checked during the initial data collection, in order to ensure that the spectra was not saturated and that they were as expected for typical, healthy vegetation. Although several errors were identified and corrected during the field campaign, some errors (see Figure 10(c)) may have been missed during data collection.

Figures 12 and 13 below show the reflectance spectra for the Cabernet Franc and Riesling blocks, respectively, collected during the veraison growth period. Again, it was observed that for the Cabernet Franc block in both the leaf view and canopy nadir view, we have an outlier spectral sample. There once again was no specific reason why this specific sample would be different; the erroneous sample was removed from the data analysis, resulting in only 30 spectral samples for each of these two view angles.

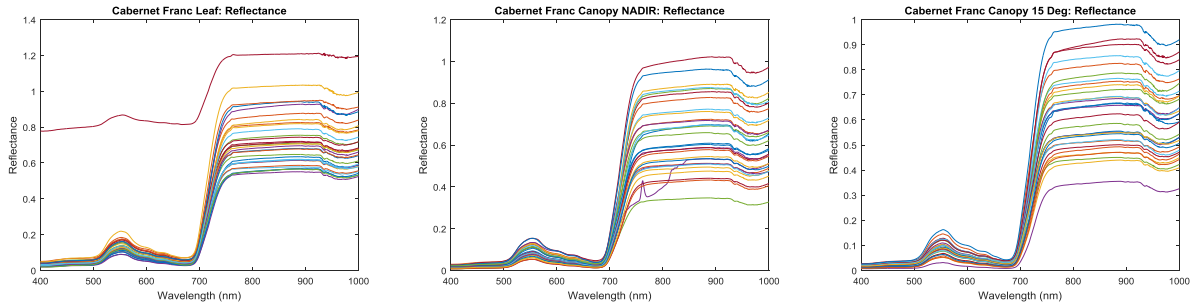

Figure 12: Reflectance for the Cabernet Franc grape cultivar for the different view angles during veraison (a) leaf view, (b) canopy nadir view, and (c) canopy 15° off-nadir view

From the collected Riesling spectrum, we can see in Figure 13(b) that a single sample spectrum had unexpectedly high values in the 400-700nm range; this spectrum was removed for the data analysis, leaving 23 samples for this view angle. These data omissions are mentioned for the sake of

completeness. Field-based data collection does not always go according to plan, with extraneous influences (atmosphere, pointing accuracy, etc.) that can impact spectral data. We contend that these omissions have limited impact on the results, given the small number that were omitted, relative to the larger overall sample size.

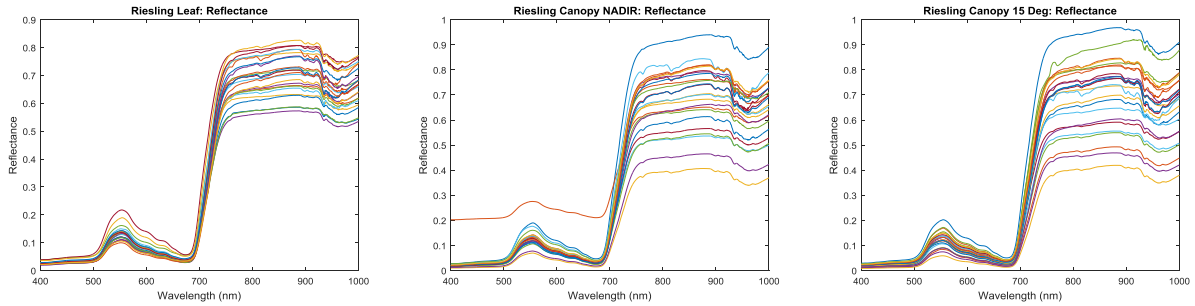

Figure 13: Reflectance for the Riesling grape cultivar for the different view angles during veraison (a) leaf view, (b) canopy nadir view, and (c) canopy 15° off-nadir view

The next step involved generation of normalized indices, based on the now consistent and error-free spectral data.

4.1.2 Index creation – 1nm data

Two different index types were created for evaluation against nutrient data. The first type of index was a normalized difference index (NDI), of the same form as the standard NDVI index found in Eismann (2012), which is commonly used for vegetation analysis in remote sensing studies (Equation 4):

$$NDI = \frac{(\lambda_1 - \lambda_2)}{(\lambda_1 + \lambda_2)} \quad (4)$$

where λ_1 and λ_2 are reflectance values at different 1 nm wavelengths.

The second index utilized a simple ratio between two different wavelengths (RI), as seen in Equation 5:

$$RI = \frac{\lambda_1}{\lambda_2} \quad (5)$$

where λ_1 and λ_2 are reflectance values at different 1 nm wavelengths.

For both the NDI and RI approaches, the wavelengths were iterated over the complete silicon photodiode spectral range in order to generate all possible combinations.

4.1.3 Calculation of the 1 nm Wavelength Correlation Coefficients

After permuting and reshaping the data into a usable form, each of these generated index types was then evaluated in terms of their correlation with the respective nutrients. This was achieved using the MATLAB command 'corrcoef', which calculates the correlation coefficient (CC or "*correlation*" from here onwards) between the two data sets. The formula, as explained in the MATLAB documentation (2016), is seen below in Equation 6:

$$R(i,j) = \frac{C_{(ij)}}{\sqrt{C_{(ii)} * C_{(jj)}}} \qquad (6)$$

where C is the covariance matrix of the indices, for wavelengths *i* and *j*.

The α-level for the correlation coefficient calculation was left at the default level of 0.05, resulting in a 95% confidence level. The highest correlation values were recorded for each of the view angle-nutrient combinations.

We next attempted to calculate the linear fit for all the above nutrient-view angle combinations. This involved 321,601 variables, which MATLAB could not resolve. We decided to limit the scope, since this method didn't give us a functional result. We started by focusing only on the nutrient-view angle combinations that had a CC ≥ 0.70, followed by limiting the wavelengths to only those of the 601 that yielded these high CC values. Finally, we calculated the linear fit for the combinations of interest using this reduced list. As there was a number of nutrient-view angle combinations that were not tested, i.e., the CC values was lower than the 0.7 cutoff value, we decided, in the interest of being thorough, to use the bands that achieved the highest CC value at a $p < 0.05$ level. This was done to ensure that i) all nutrients, phenological stages, and view angles yielded models and ii) that the selected bands were in fact correlated to a specific nutrient, hence the $p < 0.05$ selection criterion. For the two cultivars, sampled at each of the three view angles, the number of bands that were selected for the analysis at the $p < 0.05$ level matched the number of actual data samples for that view-angle. For the Riesling cultivar this was typically 24 bands, except when an erroneous band was removed. For Cabernet Franc the top 31 bands were used in general, reduced to 30 bands when an erroneous band had to be removed from the spectral data set. Using these bands, the linear fit was calculated and included in the tables for comparison against the linear fit method only; note – these bands were not included in the final summary results.

4.1.4 Wavelength and NDI Step-wise Linear Regression – 1nm data

We used the list of wavelengths that were highly correlated with the nutrient data to run a stepwise linear regression on the spectral data to improve our model fit with the nutrients. Three different model criteria were used to evaluate model terms: upper-linear-AIC, upper-linear-BIC, and upper-linear-R^2. In all three models the 'upper linear' model was used with the criterion for the addition or removal of terms. The model specification of 'upper' describes the largest set of terms that can be used in the model fit. The model type to be used further refines this model specification - we used the 'linear' model type. This implies that the model will contain only a constant and linear terms for each predictor. Three model fit criteria were used to assess the predictive wavelength-nutrient relationships, namely AIC, BIC and R^2. AIC refers to a change in the value related to the Akaike information criterion; BIC refers to a change in the value related to the Bayesian information criterion; and finally R^2 refers to an increase in the value of R^2 (coefficient of determination). In each case, if a predictor value causes an increase in the criterion, then that variable is added to the model. The step-wise linear regression was run in both a forward and backwards mode, implying that predictors (independent variables) were added in an iterative, forward method, but the model also assesses previous entries and removes those that does not cause a decrease in the criterion value. These models were run for each of the three view angles, for both cultivars, and for both growing seasons. In a brute-force approach, the complete spectrum of 601 values were used for the list of input variables in the SLR, if it was found that a given cultivar in a particular growing season had no indices that were correlated to nutrient values at or above the cut-off level.

After the highly correlated *wavelengths* were run through SLR, the *indices* that were highly correlated also were then run through SLR; the same model criteria used for the wavelengths were used for the indices. As done for the linear fit, the top correlated bands at $p < 0.05$ were also used in the SLR to evaluate how they performed against the reduced data set.

The next steps involved a look at more complicated forms of the data, following the wavelength and index modeling approaches. The first additional analysis was performed using the derivative (slope) of the reflectance spectra.

4.1.5 Derivative Analysis – 1nm data

The prepared data were used for the derivative analysis, as per the process outlined below. First, the 1nm spectral data were smoothed to limit the sensitivity of derivative analysis to erratic values (Horler *et al.* 1983); smoothing was applied to the spectra using the 'smooth' function in MATLAB. The 'moving' command was applied to ensure that the smoothing window "slide" along spectra,

incorporating new values for the smoothing operation at each new wavelength. The settings were left at the default value of five wavelengths for calculation of the smoothing effect. The next steps involved calculation of the actual 1st derivative.

It is possible to approximate a partial derivative of a vector in MATLAB through of use of the 'diff' function. The first step is to select the step spacing that would be used in calculating the derivative. Our data were at consistent 1nm spacing, so that is the spacing that was selected. Division of the 'diff' function by the spacing results in the derivative of the vector (Equation 7):

$$Y = \frac{diff(x)}{h} \tag{7}$$

where Y is the derivative, x is the data vector, and h is the step spacing of the derivative.

Figures 14-17 show the 1st derivative of the spectra for both cultivars in both growing seasons.

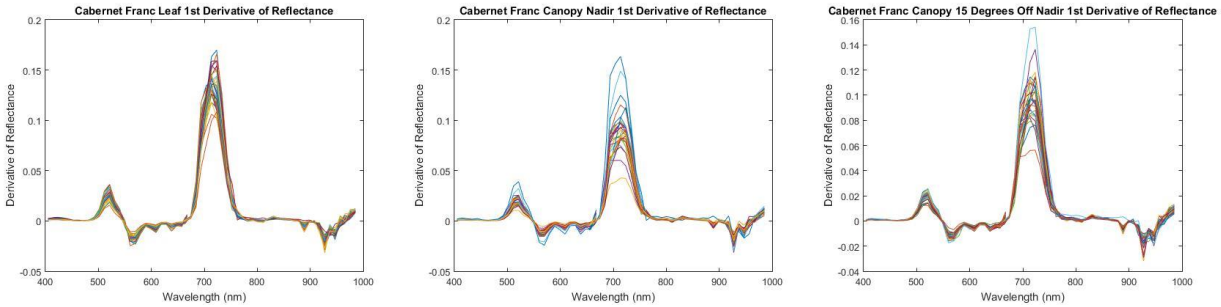

Figure 14: The 1st derivative of the reflectance for the Cabernet Franc grape cultivar for the different view angles during bloom (a) leaf view, (b) canopy nadir view, and (c) canopy 15° off-nadir view

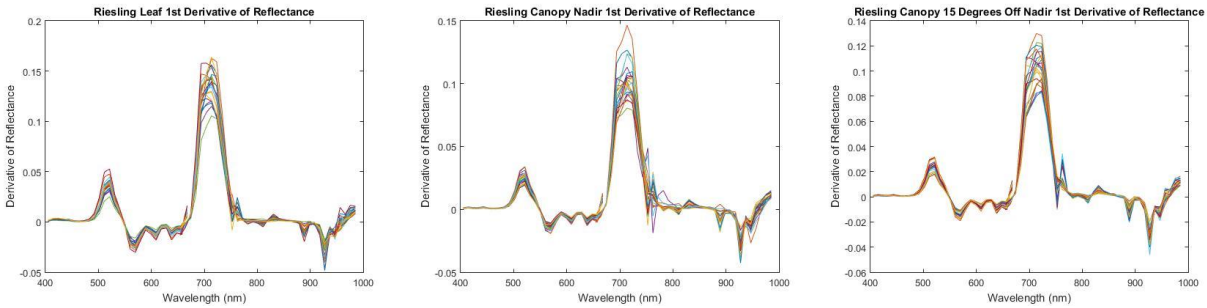

Figure 15: The 1st derivative of the reflectance for the Riesling grape cultivar for the different view angles during bloom (a) leaf view, (b) canopy nadir view, and (c) canopy 15° off-nadir view

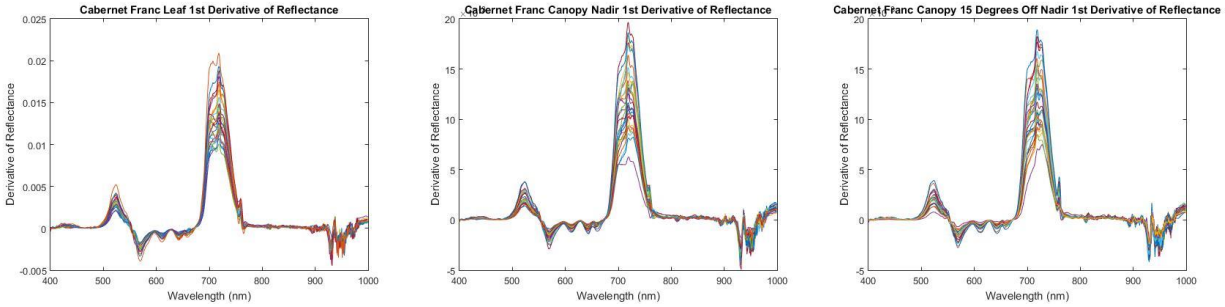

Figure 16: The 1st derivative of the reflectance for the Cabernet Franc grape cultivar for the different view angles during veraison (a) leaf view, (b) canopy nadir view, and (c) canopy 15° off-nadir view

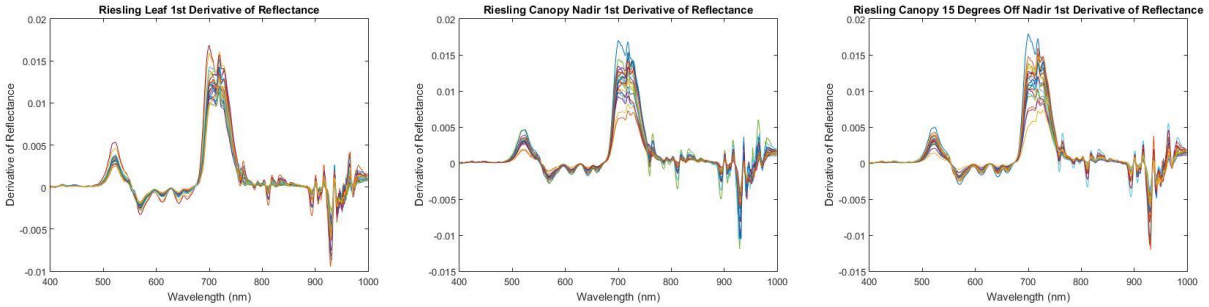

Figure 17: The 1st derivative of the reflectance for the Riesling grape cultivar for the different view angles during veraison (a) leaf view, (b) canopy nadir view, and (c) canopy 15° off-nadir view

The 601 unique wavelengths produced 600 derivative values. Correlation coefficients were then calculated for these derivatives against the nutrients in each cultivar-growing season combination. This was done in order to identify a reduced set of derivatives that was highly correlated against a particular nutrient, giving six unique nutrients. The cut-off value used to decide if the derivative value was highly correlated, was the same that as used before for the indices, i.e., a value of CC ≥ 0.70. This reduced set of wavelength derivatives was then run through SLR to find the best model fit for that nutrient. A second SLR was run using the complete set of 600 derivative values as the input variables, if it was found that the spectrum from a nutrient-growing season combination did not produce any derivatives that correlated highly with the nutrient data. Having examined the effectiveness of using the spectrum derivative for determination of nutrient content, we next evaluated absorption features of the spectrum directly through the process of continuum removal.

4.1.6 Continuum Removal – 1nm data

We used the technique of continuum removal in order to evaluate nutrient model fits, based on specific absorption features. Proposed by Kokaly and Clark (1999), we followed the same continuum removal techniques, but used different spectral regions. The steps laid out in their paper are to i) select the feature you wish to use and establish a continuum line spanning that feature; ii)

calculate the continuum-removed spectra by dividing the original reflectance values for each point in the feature by the corresponding continuum line values; followed by iii) calculating the band depth (D) at all the points along the feature by subtracting the continuum-removed spectra values from 1. This band depth can then be used in a step-wise linear regression to fit the nutrient data. The authors suggest a normalization of the band depth (calculate D_n) by dividing the band depth by the depth at the band center (D_c) of the feature. The band center in this case is not the physical center, but is instead defined as the deepest band in the feature. This gives the following equations, for continuum-removed reflectance (R')

$$R' = \frac{R}{CL} \tag{8}$$

where R is the reflectance data and CL is the values of the continuum line.

for the band depth (D)

$$D = 1 - R' \tag{9}$$

and for the normalized band depth (D_n)

$$D_n = \frac{D}{D_c} \tag{10}$$

where D_c is the band center.

Two different techniques were used to select the regions on which continuum removal would be applied. The first approach was to select a common area present in all cultivar-growing season combinations, the red trough. The majority of absorption features attempted by Kokaly and Clark (1999) and the typical regions in which continuum removal is applied, all fall outside the silicon range that we have limited ourselves to. Therefore we selected the red trough that is pronounced in all spectra for live vegetation (Eismann 2012). We needed to select an area that worked for the complete set of spectra, before analyzing the spectra for all four cultivar-growing season combinations and across all three view-angles. We enhanced red through absorption by using a linear fit line, where the two end points spanned the majority of the red trough, without cresting either end. Therefore, a point just to the right of the green peak was selected for the first point of the continuum removal line, at 560nm, while the second end point was selected just to the left of the NIR peak, at 750nm. This line was then used in the procedure explained above. An example is shown in Figure 18 below.

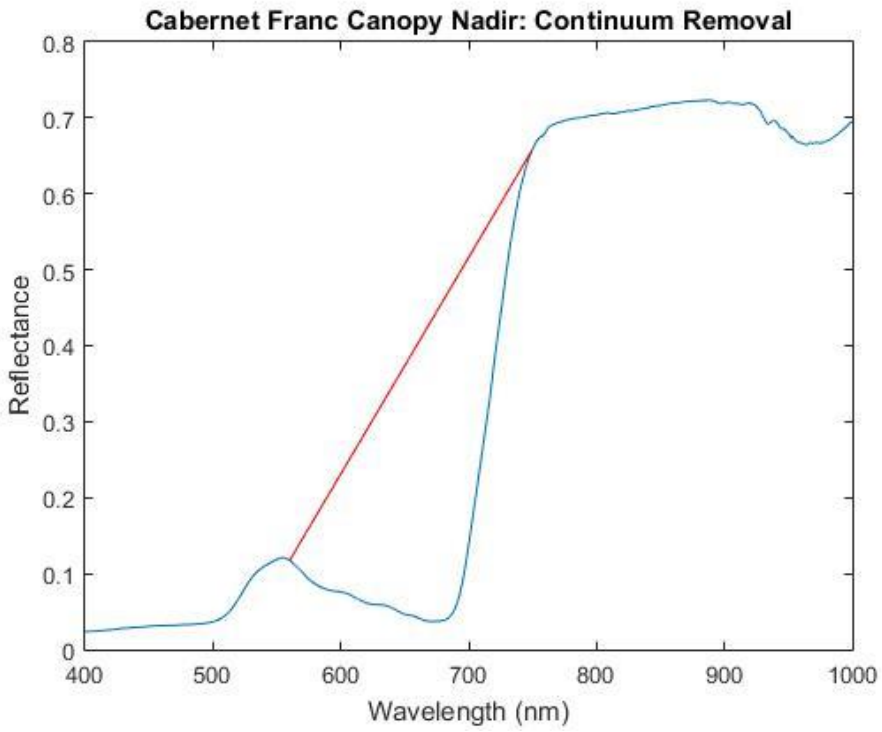

Figure 18: An example of the continuum line removal approach

The second technique that was applied was to select a spectral range specific to each of the nutrients, based on wavelengths that exhibited high correlations for that nutrient. This implied that the wavelengths with high correlation would be plotted for the spectra, followed by an examination to see if there are any dips or features in those wavelength regions that could be exploited for the continuum removal procedure outlined above. If no wavelengths came back with a high level of correlation, or no usable features were found in the location of the highly correlated wavelengths, then this second technique was not used.

4.2 1 Analysis methods – 10nm data

The next phase of the analysis involved the use of data at a 10nm spectral resolution, in order to evaluate how the lack of fine, 1nm spectral features in the spectral data influence the results, towards implementation in more common, coarser spectral resolution airborne imaging spectrometers.

4.2.1 Data Preparation – 10nm data

The data preparation for the 10nm spectral bands used the same procedures as those used for the 1nm bands, e.g., the data were read into MATLAB using the FSF post processing toolbox. The uneven spectral sampling from the SVC spectrometer was not an issue for the 10nm spectral bands,

since we needed to modify the data interpolation in either case. It was decided that, in order to make the data more relevant to the remote sensing community, instead of using arbitrary 10nm bands, we would calibrate our bands to match that of a commonly used remote sensing platform. Several options were available to use for calibration: GOES, Landsat, and IKONOS, among others. However, we decided to use AVIRIS as our calibration target. Although this platform is unlikely to be used for agricultural purposes, it was selected because it is a well-known and long running system. Table 5 shows the calibration data from the AVIRIS website; the data for the years 2012 and 2013 were available, and 2013 was selected for use. The table also shows the difference between the calculated wavelengths. It is evident that the AVIRIS sensor does not have a consistent 10nm bandwidth, but in fact varies between 9.15nm and 11.93nm. Therefore, we used a nominal 10nm bandwidth, resulting in 64 unique 10nm bands to use in our analysis.

Table 5: Calibration data for the 10nm AVIRIS bands

AVIRIS Calibration Data		**2013**					
Wavelength	**Difference**	**Wavelength**	**Difference**	**Wavelength**	**Difference**	**Wavelength**	**Difference**
404.61	9.65	560.05	9.18	693.99	9.73	849.94	10.57
414.29	9.60	569.80	9.17	703.78	9.71	859.65	10.70
423.98	9.56	579.56	9.16	713.56	9.70	869.34	10.85
433.67	9.51	589.32	9.16	723.33	9.70	879.04	11.00
443.37	9.47	599.08	9.15	733.10	9.70	888.72	11.17
453.07	9.44	608.85	9.15	742.87	9.72	898.41	11.34
462.77	9.40	618.63	9.15	752.63	9.75	908.08	11.53
472.48	9.37	628.40	9.16	762.38	9.79	917.76	11.72
482.19	9.34	638.19	9.16	772.13	9.84	927.42	11.93
491.91	9.31	647.97	9.17	781.88	9.89	937.08	10.78
501.63	9.29	657.77	9.18	791.62	9.96	946.74	9.76
511.35	9.26	667.56	9.19	801.35	10.04	956.39	9.76
521.08	9.24	654.79	9.91	811.08	10.12	966.04	9.76
530.82	9.22	664.60	9.85	820.80	10.22	975.68	9.76
540.56	9.21	674.40	9.80	830.52	10.33	985.31	9.76
550.30	9.19	684.20	9.76	840.24	10.44	994.94	9.76

The newly generated 10nm AVIRIS-like data subsequently were averaged in a similar fashion to that of the 1nm data, in order to match the number of sample obtained from the nutrient sampling. The spectra from each of the view-angles for both cultivars in both growing seasons were again examined, and the erroneous samples were removed as before. It should be noted that, in the AVIRIS calibration data there exist bands (rounding to the nearest integer value) at 658nm, 668nm, 655nm, and 665 nm. This duplication of bands was only found while generating the plots related to wavelengths to be used for nutrient modeling; the duplication of wavelengths did not negatively

impact the analysis in any way and from the peak values we can see that only one of the duplicate bands was used in a single instance.

4.2.2 Index Creation – 10nm data

Only the normalized difference index type was created for the 10nm data (Equation 4); NDIs were created by iterating across all combinations of the 64 bands. The ratio index was not created for the 10nm spectral data, because it was found from the results of the 1nm that the two indices performed the same to two decimal places, thus rendering additional analysis redundant.

4.2.3 Calculation of the 10nm Wavelength Correlation Coefficients

Correlation coefficients were calculated as per the procedure established for the 1nm data over the full range for the 10nm spectral data.

4.2.4 Wavelength and NDI Step-wise Linear Regression – 10nm data

The same process listed for 1nm data, as far as the examination of the highly correlated wavelengths and indices by way of SLR, was applied to the 10nm spectral data. No modifications to the process were required to account for the change in spectral resolution.

4.2.6 Derivative Analysis – 10 nm data

The steps used for the 1nm data to calculate the derivative and then use the results as variables for SLR to determine the best model fit to the nutrient data, also were applied to the 10nm data, with the exception of smoothing. We deemed the smoothing step as unnecessary, given that the 10nm already had been smoothed by way of resampling to 10nm spectral bandwidths. The derivative analysis resulted in 63 variables, which were then tested for correlation to the nutrient data in order to identify a highly correlated data set. As this resulted in no selected variables, the complete set of 63 variables were used in the SLR.

4.2.7 Continuum Removal Analysis – 10nm data

The same continuum removal process used for 1nm data, also was applied to the resampled 10nm spectral reflectance, i.e., only the red trough region was used (continuum line between from 560-752nm. These were the points that most closely matched those used for the 1nm resolution data (560nm and 750nm). Besides this change, the continuum removal process was the same as for the 1nm data.

5.0 Results and discussion

The first thing we will discuss is the results from the two nutrient analyses that were conducted, the leaf nutrient analysis and the petiole nutrient analysis. From there the results for each of the 5 methods will be discussed for the 1nm data and then the 10nm data.

5.1 Nutrient Analysis Results

The soil in which the grape vines grow, the cells and leaves of the vines, and the grapes that grow on the vines all contain varying amounts of nutrients. Pohl (2007) discusses how these nutrients change as the vines go from bloom, to veraison, then are harvested and fermented, and finally bottled into a finished product. For our discussion, we are only interested in the first two steps, bloom and veraison. Other authors, such as Christensen (1984), have examined the behavior of nutrients found in wine grapes across various cultivars and how they change over time. Romero et al. (2010; 2012) have examined the difference between nutrient analyses conducted at the leaf and the petiole levels between the two growing seasons, similar to our approach. They found that the leaves and petioles gave different results for the concentration of nutrients depending on which was examined and that one was more appropriate then another depending on the nutrient of interest. Tables 6-13 below provide a summary of the results from the two nutrient analyses that we conducted on the Cabernet Franc and Riesling cultivars, during both bloom and veraison.

As previously discussed, the Cabernet Franc cultivar had 31 unique samples. Comparing the bloom results between the leaf nutrient analysis and the petiole nutrient analysis we found that except for K, the results from the petiole analysis had a lower mean value then the leaf results. Wolf (2008) provides detail regarding the sufficiency ranges for the nutrient concentrations. When one compares the nutrient values from the two analyses against the values from Wolf (2008), it is evident that for B and Mg, the petiole analysis exhibited mean values that fell within the ideal concentration range for those nutrients, while the leaf analysis resulted in values higher than ideal. For K, both analyses had mean values that fell within the range, with leaf being towards the bottom and petiole being towards the top of the range. Both Zn and P had mean values above the ideal range, but the values from the petiole analysis were lower and therefore closer to what is aimed for. The mean N concentration for the leaf analysis was higher than the ideal range, while the values from the petiole analysis fell below the ideal range. The differences from the expected concentrations can be explained by the varied ground treatments and starting nutrient concentrations in the soil of the experimental plots.

Table 6: Nutrient concentrations for Cabernet Franc from the bloom phenological stage: leaf nutrient analysis

Cabernet Franc - Bloom (Leaf Analysis)					
Nutrient	**Mean**	**Std Dev**	**Max**	**Min**	**n**
Boron (mg/kg)	106.37	17.43	153.21	80.74	31
Magnesium (mg/kg)	5563.42	606.06	7028.93	4524.20	31
Nitrogen (%)	2.64	0.27	3.24	2.23	31
Phosphorus (mg/kg)	5550.27	450.21	6542.34	4609.07	31
Potassium (mg/kg)	18362.38	2751.24	24125.40	14258.40	31
Zinc (mg/kg)	174.76	21.13	225.74	146.00	31

Table 7: Nutrient concentrations for Cabernet Franc from the bloom phenological stage: petiole nutrient analysis

Cabernet Franc - Bloom (Petiole Analysis)					
Nutrient	**Mean**	**Std Dev**	**Max**	**Min**	**n**
Boron (mg/kg)	45.88	4.12	54.67	35.00	31
Magnesium (mg/kg)	4446.27	786.60	7087.08	2987.22	31
Nitrogen (%)	0.74	0.13	1.00	0.56	31
Phosphorus (mg/kg)	4541.08	1887.27	8236.95	1739.16	31
Potassium (mg/kg)	22813.35	7523.44	37957.50	9010.12	31
Zinc (mg/kg)	84.64	9.60	117.99	66.09	31

Table 8 and 9 below show the results from veraison. It is evident that the petiole nutrient analysis had higher mean values then the leaf analysis in five of the six nutrients, with N being the exception. For both analyses the mean B values were within expected concentrations. For the petiole analysis, Zn was also within the expected range, while both Mg and N fell below the ideal range and P and K were above it. From the leaf analysis, besides B, both P and K were within the ideal range. Zn and Mg were below and N was higher than the ranges reported in Wolf (2008).

According to Wolf (2008) there should be a decrease in the concentration of N, P, and K as the growing season progresses, whereas there should be an increase in the concentrations of Mg, while B and Zn should remain roughly the same. The behavior of the nutrients from the *petiole nutrient analyses* between the two growing seasons was mostly as expected. B decreased slightly, but stayed within range. N decreased as expected, as did P. Zn decreased, but this brought the initial higher levels it into the expected range. The two main deviations were in Mg and K: Mg saw a decrease when an increase was expected as the season progressed, while K did the opposite and increased when there should have been a decrease. From the *leaf nutrient analysis* there was a large decrease in B, when it should have remained fairly steady; however, this did bring B-values down into the

expected range. Magnesium, similar to the petiole analysis, increased, contrary to expectations. The mean N values also increased when they should have decreased. P decreased as expected, but there should have been an increase in K, while a decrease was seen. Finally, Zn had a very large decrease when it should have remained roughly the same. *Overall that implies that four of the six nutrients from the petiole analysis performed roughly as expected, while only two of the nutrients in the leaf analyses did so*.

Table 8: Nutrient concentrations for Cabernet Franc from the veraison phenological stage: leaf nutrient analysis

Cabernet Franc - Veraison (Leaf Analysis)					
Nutrient	**Mean**	**Std Dev**	**Max**	**Min**	**n**
Boron (mg/kg)	33.66	6.98	47.94	21.93	31
Magnesium (mg/kg)	2432.13	314.78	3306.43	1971.64	31
Nitrogen (%)	2.74	0.24	3.22	2.14	31
Phosphorus (mg/kg)	2408.34	289.03	2945.70	2048.47	31
Potassium (mg/kg)	13782.91	1812.31	17724.40	10713.10	31
Zinc (mg/kg)	20.13	2.17	24.52	17.14	31

Table 9: Nutrient concentrations for Cabernet Franc from the veraison phenological stage: petiole nutrient analysis

Cabernet Franc - Veraison (Petiole Analysis)					
Nutrient	**Mean**	**Std Dev**	**Max**	**Min**	**n**
Boron (mg/kg)	34.52	5.36	46.34	26.79	31
Magnesium (mg/kg)	2746.96	390.00	3697.15	2011.91	31
Nitrogen (%)	0.68	0.09	0.96	0.54	31
Phosphorus (mg/kg)	3459.48	722.20	5461.30	2457.46	31
Potassium (mg/kg)	30602.70	2325.26	37137.30	26473.90	31
Zinc (mg/kg)	47.60	4.98	63.13	41.19	31

The nutrient concentrations from the Riesling cultivar during the bloom collect are shown in Tables 10 and 11 below. As discussed previously, the sampling for the Riesling cultivar only produced 24 independent data points. From the leaf nutrient analysis of the Riesling cultivar, we see that similar to the Cabernet Franc, four of the six nutrients were higher than the ideal values, with Mg and K being in the correct range of concentrations. For the petiole analysis, five of the nutrients were found to be above the ideal concentration values and the sixth, N, was well below it.

Table 10: Nutrient concentrations for Riesling from the bloom phenological stage: leaf nutrient analysis

Riesling - Bloom (Leaf Analysis)					
Nutrient	**Mean**	**Std Dev**	**Max**	**Min**	**n**
Boron (mg/kg)	63.68	7.16	80.77	54.75	24
Magnesium (mg/kg)	4662.68	533.51	5701.06	3846.40	24
Nitrogen (%)	2.30	0.25	2.64	1.78	24
Phosphorus (mg/kg)	5835.30	943.54	7649.08	4444.96	24
Potassium (mg/kg)	15920.38	2537.62	21366.60	12452.20	24
Zinc (mg/kg)	138.99	19.63	177.99	105.95	24

Table 11: Nutrient concentrations for Riesling from the bloom phenological stage: petiole nutrient analysis

Riesling - Bloom (Petiole Analysis)					
Nutrient	**Mean**	**Std Dev**	**Max**	**Min**	**n**
Boron (mg/kg)	101.09	6.10	110.63	86.95	24
Magnesium (mg/kg)	10772.76	1120.73	12856.50	8667.49	24
Nitrogen (%)	0.68	0.10	0.87	0.54	24
Phosphorus (mg/kg)	14479.66	3514.37	20027.20	7968.83	24
Potassium (mg/kg)	37485.65	3478.64	46176.85	30585.40	24
Zinc (mg/kg)	149.43	14.61	180.72	119.56	24

During veraison, in Tables 12 and 13 below, the leaf analysis saw B, P, and K exhibit mean values in the expected range. Magnesium went from the ideal range during bloom, to below the ideal range during veraison, and Zn fell from well above to just below the ideal concentration range as the season progressed. The N value saw an increase between bloom and veraison, remaining above the expected values. From the petiole analysis during veraison we again had three nutrients in the ideal concentration range: B, as in the leaf analysis, N, and Zn. The Mg concentration came in below the ideal range, while both P and K were above the expected values.

We found, for the leaf nutrient analysis that two of the six nutrients behaved as expected when comparing the behavior of the nutrient concentration from a single analysis between growing seasons. From the other four nutrients we saw: Mg decreased when it should have increased, N and K increased when they should have decreased, and Zn greatly decreased when it should have remained roughly the same. Between the two petiole nutrient analyses, in contrast, three of the six nutrients behaved as expected. Both B and Zn saw large decreases when they should have remained the same. And N increased when it should have decreased, though this brought it into the expected

range of values. This means that looking at both cultivars, the petiole nutrient analysis performed slightly better than the leaf nutrient analysis between the two growing seasons in terms of consistency with expected nutrient levels (Wolf, 2008).

Table 12: Nutrient concentrations for Riesling from the veraison phenological stage: leaf nutrient analysis

Riesling - Veraison (Leaf Analysis)					
Nutrient	**Mean**	**Std Dev**	**Max**	**Min**	**n**
Boron (mg/kg)	45.38	6.09	59.19	2225.78	24
Magnesium (mg/kg)	3134.99	989.08	6887.98	21.70	24
Nitrogen (%)	2.39	0.20	2.82	2.00	24
Phosphorus (mg/kg)	2971.96	1021.01	7506.33	2.08	24
Potassium (mg/kg)	18803.83	14366.88	83568.40	2349.46	24
Zinc (mg/kg)	28.59	9.53	69.86	2.00	24

Table 13: Nutrient concentrations for Riesling from the veraison phenological stage: petiole nutrient analysis

Riesling - Veraison (Petiole Analysis)					
Nutrient	**Mean**	**Std Dev**	**Max**	**Min**	**n**
Boron (mg/kg)	38.53	2.33	43.82	33.95	24
Magnesium (mg/kg)	2768.35	416.68	3836.82	2018.82	24
Nitrogen (%)	0.84	0.10	1.03	0.68	24
Phosphorus (mg/kg)	4054.78	438.78	5086.15	3338.10	24
Potassium (mg/kg)	34011.35	2550.47	41000.85	28354.80	24
Zinc (mg/kg)	46.59	3.70	54.66	41.23	24

Romero *et al.* (2010) compared the nutrient analyses of the leaves and the petioles of vines and found that the petioles had higher concentrations of K, Mg and Zn than those for the leaves. For N and P, they found that the leaf level analysis resulted in higher values when compared to petiole level results. We found that K behaved as Romero et al. (2010) predicted, while for Cabernet Franc during veraison and for Riesling the results for Mg and Zn also lined up. Nitrogen also behaved as seen by Romero et al. (2010), but P did not. These differences are likely due to the fact that different cultivars were sampled in our study when compared to the Romero et al. (2010) effort. The different cultivars could require and have different nutrient concentrations. Romero *et al.* (2012), in a follow-up paper, also determined that leaf blades could be more appropriate for the analysis of N and K, while petiole analysis is more appropriate for B. For P and Mg, either approach worked for

collection of samples during bloom, but at veraison, a leaf nutrient analysis worked better. In examining our results, we found that they agreed with Romero et al. (2012) as far as K and P are concerned. Our results also agreed for B for the samples from Cabernet Franc, but were inconsistent for those collected from Riesling. Finally, comparing our data trends to those found by Christensen (1984), we find that our N values between the cultivars behaved as seen by that author, in being fairly consistent across cultivars. The other nutrients that we examined differed from Christensen (1984) findings. There are two primary reasons why our data may not match the results derived from these previous studies: The first is that though both papers examined a multitude of cultivars, none of them were either Riesling or Cabernet Franc; the other reason is that we took samples from an experimental farm; a variety of ground treatments had been applied to the different cultivars, meaning that the nutrient concentrations do not conform exactly to the expected starting values either in the papers or the wine grape production guide by Wolfe (2008). However, this induced variability arguably could contribute to more robust modeling across a range of nutrient levels.

We proceeded to further compare the nutrient analyses, since an examination of the mean values for the nutrient concentrations were complete. To this end we plotted the leaf vs. petiole analyses against each other to evaluate potential differences. If both analyses exhibited similar results or trends for each nutrient, we should see a linear relationship on the plot. In Figures 19-22 below are the results of the leaf vs. petiole nutrient data, plotted against each other, as well as a linear fit being based on the 'fitlm' command in MATLAB. Figures 19 and 20 are the results from the Cabernet Franc cultivar during bloom and veraison, respectively. In linear fit plots shown below the 95% confidence bounds are shown by the dotted line.

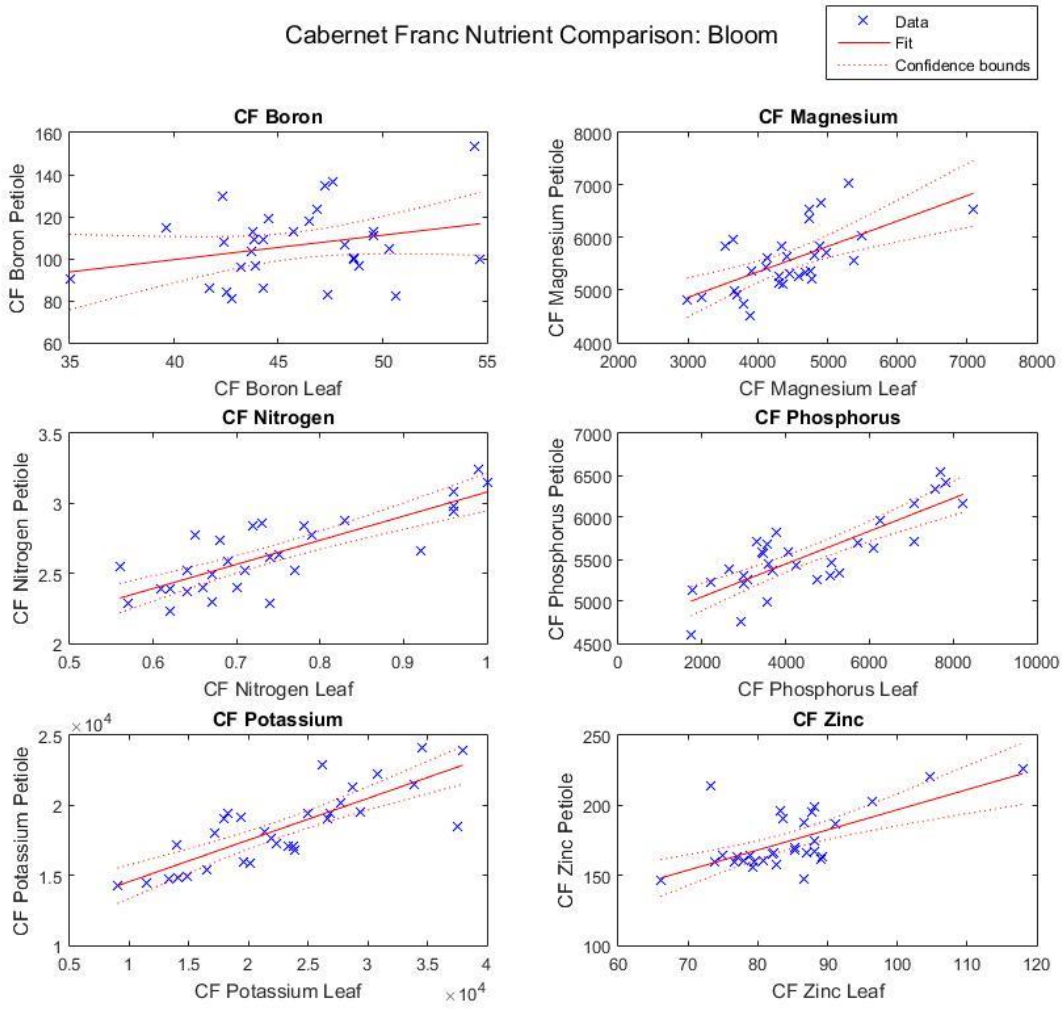

Figure 19: Plot of Cabernet Franc leaf nutrient analysis versus the petiole nutrient analysis (bloom phenological stage)

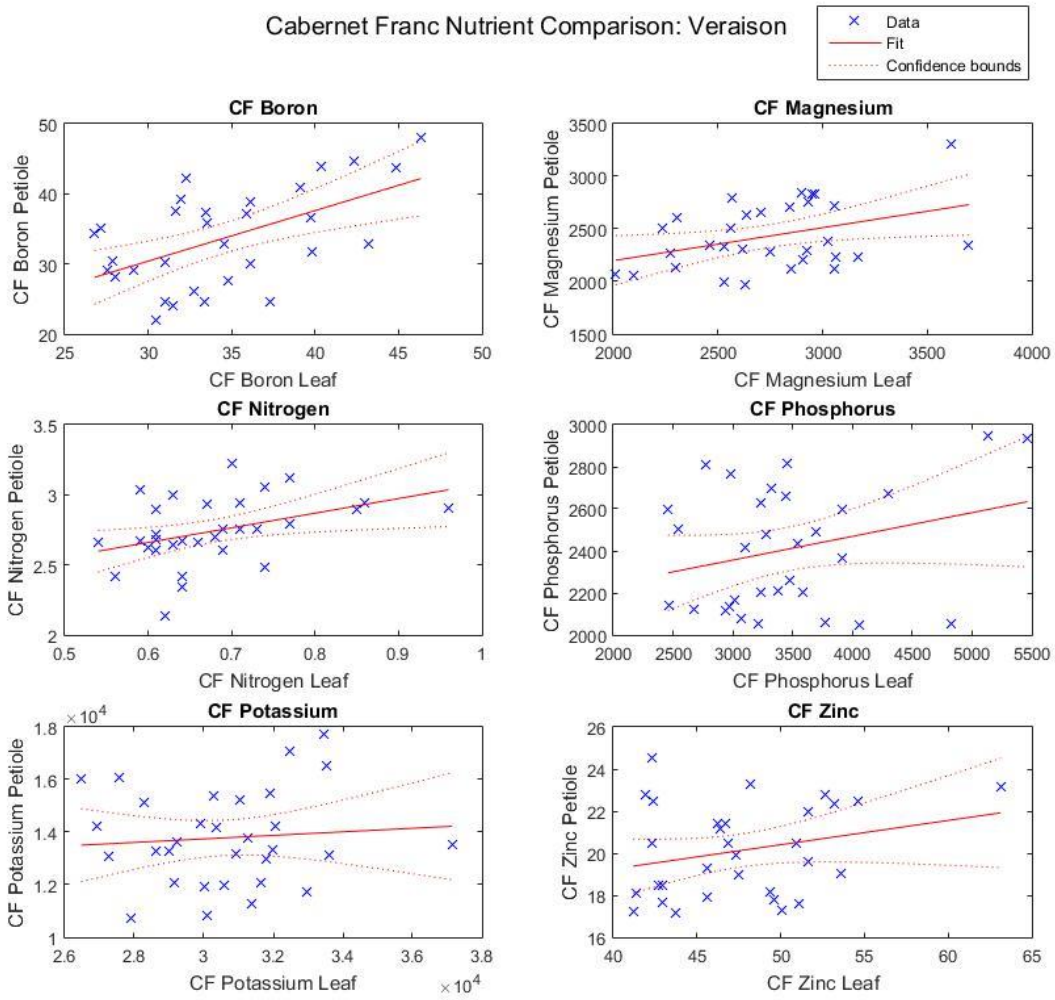

Figure 20: Plot of Cabernet Franc leaf nutrient analysis versus the petiole nutrient analysis (veraison phenological stage)

The R^2 and adjusted- R^2 values, as well as the root mean squared error (RMSE) of the calculations from the linear fits are provided in Table 14 below. We found that for N, P and K the two nutrient analyses during bloom agree with each other, at a 66% explained-variability level. Zinc and N were slightly lower, but B presented a concern: Only 8% of the variability between the leaf and petiole analyses was explained by the fitted linear relationship, which was a value considerably lower than expected.

Table 14: R^2 results from the linear fit comparison between the leaf and petiole nutrient analysis for Cabernet Franc during bloom and veraison

	Cabernet Franc - Bloom			Cabernet Franc - Veraison		
	R^2	**R^2 Adjusted**	**RMSE**	**R^2**	**R^2 Adjusted**	**RMSE**
Boron	0.08	0.04	17.05 (mg/kg)	0.31	0.28	5.91 (mg/kg)
Magnesium	0.39	0.37	479.51 (mg/kg)	0.01	0.12	295.09 (mg/kg)
Nitrogen	0.66	0.65	0.16 (%)	0.15	0.14	0.22 (%)
Phosphorus	0.67	0.66	262.11 (mg/kg)	0.17	0.05	282.06 (mg/kg)
Potassium	0.66	0.65	1630.42 (mg/kg)	0.08	-0.03	1836.39 (mg/kg)
Zinc	0.43	0.41	16.27 (mg/kg)	0.07	0.04	2.13 (mg/kg)

When examining the results of the linear fit between the two nutrient analyses from the veraison growing season, we found an increase in the agreement regarding the nutrient concentration of B between the two analyses (from 8 % up to 31%), while all other nutrients decreased dramatically. There appears to be no linear relationship between the two levels of nutrient analyses for Cabernet Franc during veraison. Figures 21 and 22 show the plotted linear fit between the leaf and petiole nutrient analyses obtained for the Riesling cultivar during bloom and veraison.

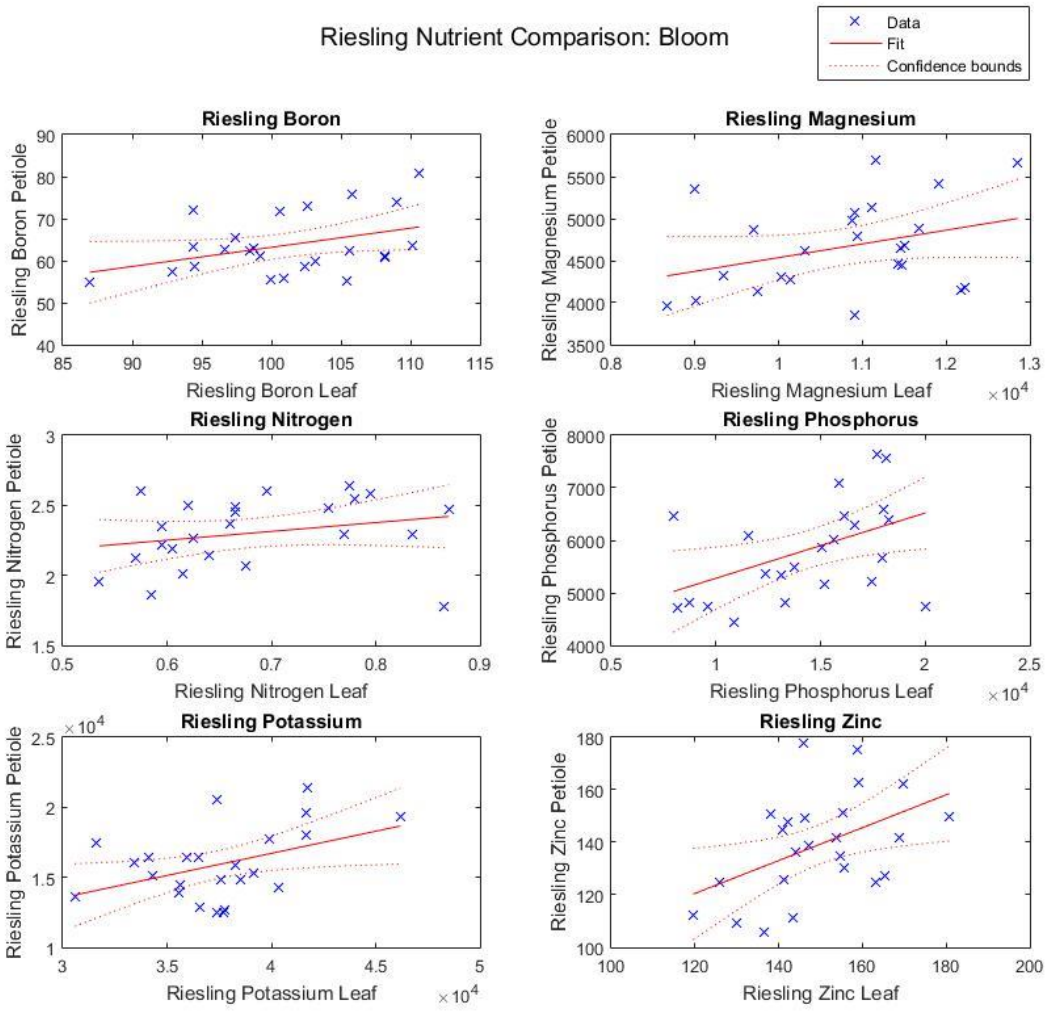

Figure 21: Plot of Riesling leaf nutrient analysis versus the petiole nutrient analysis (bloom phenological stage)

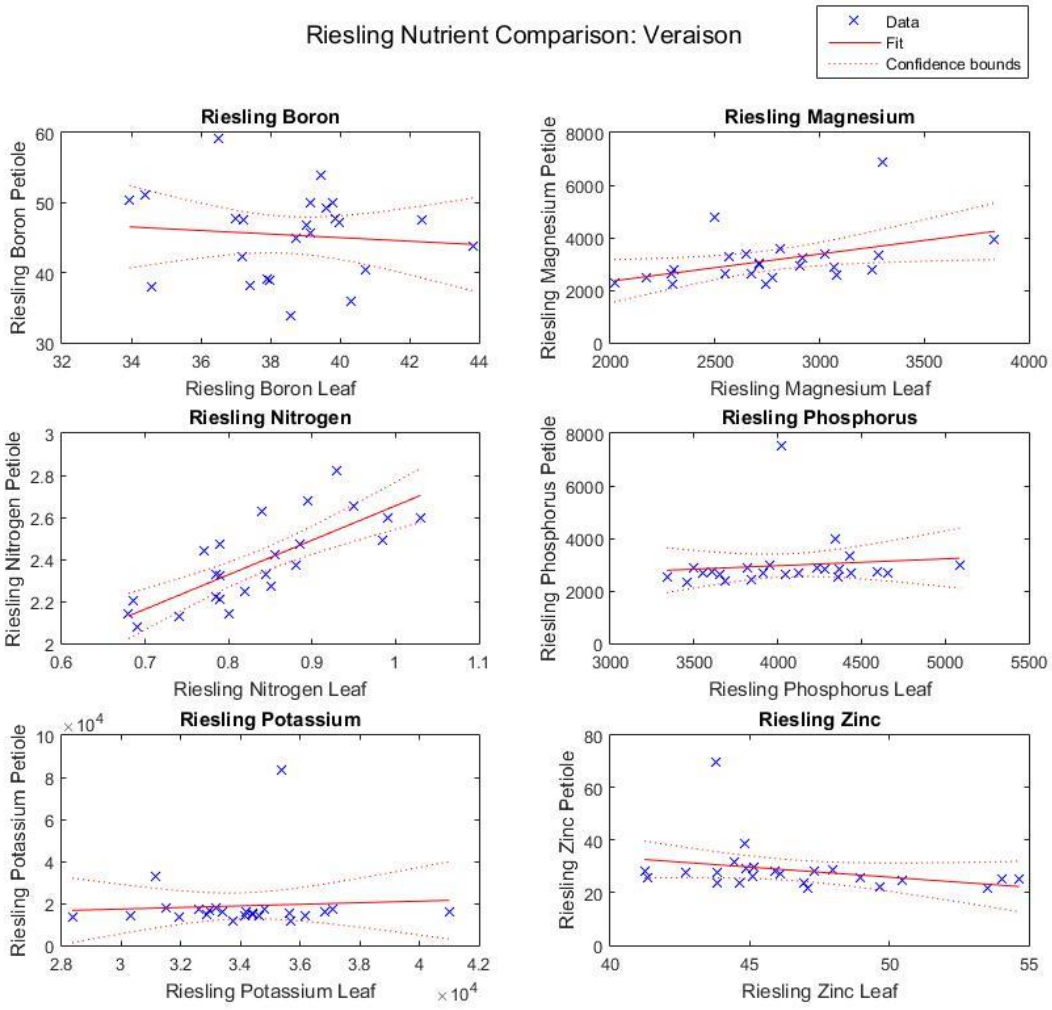

Figure 22: Plot of Riesling leaf nutrient analysis versus the petiole nutrient analysis (veraison phenological stage)

Based on the bloom results in Table 15 below, it was found that little linearity between the two nutrient analyses exist, with the peak value being only 22% (for Zn). During veraison, N achieved a linear fit that explains 60% of the data variability, but all other fits are significantly lower, at less than 10%.

Table 15: R^2 results from the linear fit comparison between the leaf and petiole nutrient analysis for Riesling during bloom and veraison

	Riesling - Bloom			Riesling - Veraison		
	R^2	**R^2 Adjusted**	**RMSE**	**R^2**	**R^2 Adjusted**	**RMSE**
Boron	0.15	0.11	6.74 (mg/kg)	0.01	-0.04	6.19 (mg/kg)
Magnesium	0.12	0.08	512.46 (mg/kg)	0.19	0.15	909.65 (mg/kg)
Nitrogen	0.06	0.02	0.24 (%)	0.60	0.58	0.13 (%)
Phosphorus	0.21	0.18	855.10 (mg/kg)	0.01	-0.03	1037.31 (mg/kg)
Potassium	0.19	0.15	2338.52 (mg/kg)	0.00	-0.04	1465.69 (mg/kg)
Zinc	0.22	0.18	17.76 (mg/kg)	0.09	0.05	9.30 (mg/kg)

There therefore seems to be little in the way of agreement between the two nutrient analyses over the two cultivars and growing seasons. Owing to this fact, the reflectance data analysis will proceed using only one of the nutrient analyses. The petiole analysis had better performance between the growing seasons as far as matching the expected behavior of the nutrient concentrations is concerned. It is also the industry standard, which would allow easier comparison of our data to other studies' results. The petiole nutrient analysis therefore was selected to constitute the nutrient data, which we next will attempt to model using the reflectance spectra collected. The obvious drawback to our approach is that our spectral measurements were collected at the leaf-, or upscaled leaf, i.e., canopy levels. One could thus argue that a reflectance-to-nutrient comparison at the leaf level should constitute a better match. However, with this caveat in mind, we still deemed it more appropriate to relate our remote sensing samples to petiole analyses, based on the reasons provided earlier.

5.2 Modeling results - 1nm data

The first set of reflectance data analyzed had a spectral resolution of 1nm. For both the 1nm data analysis and the 10nm data analysis, a threshold for the correlation coefficient needed to be

established in order to limit the number of variables. This cut-off level, as stated earlier, was set at CC ≥ 0.70. This implies that only if a correlation coefficient produced a value of 0.70 or higher, was it considered highly correlated. Taylor (1990) stated in their paper discussing the interpretation of the correlation coefficient that a strong or high correlation is an R^2 value between 0.68 and 1.0, with those over 0.90 implying high correlations. Calkins (2005) argued that an R value between 0.70-0.90 could be deemed highly correlated. We set our threshold level at R ≥ 0.70, i.e., indicating a high level of correlation, based on these studies.

5.2.1 Index results

Using the threshold described above, the correlation coefficient results that were achieved using the normalized difference index, when run against the bloom nutrient data, are shown below in Table 16. Gil-Perez et al. (2010) used narrow-band hyperspectral imagery to evaluate the nutrient content in vineyards. Similar to this study, the authors used 1nm spectral resolution data for the analysis. Four of the nutrients examined in their paper lined up with this investigation: N, P, K, and Mg. Using narrow-band indices they achieved correlation values between 0.50-0.69. Our results (Tables 16 and 18) therefore were comparable or better in a number of cases then the correlation values achieved by Gil-Perez *et al* (2010).

We furthermore saw that, when examining the results from Cabernet Franc, two separate nutrient-view angle combinations performed at or above our threshold level. These results were spread between both canopy view-angles, with a maximum CC value of 0.72 being achieved by both B and P. Examining the correlations obtained from Riesling, we see that for the petiole analysis seven different nutrient-view angle combinations were highly correlated. While the high correlations were observed across all three view-angles, concentration was in the leaf-view results. The correlations were spread across five of the nutrients, with two nutrients performing well in more than one view-angle. The highest CC achieved from Riesling data was a CC=0.82, for N. However, between the two cultivars there were no nutrient-view angle combinations that had a high correlation in both cultivars. For the one nutrient, B, that achieved a high correlation in both cultivars, they each had a different view-angle for which this occurred (the CC values was within 0.01 of each other).

Table 16: Correlation coefficient results for Cabernet Franc and Riesling from the bloom phenological stage for the normalized difference index

Bloom Data, 1nm Bands NDI Index				
Correlation Coefficient				
	Field:	Cabernet Franc		
	View:	Leaf	Canopy NADIR	Canopy 15 Deg
Petiole Nutrient Analysis	Boron	0.57	**0.72**	0.58
	Potassium	0.58	0.55	0.61
	Magnesium	0.66	0.55	0.67
	Nitrogen	0.64	0.61	0.50
	Phosphorus	0.65	0.65	**0.72**
	Zinc	0.64	0.68	0.58

Bloom Data, 1nm Bands NDI Index				
Correlation Coefficient				
	Field:	Riesling		
	View:	Leaf	Canopy NADIR	Canopy 15 Deg
Petiole Nutrient Analysis	Boron	**0.71**	0.69	0.57
	Potassium	**0.74**	**0.71**	0.62
	Magnesium	**0.81**	0.57	0.67
	Nitrogen	**0.82**	0.66	**0.71**
	Phosphorus	0.62	0.64	0.66
	Zinc	**0.71**	0.62	0.60

Table 17 shows the CC results achieved using the ratio index (RI) instead of the NDI approach. We found that all the results were the same to two decimal places via a comparison of the two tables. This pattern of matching results continued for all cultivar and growing season combinations. Instead of showing duplicate results, the ratio index results will not be shown for the remainder of the 1nm index analysis. It should also be noted that none of the follow-on analyses, such as the step-wise linear regression of the index results, was done using the ratio index.

Table 17: Correlation coefficient results for Cabernet Franc and Riesling from the bloom phenological stage for the ratio index

Bloom Data, 1nm Bands Ratio Index				
Correlation Coefficient				
	Field:	Cabernet Franc		
	View:	Leaf	Canopy NADIR	Canopy 15 Deg
Petiole Nutrient Analysis	Boron	0.57	**0.72**	0.58
	Potassium	0.59	0.55	0.61
	Magnesium	0.66	0.55	0.67
	Nitrogen	0.65	0.62	0.50
	Phosphorus	0.65	0.66	**0.72**
	Zinc	0.64	0.68	0.59

Bloom Data, 1nm Bands Ratio Index				
Correlation Coefficient				
	Field:	Riesling		
	View:	Leaf	Canopy NADIR	Canopy 15 Deg
Petiole Nutrient Analysis	Boron	**0.71**	0.69	0.57
	Potassium	**0.74**	**0.71**	0.62
	Magnesium	**0.81**	0.57	0.67
	Nitrogen	**0.82**	0.66	**0.71**
	Phosphorus	0.62	0.64	0.66
	Zinc	**0.71**	0.62	0.61

Table 18 below shows the CC results achieved from the NDI during the veraison collect; it is worth noting that the nutrient-view angle combinations that perform satisfactorily have shifted. In the case of the Cabernet Franc data, we observed that only B correlated highly, approximately at the threshold of CC=0.70, and only for a single view angle (leaf-view). Between the two growing seasons, B remained the only nutrient that had a high correlation between the spectral reflectance and the nutrient concentrations found in the petiole of the plant. While B remained consistent, the

view-angle that achieved this high correlation shifted from the canopy, viewed at nadir during bloom, to the leaf level view.

However, for the Riesling results we noted a marked increase in high correlations: Mg, N, and P had high correlations for all three view angles and Zn correlated highly at the leaf view-angle. The maximum correlation value achieved was CC=0.80. Though there is a slight decrease in maximum correlation from the bloom value of CC=0.82, the number of nutrient-view angle combinations that achieved a correlation value above the CC≥0.70 threshold increased from seven to ten. Finally, it is clear that for both the bloom and veraison results (Tables 16 and 18), the correlations achieved from our NDI method produced correlation values superior to the values produced by the GM, VOG, or GLI indices that we tested earlier.

Table 18: Correlation coefficient results for Cabernet Franc and Riesling from the veraison phenological stage for the normalized difference index

Veraison Data, 1nm Bands NDI Index				
Correlation Coefficient				
	Field:	Cabernet Franc		
	View:	Leaf	Canopy NADIR	Canopy 15 Deg
Petiole Nutrient Analysis	Boron	**0.70**	0.63	0.69
	Potassium	0.58	0.64	0.66
	Magnesium	0.55	0.53	0.54
	Nitrogen	0.62	0.46	0.67
	Phosphorus	0.50	0.51	0.55
	Zinc	0.52	0.58	0.50

Veraison Data, 1nm Bands NDI Index				
Correlation Coefficient				
	Field:	Riesling		
	View:	Leaf	Canopy NADIR	Canopy 15 Deg
Petiole Nutrient Analysis	Boron	0.54	0.67	0.60
	Potassium	0.50	0.59	0.52
	Magnesium	**0.75**	**0.73**	**0.71**
	Nitrogen	**0.77**	**0.80**	**0.78**
	Phosphorus	**0.70**	**0.78**	**0.76**
	Zinc	**0.71**	0.68	0.68

When one compares the similar nutrient-view angle combinations between nutrient analyses, there are four in common: Mg and Zn viewed at the leaf level, as well as N compared against both the leaf and canopy 15^{o} off-nadir results. Following the previous trend in the maximum correlation value, there was a general decrease in the correlation result for three of the four consistently high combinations by between 0.05-0.07. The correlation results achieved by Zn, when viewed at the leaf level, remained constant between the two growing seasons.

The fact that there were combinations that performed well in both growing seasons, led us to believe that it could be feasible to identify wavelengths that will work for both growth seasons in terms of producing high correlation values. Next we further analyzed the wavelengths that produced the high correlation coefficients.

5.2.2 Analysis of correlation coefficient heat maps

We plotted "heat maps" of the correlations from the determination of the peak CCs in order to evaluate how well the various wavelength combinations performed. For each of the heat maps, the brighter the yellow, the higher the correlation coefficient produced and the darker the blue, the lower the corresponding correlation value. Note that only the nutrient-view angle combinations that produced a CC value at or above cutoff level are shown below.

5.2.2.1 Cabernet Franc Heat Maps

The heat map results from the Cabernet Franc cultivar during both seasons are discussed next. We concluded that, based on the bloom data, there were two nutrient-view angle combinations that produced high correlation coefficients. The heat map from B viewed at canopy nadir (Figure 23) shows that the peak values were generated from row 501; column 522, which corresponds to wavelengths 900nm and 921nm, respectively. Besides the peak values, high areas of correlation were produced by a combination of two NIR bands, as well as areas created by combining two visible wavelengths.

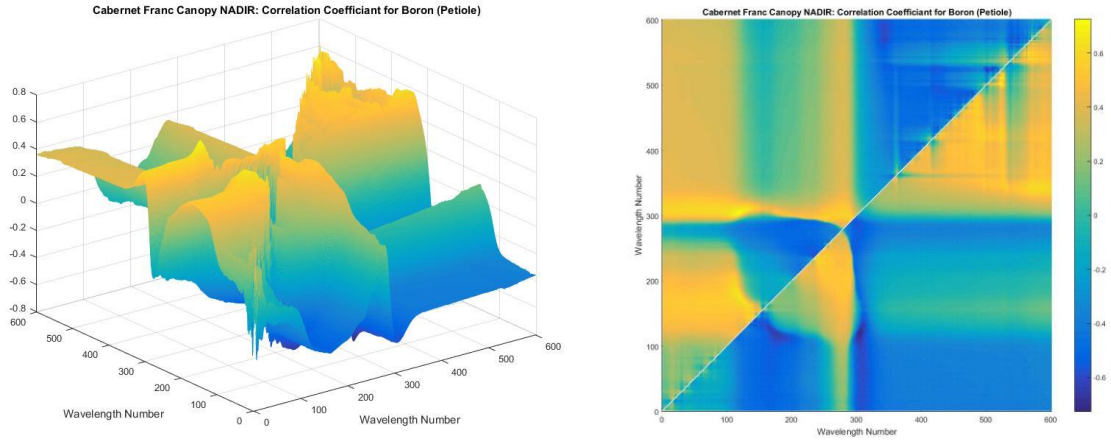

Figure 23: The boron wavelength correlation coefficients for Cabernet Franc bloom phenological stage at the canopy nadir view angle: (a) 3-D view, (b) 2-D view

Figure 24, on the other hand, shows that P exhibited a low average correlation. It has a relatively small peak area, formed by combining blue and green wavelengths. Peak CC values were from row 63; column 54, or wavelengths 462nm and 453nm, respectively.

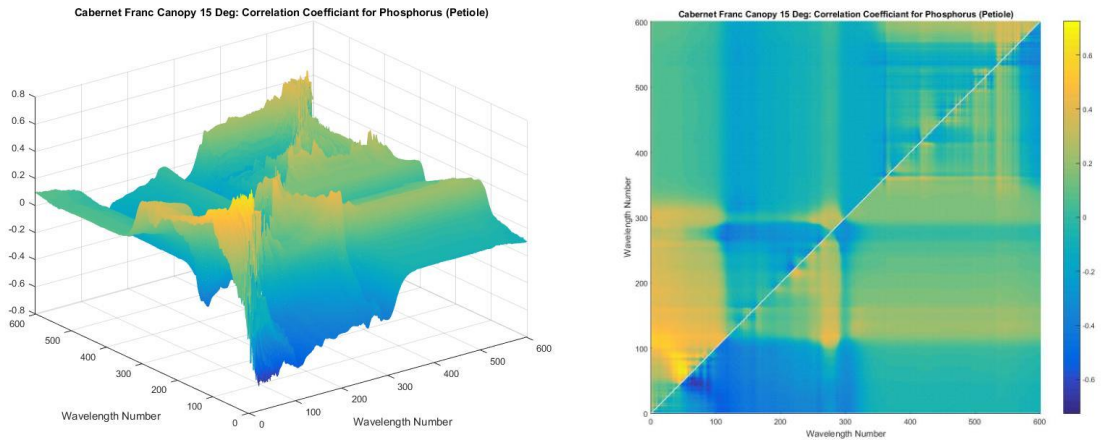

Figure 24: The phosphorus wavelength correlation coefficients for Cabernet Franc bloom phenological stage at the canopy 15° off-nadir view angle: (a) 3-D view, (b) 2-D view

For Cabernet Franc during veraison there was only a single nutrient-view angle combination that produced high CCs, with B at leaf view. The heat map in Figure 25 has a small peak value made from a combination of blue bands (row 70; column 75), or wavelengths 469nm and 474nm. Apart from these wavelengths, there is another region of fairly high correlation created by combining two NIR bands. The wavelengths creating the peak value here differ greatly from what was found in bloom, which was a combination of wavelengths around 900nm - for veraison we see that the peak value was formed by two blue wavelengths.

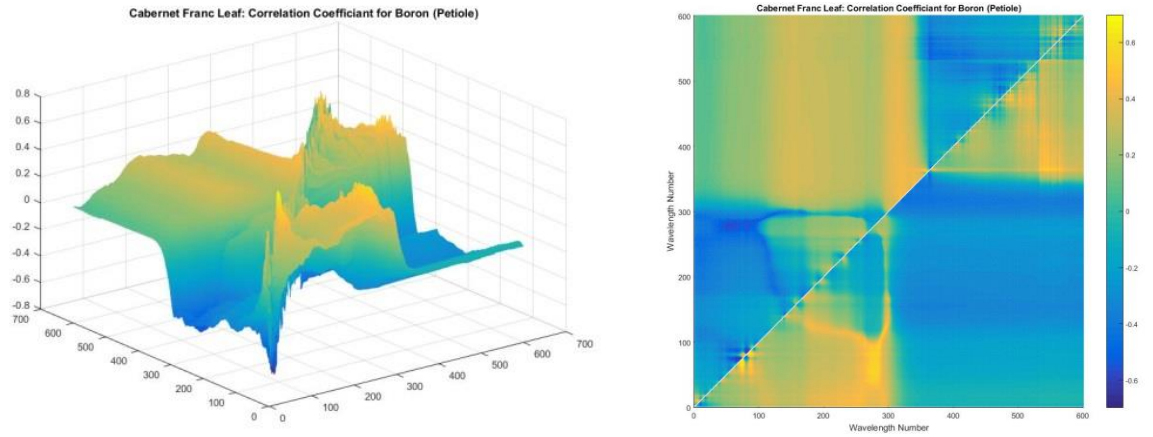

Figure 25: The boron wavelength correlation coefficients for Cabernet Franc veraison phenological stage at the leaf view angle: (a) 3-D view, (b) 2-D view

5.2.2.1 Riesling Heat Maps

The heat maps produced from the Riesling cultivar are displayed below. The bloom collection resulted in seven nutrient-view angle combinations above the threshold (CC≥0.70). These were spread over five of the six nutrients and all three view-angles. The heat map for the leaf-view of B

shows that, both the cutoff criteria was barely met and that only a very small number of wavelengths combined to do this. Row 523 (922nm) and column 508 (907nm) form the peak correlation value.

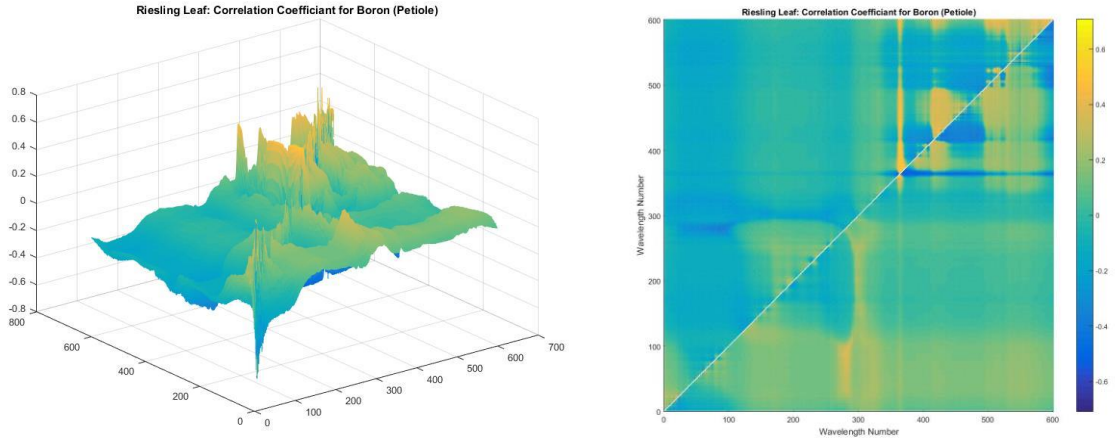

Figure 26: The boron wavelength correlation coefficients for Riesling bloom phenological stage at the leaf view angle: (a) 3-D view, (b) 2-D view

Magnesium viewed at leaf level had a greater number of high correlations, formed predominantly from visible bands. The peak was from row 243; column 295, corresponding to wavelengths 642nm and 694nm, respectively.

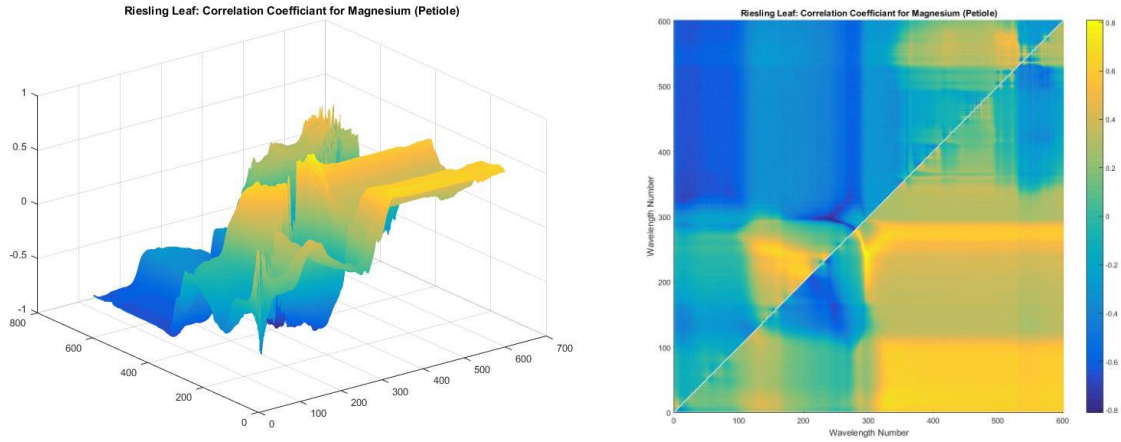

Figure 27: The magnesium wavelength correlation coefficients for Riesling bloom phenological stage at the leaf view angle: (a) 3-D view, (b) 2-D view

Nitrogen at the leaf level exhibited few high correlations, with the peak values from row 24; column 20, corresponding to wavelengths 423nm and 419nm, respectively. This peak is in the same region as we see for N when viewed at canopy 15^{o} off-nadir (Figure 29). In that case it was row 53; column

55, corresponding to wavelengths 452nm and 454nm, respectively; all of these wavelengths were located in the blue wavelength region.

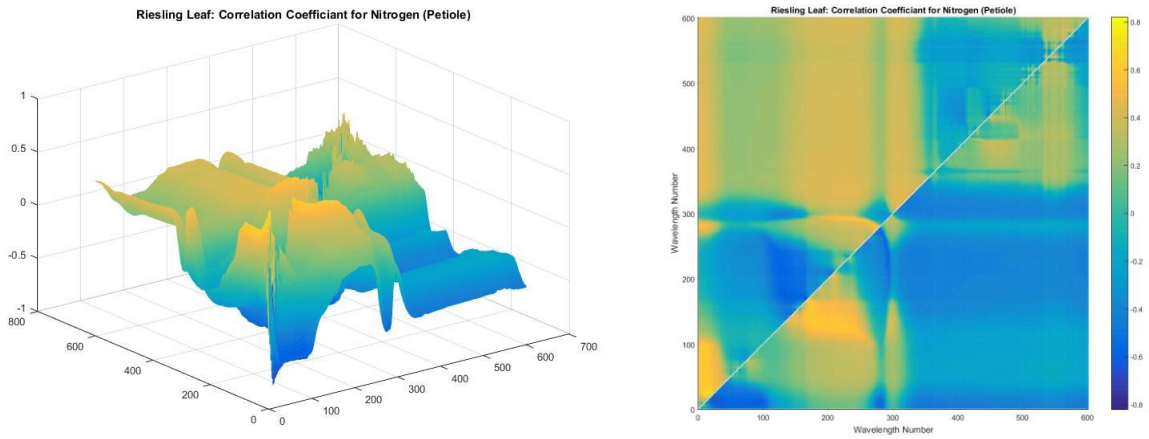

Figure 28: The nitrogen wavelength correlation coefficients for Riesling bloom phenological stage at the leaf view angle: (a) 3-D view, (b) 2-D view

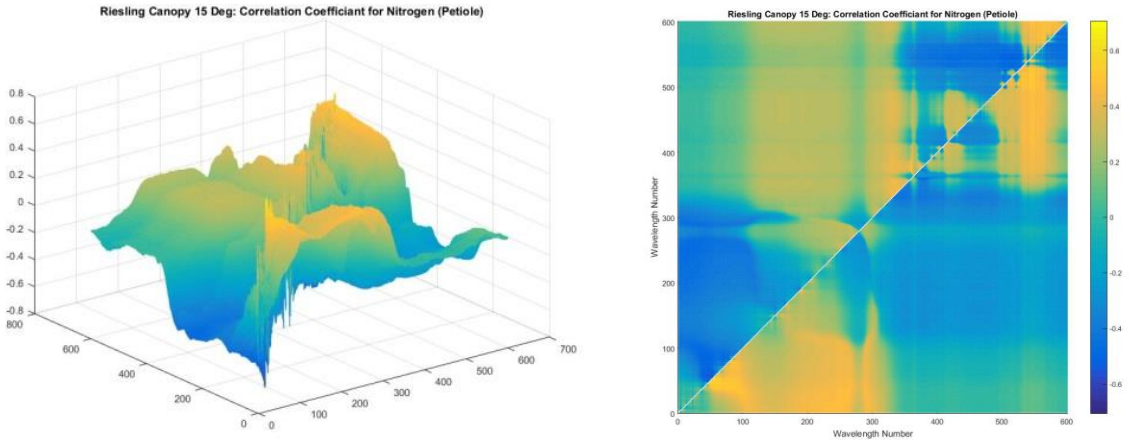

Figure 29: The nitrogen wavelength correlation coefficients for Riesling bloom phenological stage at the canopy 15^{o} off-nadir view angle: (a) 3-D view, (b) 2-D view

For K viewed at leaf level we see strong responses when two visible bands are combined and when two NIR bands are combined. The peak values were generated from row 579 (987nm); column 574 (973nm). Viewed at canopy nadir, the results for K shifted from two NIR bands which interacted well, to a combination of NIR and visible region bands. Also the peak value shifts from being produced by NIR bands to being created by two blue bands: row 64 (463nm); column 65 (464nm).

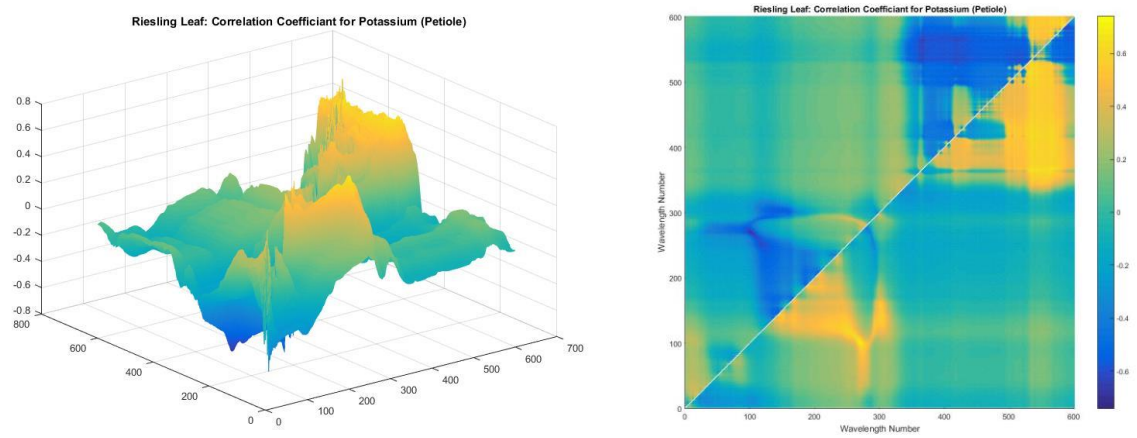

Figure 30: The potassium wavelength correlation coefficients for Riesling bloom phenological stage at the leaf view angle: (a) 3-D view, (b) 2-D view

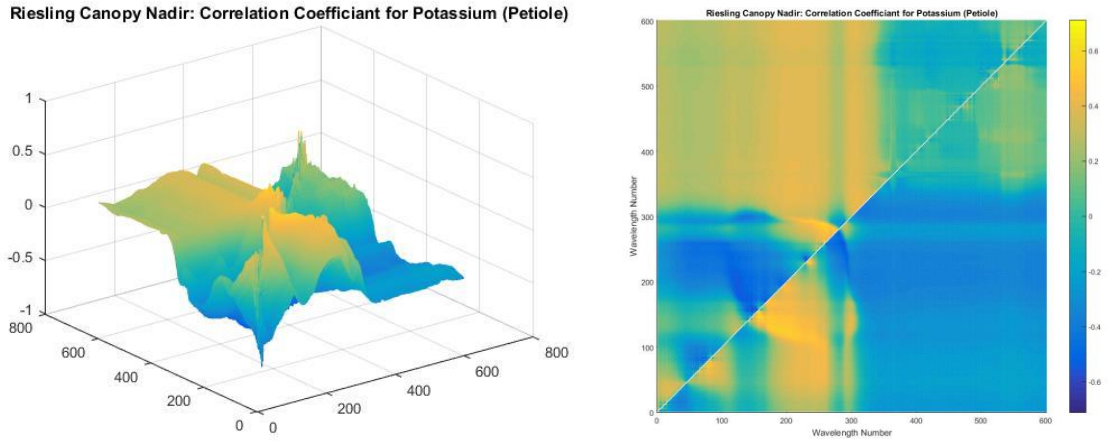

Figure 31: The potassium wavelength correlation coefficients for Riesling bloom phenological stage at the canopy nadir view angle: (a) 3-D view, (b) 2-D view

The final nutrient-view angle combination with high correlation for Riesling during bloom is for Zn, viewed at leaf level. There is one small peak in the visible-visible range, but the main area of high correlation, as well as the peak (row 475, column 477, corresponding to wavelengths 874 nm and 876 nm, respectively), fall in the NIR region.

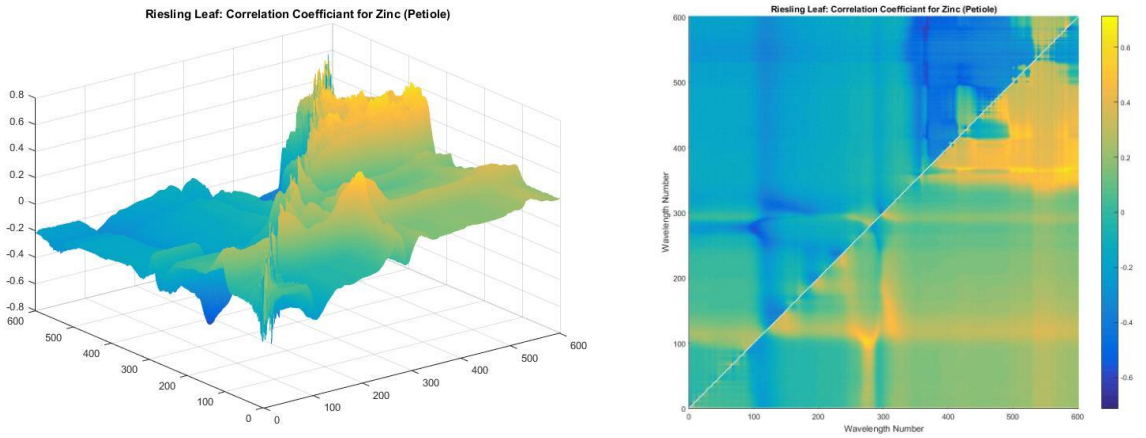

Figure 32: The zinc wavelength correlation coefficients for Riesling bloom phenological stage at the leaf view angle: (a) 3-D view, (b) 2-D view

Based on the veraison data, there were 10 nutrient-view angle combinations that met the threshold criterion. The first is Mg when viewed at leaf level - the peak is formed by row 449 and column 453, corresponding to wavelengths 848nm and 852nm, respectively. There is a small hotspot area, formed by other NIR bands that were also highly correlated.

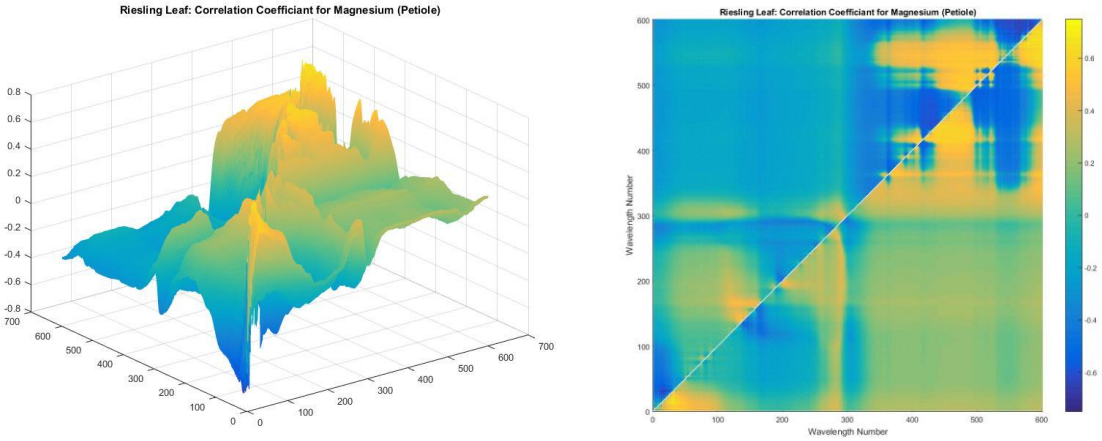

Figure 33: The magnesium wavelength correlation coefficients for Riesling veraison phenological stage at the leaf view angle: (a) 3-D view, (b) 2-D view

In comparison to the leaf view, the nadir-view for Mg has a peak CC value that was formed by two blue bands, row 76 (475nm) and column 68 (467nm). It also had larger regions of high correlation, formed by other visible bands and a combination of a visible and NIR band.

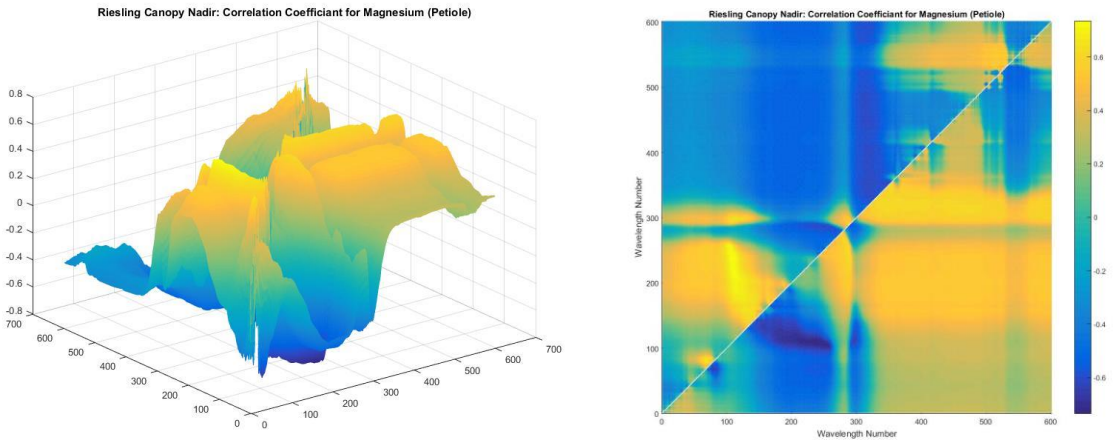

Figure 34: The magnesium wavelength correlation coefficients for Riesling veraison phenological stage at the canopy nadir view angle: (a) 3-D view, (b) 2-D view

Magnesium at the canopy 15º off-nadir view-angle has an isolated peak, formed by two NIR wavelengths; row 429 (828nm) and column 425 (824nm). Besides this peak, the main area of correlation was formed by two wavelengths, one around 600nm and the other from either the blue or green regions of the spectra.

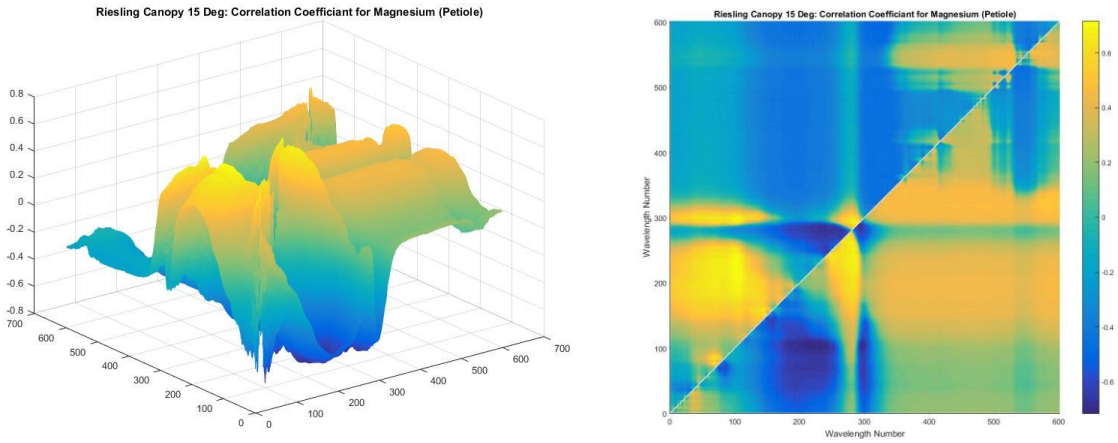

Figure 35: The magnesium wavelength correlation coefficients for Riesling veraison phenological stage at the canopy 15º off-nadir view angle: (a) 3-D view, (b) 2-D view

When evaluating the three view-angles for N from Riesling during veraison, we observe that they all exhibited similar patterns. There was a high correlation area formed by two wavelengths, one around 600nm and the other from either the blue or green regions of the spectra, and another region formed by a 600nm band and a NIR band. For the leaf view, the peak correlation value was located at row 21 (420nm) and column 4 (403nm).

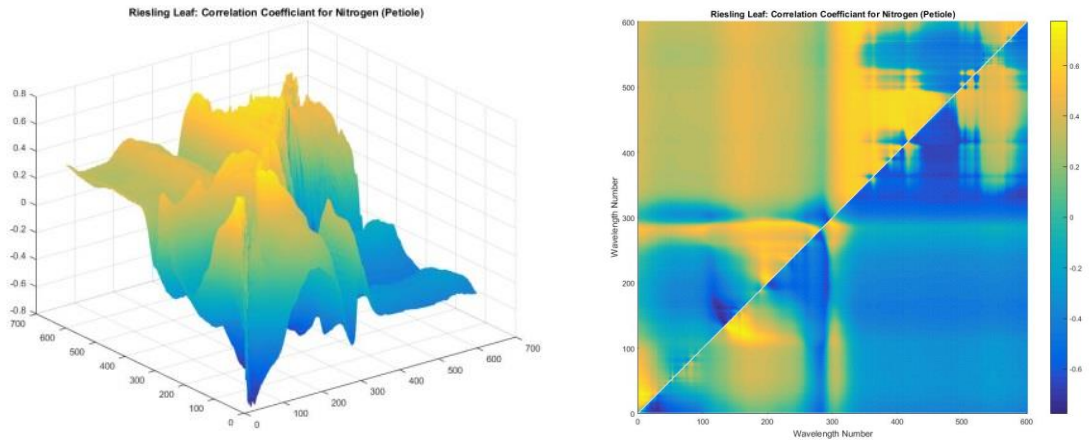

Figure 36: The nitrogen wavelength correlation coefficients for Riesling veraison phenological stage at the leaf view angle: (a) 3-D view, (b) 2-D view

For the nadir view-angle the peak correlation was also in the blue region, at row 76 and column 68, corresponding to wavelengths 475nm and 467nm, respectively. Despite a similar shape as the one found for the nadir view-angle heat map, the peak region for the 15^{o} off-nadir view angle was created by a combination of row 429 (828nm) and column 425 (824nm).

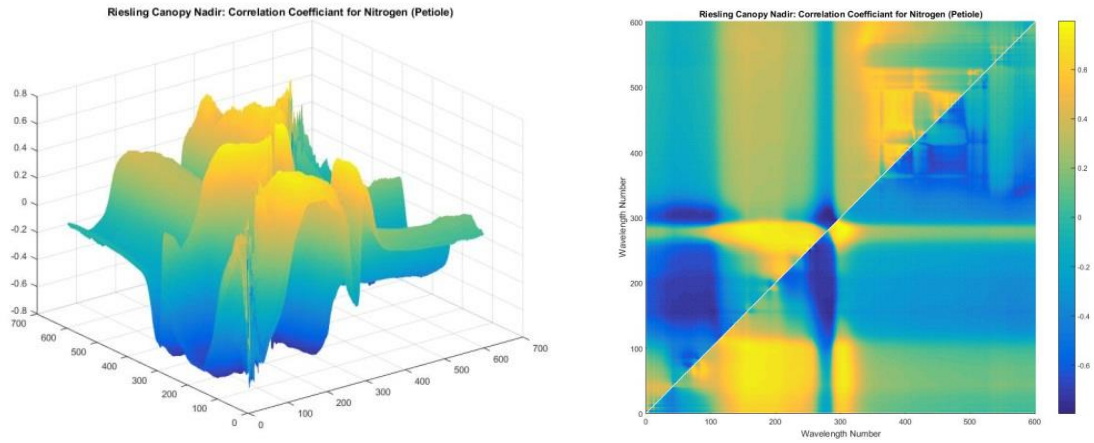

Figure 37: The nitrogen wavelength correlation coefficients for Riesling veraison phenological stage at the canopy nadir view angle: (a) 3-D view, (b) 2-D view

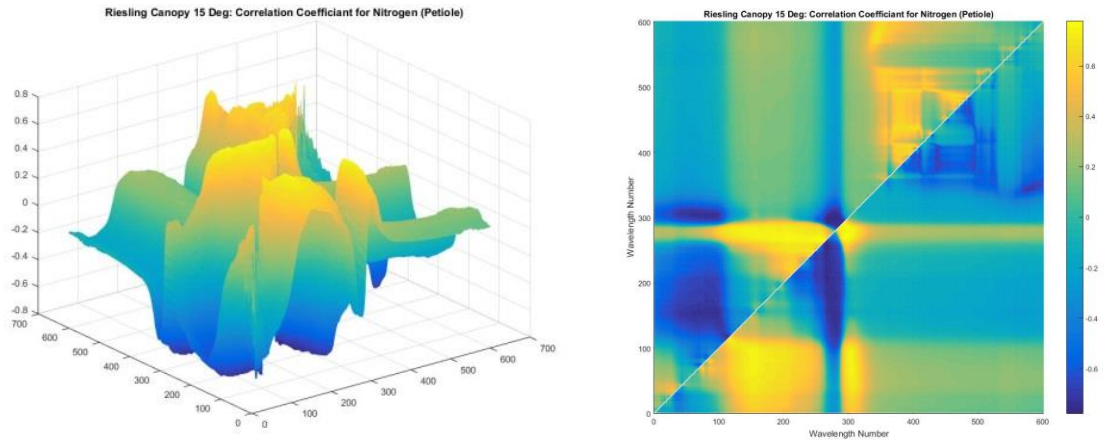

Figure 38: The nitrogen wavelength correlation coefficients for Riesling veraison phenological stage at the canopy 15^{o} off-nadir view angle: (a) 3-D view, (b) 2-D view

The leaf-view for P during veraison exhibited a peak CC value at row 547 and column 535, corresponding to wavelengths 946nm and 934nm, respectively. This is an isolated peak, but there are other areas of high correlation that formed via a combination of bands in the 800nm range and again by combining a red and a green band.

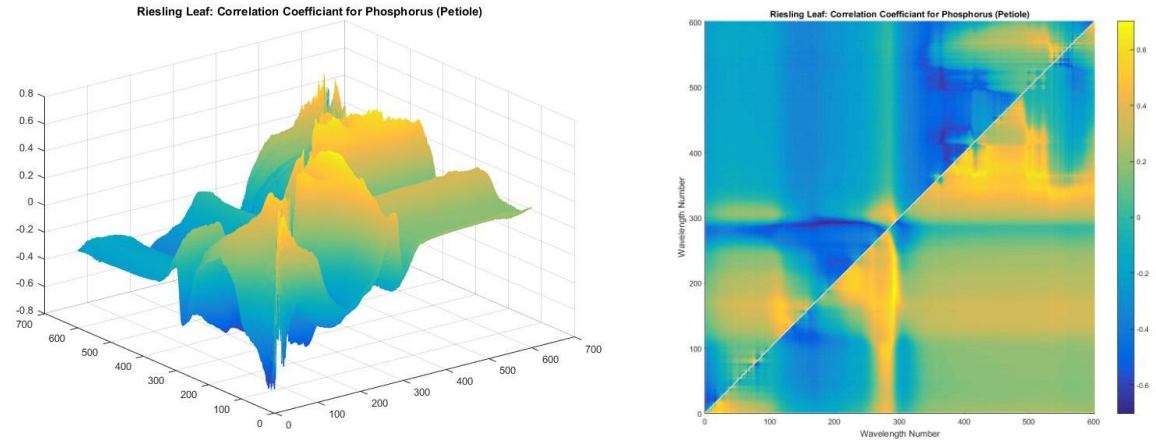

Figure 39: The phosphorus wavelength correlation coefficients for Riesling veraison phenological stage at the leaf view angle: (a) 3-D view, (b) 2-D view

For the nadir-view the peak CC value was located at row 365 (764nm) and column 417 (816nm). Despite the peak being formed by two NIR bands, the largest area of high correlation was created through a combination of bands between the blue and green regions.

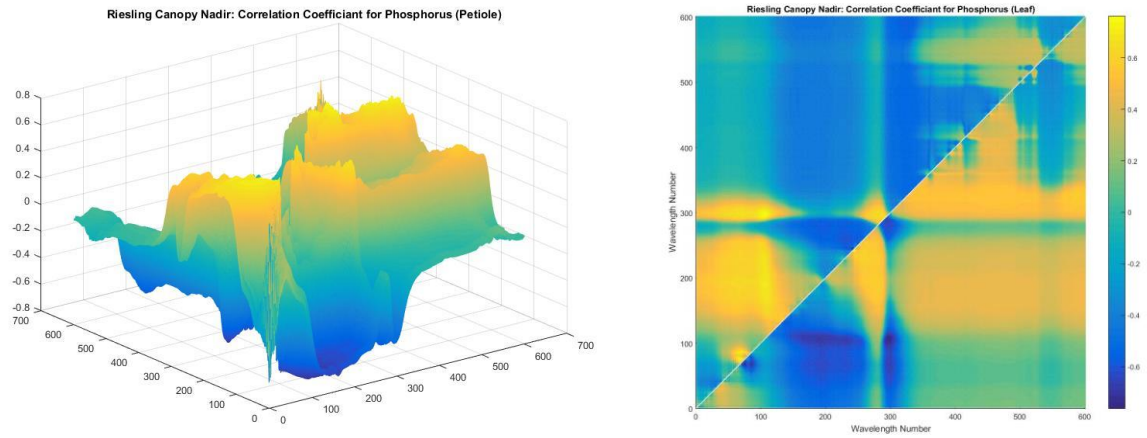

Figure 40: The phosphorus wavelength correlation coefficients for Riesling veraison phenological stage at the canopy nadir view angle: (a) 3-D view, (b) 2-D view

Figure 41, in turn, shows that for the canopy 15^{o} off-nadir view angle the peak value was located at row 429 (828nm) and column 425 (824nm). As was the case for the nadir-view, there was a region of high correlation through a combination of visible bands, but in this case the correlation was driven by two bands around 500nm, a little lower in the spectrum then for the nadir-view. Unlike the nadir-view, there were some additional regions in the NIR/NIR region with high correlation values.

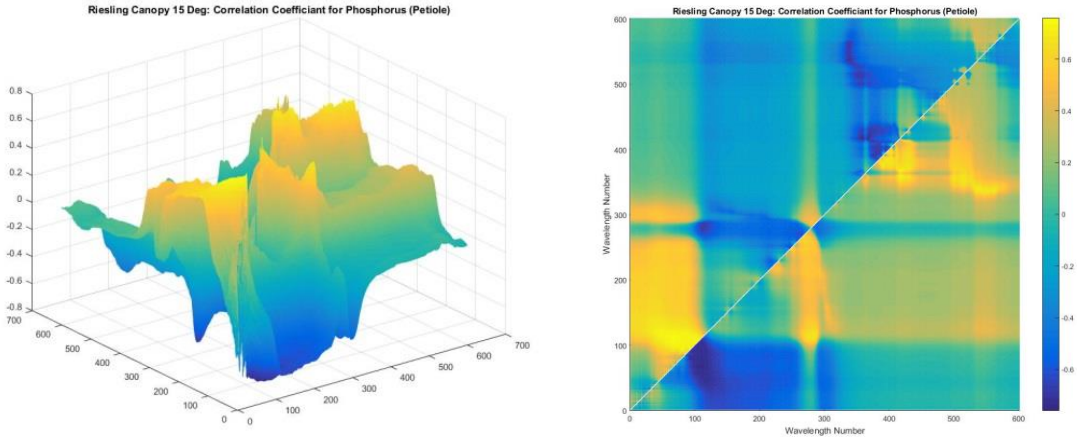

Figure 41: The phosphorus wavelength correlation coefficients for Riesling veraison phenological stage at the canopy 15^{o} off-nadir view angle: (a) 3-D view, (b) 2-D view

For Zn we found that the highest correlations tended to be created by a combination of two NIR bands (Figure 42). The peak CC value was at row 477 column 472, corresponding to wavelengths 876nm and 871nm, respectively. There was also a heat map region of high correlation, based on similar bands in the red wavelengths.

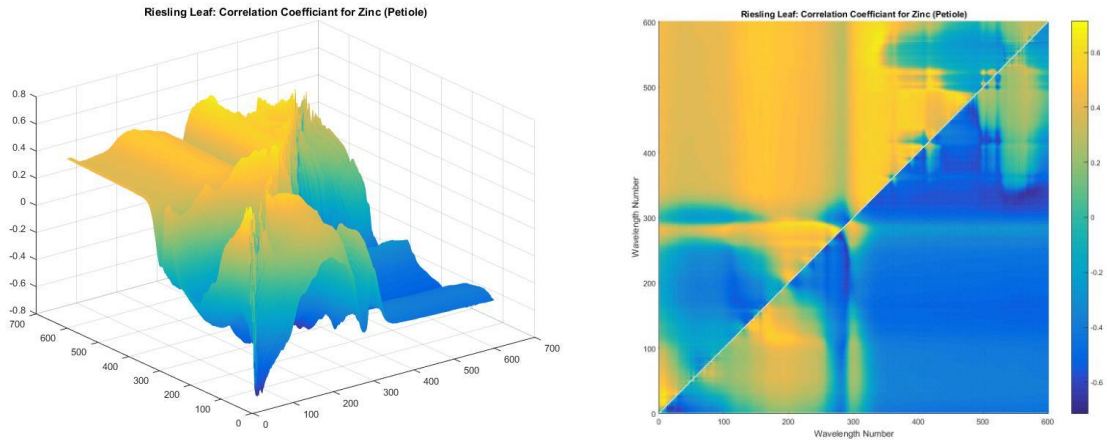

Figure 42: The zinc wavelength correlation coefficients for Riesling veraison phenological stage at the leaf view angle: (a) 3-D view, (b) 2-D view

We identified a number of evident trends based on the examination and comparison of individual nutrient heat maps. The peak values for B during bloom came from wavelengths in the 900nm range. For N, four of the five heat maps had peak values constituted by two wavelengths in the 400nm range. And finally, for both heat maps from Zn, the peak values in each came from wavelengths in the mid 800nm area. However, no pattern was evident for the other three nutrients.

5.2.3 R^2 Analysis

The number of potential independent variables was too great to get convergence in most linear selection routines and compute a viable solution for all cases, which resulted in an approach whereby the R^2 values were only computed for the nutrient-view angle combinations that produced CC≥0.70. Even then it was necessary to limit the wavelengths, as described in the methods section. We calculated the coefficient of determination for each nutrient-view angle pair that produced a high CC, using the combined highly correlated wavelengths from their respective cultivars and growing seasons. The results from this are seen in tables below. The R^2 values calculated using the top bands, i.e., those bands correlated at $p < 0.05$, have also been included in the tables.

For Cabernet Franc during bloom we know that only two nutrient-view angle combinations had values above the CC=0.70 threshold. The number of indices that generated CC values above this threshold is shown in Table 19 below.

Table 19: Number of highly correlated indices produced using the normalized difference index for Cabernet Franc from the bloom phenological stage

Bloom Data, 1nm Bands NDI Index				
Number of Highly Correlated Indices				
	Field:	Cabernet Franc		
	View:	Leaf	Canopy NADIR	Canopy 15 Deg
		# of indices	# of indices	# of indices
Petiole Nutrient Analysis	Boron		35	
	Potassium			
	Magnesium			
	Nitrogen			
	Phosphorus			2
	Zinc			

In the case of B, 35 separate indices had a CC value of 0.70 or greater. These 35 indices were then used as the input variables for the linear fit that was run against the B nutrient data to generate the R^2 results seen in Table 20 below. The same goes for the two indices that correlated highly for Zn.

Table 20: R^2 results using the normalized difference index for Cabernet Franc from the bloom phenological stage

Bloom Data, 1nm Bands NDI Index													
R^2													
	Field:	Cabernet Franc											
	View:	Leaf				Canopy NADIR				Canopy 15 Deg			
		R^2 Ordinary	R^2 Adjusted	RMSE	Top Bands	R^2 Ordinary	R^2 Adjusted	RMSE	Top Bands	R^2 Ordinary	R^2 Adjusted	RMSE	Top Bands
Petiole Nutrient Analysis	Boron				0.00	0.51	0.49	2.95	0.36				0.00
	Potassium				0.04				0.00				0.00
	Magnesium				0.00				0.00				0.00
	Nitrogen				0.00				0.10				0.00
	Phosphorus				0.02				0.02	0.53	0.51	1335.53 (mg/kg)	0.02
	Zinc				0.01				0.02				0.01

As we can see from Table 20, the highest R^2 value achieved by our data from Cabernet Franc (bloom) was able to explain 53% of the variation in the nutrient data. The inclusion of correlated bands at $p < 0.05$ resulted in no models being generated at any view angle.

Moving onto Riesling, there were seven nutrient-view angle combinations reaching the CC threshold. The number of indices that did this for each combination varied from a single index to 322 different indices.

Table 21: Number of highly correlated indices produced using the normalized difference index for Riesling from the bloom phenological stage

Bloom Data, 1nm Bands NDI Index				
Number of Highly Correlated Indices				
	Field:	Riesling		
	View:	Leaf	Canopy NADIR	Canopy 15 Deg
		# of indices	# of indices	# of indices
Petiole Nutrient Analysis	Boron	1		
	Potassium	6	2	
	Magnesium	322		
	Nitrogen	33		1
	Phosphorus			
	Zinc	1		

Again the highly correlated indices were used for a linear fit and the coefficients of determination are shown below. The Riesling cultivar, despite achieving higher correlation coefficients than Cabernet Franc, actually performed slightly worse with a maximum $R^2 = 0.51$ being reached. Despite a correlation coefficient of 0.82 for N at leaf level, our method of calculating the R^2 value using only the wavelengths that correlated highly did not work well, resulting in a $R^2 = 0.02$.

Table 22: R^2 results using the normalized difference index for Riesling from the bloom phenological stage

Bloom Data, 1nm Bands NDI Index													
R^2													
	Field:	Riesling											
	View:	Leaf				Canopy NADIR				Canopy 15 Deg			
		R^2 Ordinary	R^2 Adjusted	RMSE	Top Bands	R^2 Ordinary	R^2 Adjusted	RMSE	Top Bands	R^2 Ordinary	R^2 Adjusted	RMSE	Top Bands
Petiole Nutrient Analysis	Boron	0.50	0.48	4.41 (mg/kg)	0.00				0.00				0.00
	Potassium	0.00	-0.05	3556.54 (mg/kg)	0.00	0.51	0.48	2500.43 (mg/kg)	0.00				0.00
	Magnesium	0.05	0.01	1114.12 (mg/kg)	0.20				0.24				0.16
	Nitrogen	0.02	-0.03	0.10 (%)	0.00				0.00	0.50	0.47	0.07 (%)	0.00
	Phosphorus				0.00				0.00				0.10
	Zinc	0.02	-0.03	14.80 (mg/kg)	0.00				0.11				0.00

We observed similar results for veraison in terms of the R^2 that were calculated. For Cabernet Franc, none of the CC values reached the threshold level, therefore indices could be used for the linear fit. Of note, one combination reached CC=0.70 at only two significant digits, but fell below when using more than two. The data as read by MATLAB were used at more than two significant digits, hence the value of 0.6961 did not reach the CC threshold of 0.7 in MATLAB.

Table 23: Number of highly correlated indices produced using the normalized difference index for Cabernet Franc from the veraison phenological stage

Veraison Data, 1nm Bands NDI Index													
R^2													
	Field:	Cabernet Franc											
	View:	Leaf				Canopy NADIR				Canopy 15 Deg			
		R^2 Ordinary	R^2 Adjusted	RMSE	Top Bands	R^2 Ordinary	R^2 Adjusted	RMSE	Top Bands	R^2 Ordinary	R^2 Adjusted	RMSE	Top Bands
Petiole Nutrient Analysis	Boron	N/A	N/A	N/A	0.38				0.62				0.39
	Potassium				0.30				0.27				0.29
	Magnesium				0.00				0.01				0.00
	Nitrogen				0.00				0.00				0.00
	Phosphorus				0.00				0.03				0.00
	Zinc				0.00				0.06				0.06

We found that for the correlated bands ($p < 0.05$), only B resulted in a decent model fit for the Cabernet Franc cultivar during the veraison phenological stage.

Despite a large number of indices that correlated highly in some of the nutrient-view angle combinations, the results from the Riesling cultivar during veraison, seen in Tables 24 and 25 below, performed similar to the results from bloom, with a maximum R^2 value of just over 0.50. Again, like bloom, some of the combinations that generated the highest CC values had the lowest R^2 values.

Table 24: Number of highly correlated indices produced using the normalized difference index for Riesling from the veraison phenological stage

Veraison Data, 1nm Bands NDI Index				
Number of Highly Correlated Indices				
	Field:	Riesling		
	View:	Leaf	Canopy NADIR	Canopy 15 Deg
		# of indices	# of indices	# of indices
Petiole Nutrient Analysis	Boron			
	Potassium			
	Magnesium	14	540	6783
	Nitrogen	407	9389	6783
	Phosphorus	1	4436	1688
	Zinc	3		

Table 25: R^2 results using the normalized difference index for Riesling from the veraison phenological stage

Veraison Data, 1nm Bands NDI Index													
R^2													
	Field:	Riesling											
	View:	Leaf				Canopy NADIR				Canopy 15 Deg			
		R^2 Ordinary	R^2 Adjusted	RMSE	Top Bands	R^2 Ordinary	R^2 Adjusted	RMSE	Top Bands	R^2 Ordinary	R^2 Adjusted	RMSE	Top Bands
Petiole Nutrient Analysis	Boron				0.00				0.15				0.00
	Potassium				0.15				0.00				0.00
	Magnesium	0.02	-0.03	422.76 (mg/kg)	0.23	0.49	0.47	299.18 (mg/kg)	0.28	0.49	0.47	304.21 (mg/kg)	0.28
	Nitrogen	0.00	-0.04	0.10 (%)	0.48	0.52	0.49	0.07 (%)	0.46	0.51	0.49	0.07 (%)	0.18
	Phosphorus	0.01	-0.04	447.09 (mg/kg)	0.00	0.49	0.47	426.20 (mg/kg)	0.02	0.49	0.47	320.16 (mg/kg)	0.03
	Zinc	0.17	0.13	3.45 (mg/kg)	0.52				0.13				0.00

Correlation coefficients do not guarantee a good fit with the nutrient data; they just indicate the level to which the wavelengths are correlated. The peak CC result of 0.82 only produced a coefficient of determination of 0.02. This would indicate that the method we adopted for using only the wavelengths that were strongly correlated might not be the best method with which to fit the nutrient data. The usage of all correlated bands ($p < 0.05$) to generate a specific nutrient model did not generally improve the model fits, nor did this approach generate good modeling results when compared to those nutrient-view angle combinations which had indices that did not have CC > 0.7 values.

To that end, another method was employed, namely step-wise linear regression.

5.2.4 Wavelength and NDI SLR results

We next wanted to determine what results could be achieved using step-wise linear regression, following the standard linear fit attempt for the nutrients, focused on the nutrient-view angle combinations that correlated highly. The first objective for this was to evaluate this approach using the individual wavelengths and the correlated indices.

The CC was run for all the wavelengths to find a subset that highly correlated for a given nutrient from each view-angle. The results came back without any individual wavelengths correlating at the CC≥0.70 level for both cultivars in both growing seasons. Therefore, we were unable to find a correlated subset. In this case, the complete set of 601 wavelengths was used as the input variables for running SLR on each of the nutrients. Once SLR had been run using the complete set of wavelengths, it was again ran using the highly correlated indices as the input variables. The results from these two analyses are shown below in Tables 26-49. Of note, for all the following tables, the criterion column refers to the criterion model specification used for the SLR that gave the highest R^2 value for that given nutrient.

Examining the results from Cabernet Franc first, the values achieved from the three view-angles during bloom are seen in Tables 26-27. We found that for the results that gave an R^2 value above zero, five out of six of them were achieved based on the AIC criterion. Also, if the results from the three view angles were combined, all six nutrients had R^2 values greater than zero; however, no more than two nutrients achieved this feat in a single view angle. This is a unique occurrence that was not observed in any of the other cultivar-growing season combinations. The results achieved varied between 0.22-0.82, depending on the nutrient for the Cabernet Franc bloom data.

Table 26: R^2 results for step-wise linear regression using all wavelengths for Cabernet Franc from the bloom phenological stage at the leaf view angle

Nutrient	SLR - All Wavelengths			
	R^2	R^2 Adjusted	Criterion	RMSE
Boron	0.00	0.00	BIC/R^2	4.12 (mg/kg)
Magnesium	0.00	0.00	AIC/BIC/ R^2	786.60 (mg/kg)
Nitrogen	0.68	0.61	AIC	0.08 (%)
Phosphorus	0.00	0.00	BIC/ R^2	1887.27 (mg/kg)
Potassium	0.00	0.00	AIC/BIC/ R^2	7523.44 (mg/kg)
Zinc	0.58	0.51	AIC	6.71 (mg/kg)

Table 27: R^2 results for step-wise linear regression using all wavelengths for Cabernet Franc from the bloom phenological stage at the canopy nadir view angle

Nutrient	SLR - All Wavelengths			
	R^2	R^2 Adjusted	Criterion	RMSE
Boron	0.00	0.00	BIC/ R^2	4.12 (mg/kg)
Magnesium	0.22	0.16	AIC	719.77 (mg/kg)
Nitrogen	0.00	0.00	AIC/BIC/ R^2	0.13 (%)
Phosphorus	0.00	0.00	AIC/BIC/ R^2	1887.27 (mg/kg)
Potassium	0.48	0.42	BIC/ R^2	5748.85 (mg/kg)
Zinc	0.00	0.00	AIC/BIC/ R^2	9.60 (mg/kg)

Table 28: R^2 results for step-wise linear regression using all wavelengths for Cabernet Franc from the bloom phenological stage at the canopy 15^o off-nadir view angle

Nutrient	SLR - All Wavelengths			
	R^2	R^2 Adjusted	Criterion	RMSE
Boron	0.54	0.44	AIC	3.09 (mg/kg)
Magnesium	0.00	0.00	AIC/BIC/ R^2	798.03 (mg/kg)
Nitrogen	0.00	0.00	AIC/BIC/ R^2	0.12 (%)
Phosphorus	0.82	0.78	AIC	898.85 (mg/kg)
Potassium	0.00	0.00	AIC/BIC/ R^2	7557.50 (mg/kg)
Zinc	0.00	0.00	AIC/BIC/ R^2	9.76 (mg/kg)

The results from veraison are presented in Tables 29-31. We observed that a positive R^2 value was generated for B from a combination of wavelengths from any of the three view angles, with those collected at canopy 15^o off-nadir accounting for 82% of the variation in the nutrient data. Besides B,

only K and Zn are also represented from this data set. The AIC criterion again generated the highest R^2 values, similar to what was seen in the bloom analysis.

Table 29: R^2 results for step-wise linear regression using all wavelengths for Cabernet Franc from the veraison phenological stage at the leaf view angle

	SLR - All Wavelengths			
Nutrient	R^2	R^2 Adjusted	Criterion	RMSE
Boron	0.31	0.26	BIC/ R^2	4.52 (mg/kg)
Magnesium	0.00	0.00	AIC/BIC/ R^2	396.67 (mg/kg)
Nitrogen	0.40	0.36	AIC/BIC/ R^2	0.08 (%)
Phosphorus	0.00	0.00	AIC/BIC/ R^2	710.37 (mg/kg)
Potassium	0.33	0.22	AIC	2008.19 (mg/kg)
Zinc	0.57	0.48	AIC	3.65 (mg/kg)

Table 30: R^2 results for step-wise linear regression using all wavelengths for Cabernet Franc from the veraison phenological stage at the canopy nadir view angle

	SLR - All Wavelengths			
Nutrient	R^2	R^2 Adjusted	Criterion	RMSE
Boron	0.30	0.27	AIC/BIC/ R^2	4.53 (mg/kg)
Magnesium	0.00	0.00	AIC/BIC/ R^2	387.64 (mg/kg)
Nitrogen	0.00	0.00	AIC/BIC/ R^2	0.09 (%)
Phosphorus	0.00	0.00	AIC/BIC/ R^2	733.35 (mg/kg)
Potassium	0.00	0.00	BIC/ R^2	2324.46 (mg/kg)
Zinc	0.21	0.15	AIC	3.80 (mg/kg)

Table 31: R^2 results for step-wise linear regression using all wavelengths for Cabernet Franc from the veraison phenological stage at the canopy 15° off-nadir view angle

Nutrient	SLR - All Wavelengths			
	R^2	R^2 Adjusted	Criterion	RMSE
Boron	0.86	0.80	AIC	2.39 (mg/kg)
Magnesium	0.00	0.00	AIC/BIC/ R^2	390.00 (mg/kg)
Nitrogen	0.00	0.00	AIC/BIC/ R^2	0.09 (%)
Phosphorus	0.00	0.00	AIC/BIC/ R^2	722.20 (mg/kg)
Potassium	0.00	0.00	BIC/ R^2	2325.26 (mg/kg)
Zinc	0.00	0.00	AIC/BIC/ R^2	4.98 (mg/kg)

Staying with the Cabernet Franc cultivar, the results from the SLR run using the highly correlated indices from the initial analysis were generated. For the three different view angles, only the combinations of the view angles and the nutrients which resulted in a CC≥0.70 were tested. All other combinations, i.e., those that did not reach the required threshold level, were ignored as they did not have any highly correlated indices to use as input variables. Tables 32-34 show the results from bloom.

We observed that only two of the nutrient-view angle combinations were highly correlated for bloom. For these two, R^2 values matching those generated using the standard linear fit were found. This is likely due to the fact that a low number of indices for each of these models were found to be highly correlated. The SLR found the best result using only a single index based on the small input data set, which matched the results from the standard linear fit approach.

Table 32: R^2 results for step-wise linear regression using the highly correlated normalized difference indices for Cabernet Franc from the bloom phenological stage at the leaf view angle

Nutrient	SLR - Correlated NDI				
	R^2	R^2 Adjusted	Criterion	RMSE	Top Bands
Boron	N/A	N/A	N/A	N/A	0.00
Magnesium	N/A	N/A	N/A	N/A	0.00
Nitrogen	N/A	N/A	N/A	N/A	0.00
Phosphorus	N/A	N/A	N/A	N/A	0.00
Potassium	N/A	N/A	N/A	N/A	0.00
Zinc	N/A	N/A	N/A	N/A	0.00

Table 33: R^2 results for step-wise linear regression using the highly correlated normalized difference indices for Cabernet Franc from the bloom phenological stage at the canopy nadir view angle

Nutrient	SLR - Correlated NDI				
	R^2	R^2 Adjusted	Criterion	RMSE	Top Bands
Boron	0.51	0.49	AIC/BIC/ R^2	2.69 (mg/kg)	0.36
Magnesium	N/A	N/A	N/A	N/A	0.00
Nitrogen	N/A	N/A	N/A	N/A	0.10
Phosphorus	N/A	N/A	N/A	N/A	0.00
Potassium	N/A	N/A	N/A	N/A	0.00
Zinc	N/A	N/A	N/A	N/A	0.00

Table 34: R^2 results for step-wise linear regression using the highly correlated normalized difference indices for Cabernet Franc from the bloom phenological stage at the canopy 15° off-nadir view angle

Nutrient	SLR - Correlated NDI				
	R^2	R^2 Adjusted	Criterion	RMSE	Top Bands
Boron	N/A	N/A	N/A	N/A	0.00
Magnesium	N/A	N/A	N/A	N/A	0.00
Nitrogen	N/A	N/A	N/A	N/A	0.00
Phosphorus	0.53	0.51	AIC/BIC/ R^2	1335.53 (mg/kg)	0.00
Potassium	N/A	N/A	N/A	N/A	0.00
Zinc	N/A	N/A	N/A	N/A	0.00

Recall that veraison had no highly correlated indices; hence there were no input variables to use with the SLR modeling approach. In the case of the Cabernet Franc cultivar, the use of step-wise linear regression gave us the best results when used with the full spectrum of wavelengths, rather than the highly correlated indices. We will examine the Riesling results next, starting with SLR using the full spectrum of wavelengths from 400-1000nm.

Tables 35-37 show that of the six nutrients, only for Zn was the SLR unable to produce a non-zero R^2 value. In other words, for the other five nutrients the R^2 values varied between 0.15-0.71 and were spread between the three different criteria, with the R^2 criterion performing the best overall. This is a change from the Cabernet Franc results, in which the AIC criterion worked the best. From the Riesling results, we found that while the highest R^2 values came from the leaf-view, the largest number of nutrients was represented from the spectrum collected at canopy 15° off-nadir.

Table 35: R^2 results for step-wise linear regression using all wavelengths for Riesling from the bloom phenological stage at the leaf view angle

Nutrient	SLR - All Wavelengths			
	R^2	R^2 Adjusted	Criterion	RMSE
Boron	0.00	0.00	AIC/BIC/ R^2	6.10 (mg/kg)
Magnesium	0.53	0.46	AIC	821.02 (mg/kg)
Nitrogen	0.71	0.67	R^2	0.06 (%)
Phosphorus	0.49	0.44	R^2	2624.69 (mg/kg)
Potassium	0.00	0.00	AIC/BIC/ R^2	3478.64 (mg/kg)
Zinc	0.00	0.00	AIC/BIC/ R^2	14.61 (mg/kg)

Table 36: R^2 results for step-wise linear regression using all wavelengths for Riesling from the bloom phenological stage at the canopy nadir view angle

Nutrient	SLR - All Wavelengths			
	R^2	R^2 Adjusted	Criterion	RMSE
Boron	0.00	0.00	AIC/BIC/ R^2	6.10 (mg/kg)
Magnesium	0.00	0.00	AIC/BIC/ R^2	1120.73 (mg/kg)
Nitrogen	0.00	0.00	BIC/ R^2	0.10 (%)
Phosphorus	0.00	0.00	AIC/BIC/ R^2	3514.37 (mg/kg)
Potassium	0.52	0.45	AIC/ R^2	2589.97 (mg/kg)
Zinc	0.00	0.00	AIC/BIC/ R^2	14.61 (mg/kg)

Table 37: R^2 results for step-wise linear regression using all wavelengths for Riesling from the bloom phenological stage at the canopy 15° off-nadir view angle

Nutrient	SLR - All Wavelengths			
	R^2	R^2 Adjusted	Criterion	RMSE
Boron	0.39	0.30	R^2	5.1 (mg/kg)
Magnesium	0.58	0.49	BIC	800.47 (mg/kg)
Nitrogen	0.47	0.28	AIC	0.08 (%)
Phosphorus	0.15	0.11	AIC/BIC/ R^2	3316.02 (mg/kg)
Potassium	0.53	0.43	R^2	2636.00 (mg/kg)
Zinc	0.00	0.00	AIC/BIC/ R^2	14.61 (mg/kg)

The R^2 values for the veraison results can be seen in Tables 38-40. None of the spectra collected from any of the three view-angles could generate a non-zero coefficient of determination for either B or K. based on our modeling of the veraison nutrient data for Riesling. For the other four nutrients, both the leaf view and the canopy at 15° off-nadir generated R^2 values for N and Zn, while the canopy nadir view generated R^2 values for both Mg and P. The values ranged between 0.32-0.82 and were generated predominantly with the AIC criterion.

Table 38: R^2 results for step-wise linear regression using all wavelengths for Riesling from the veraison phenological stage at the leaf view angle

Nutrient	SLR - All Wavelengths			
	R^2	R^2 Adjusted	Criterion	RMSE
Boron	0.00	0.00	AIC/BIC/ R^2	4.52 (mg/kg)
Magnesium	0.00	0.00	AIC/BIC/ R^2	396.67 (mg/kg)
Nitrogen	0.68	0.64	R^2	0.08 (%)
Phosphorus	0.00	0.00	AIC/BIC/ R^2	710.37 (mg/kg)
Potassium	0.00	0.00	AIC/BIC/ R^2	2008.19 (mg/kg)
Zinc	0.32	0.26	AIC/BIC/ R^2	3.65 (mg/kg)

Table 39: R^2 results for step-wise linear regression using all wavelengths for Riesling from the veraison phenological stage at the canopy nadir view angle

Nutrient	SLR - All Wavelengths			
	R^2	R^2 Adjusted	Criterion	RMSE
Boron	0.00	0.00	AIC/BIC/ R^2	4.53 (mg/kg)
Magnesium	0.64	0.56	AIC	387.64 (mg/kg)
Nitrogen	0.00	0.00	AIC/BIC/ R^2	0.09 (%)
Phosphorus	0.60	0.56	AIC	733.35 (mg/kg)
Potassium	0.00	0.00	AIC/BIC/ R^2	2324.46 (mg/kg)
Zinc	0.00	0.00	AIC/BIC/ R^2	3.80 (mg/kg)

Table 40: R^2 results for step-wise linear regression using all wavelengths for Riesling from the veraison phenological stage at the canopy 15° off-nadir view angle

Nutrient	SLR - All Wavelengths			
	R^2	R^2 Adjusted	Criterion	RMSE
Boron	0.00	0.00	BIC/R^2	3.18 (mg/kg)
Magnesium	0.00	0.00	AIC/BIC/ R^2	390.00 (mg/kg)
Nitrogen	0.53	0.49	AIC/ R^2	0.09 (%)
Phosphorus	0.00	0.00	AIC/BIC/ R^2	722.20 (mg/kg)
Potassium	0.00	0.00	AIC/BIC/ R^2	2325.26 (mg/kg)
Zinc	0.81	0.74	AIC	4.98 (mg/kg)

The Riesling veraison nutrients that generated high values do not match any obvious pattern when compared against the bloom results or against those from the Cabernet Franc cultivar. As for Cabernet Franc, we used the indices that were highly correlated from the initial analysis as the input variables for nutrient-specific SLR.

The results of the Riesling SLR using indices are seen in Tables 41-43 below. Similar to Cabernet Franc, a number of the high R^2 values matched those generated from the standard linear fit. This was because the SLR only used the one index that the linear fit also found to work best. The only other difference that stood out was that when the R^2 value was low ($R^2 \leq 0.05$), the SLR could not produce a non-zero result. This is seen in three different nutrient-view angle combinations. As shown in the results from veraison (Tables 44-46), we found that the SLR behaved in a similar fashion to bloom in the three instances when $R^2 \leq 0.05$.

Table 41: R^2 results for step-wise linear regression using the highly correlated normalized difference indices for Riesling from the bloom phenological stage at the leaf view

Nutrient	SLR - Correlated NDI				
	R^2	R^2 Adjusted	Criterion	RMSE	Top Bands
Boron	0.50	0.48	AIC/BIC/ R^2	4.41 (mg/kg)	0.00
Magnesium	0.00	0.00	AIC/BIC/ R^2	1114.12 (mg/kg)	0.20
Nitrogen	0.00	0.00	AIC/BIC/ R^2	0.10 (%)	0.00
Phosphorus	N/A	N/A	N/A	N/A	0.00
Potassium	0.00	0.00	AIC/BIC/ R^2	3556.54 (mg/kg)	0.00
Zinc	0.00	0.00	AIC/BIC/ R^2	14.80 (mg/kg)	0.00

Table 42: R^2 results for step-wise linear regression using the highly correlated normalized difference indices for Riesling from the bloom phenological stage at the canopy nadir view angle

Nutrient	SLR - Correlated NDI				
	R^2	R^2 Adjusted	Criterion	RMSE	Top Bands
Boron	N/A	N/A	N/A	N/A	0.00
Magnesium	N/A	N/A	N/A	N/A	0.24
Nitrogen	N/A	N/A	N/A	N/A	0.00
Phosphorus	N/A	N/A	N/A	N/A	0.00
Potassium	0.51	0.48	AIC/BIC/ R^2	2500.43 (mg/kg)	0.00
Zinc	N/A	N/A	N/A	N/A	0.11

Table 43: R^2 results for step-wise linear regression using the highly correlated normalized difference indices for Riesling from the bloom phenological stage at the canopy 15° off-nadir view angle

Nutrient	SLR - Correlated NDI				
	R^2	R^2 Adjusted	Criterion	RMSE	Top Bands
Boron	N/A	N/A	N/A	N/A	0.00
Magnesium	N/A	N/A	N/A	N/A	0.16
Nitrogen	0.50	0.47	AIC/BIC/ R^2	0.07 (%)	0.00
Phosphorus	N/A	N/A	N/A	N/A	0.10
Potassium	N/A	N/A	N/A	N/A	0.00
Zinc	N/A	N/A	N/A	N/A	0.00

It was found that the spectrum collected for canopy nadir could not generate non-zero R^2 values for the three nutrients when the nutrient-view angle combinations were high, but the spectrum from the canopy at 15° off-nadir did produce positive results. The SLR for Mg and N produced R^2 values slightly higher than those created from the standard linear fit approach, while for P it produced a distinctly lower value, which hints at the mixed results achieved by the SLR method.

Table 44: R^2 results for step-wise linear regression using the highly correlated normalized difference indices for Riesling from the veraison phenological stage at the leaf view

Nutrient	SLR - Correlated NDI				
	R^2	R^2 Adjusted	Criterion	RMSE	Top Bands
Boron	N/A	N/A	N/A	N/A	0.00
Magnesium	0.00	0.00	AIC/BIC/ R^2	416.68 (mg/kg)	0.23
Nitrogen	0.00	0.00	AIC/BIC/ R^2	0.10 (%)	0.48
Phosphorus	0.00	0.00	AIC/BIC/ R^2	438.78 (mg/kg)	0.00
Potassium	N/A	N/A	N/A	N/A	0.15
Zinc	0.17	0.13	AIC/BIC/ R^2	3.45 (mg/kg)	0.52

Table 45: R^2 results for step-wise linear regression using the highly correlated normalized difference indices for Riesling from the veraison phenological stage at the canopy nadir view angle

Nutrient	SLR - Correlated NDI				
	R^2	R^2 Adjusted	Criterion	RMSE	Top Bands
Boron	N/A	N/A	N/A	N/A	0.15
Magnesium	0.00	0.00	AIC/BIC/ R^2	299.18 (mg/kg)	0.00
Nitrogen	0.00	0.00	AIC/BIC/ R^2	0.07 (%)	0.46
Phosphorus	0.00	0.00	AIC/BIC/ R^2	327.27 (mg/kg)	0.00
Potassium	N/A	N/A	N/A	N/A	0.00
Zinc	N/A	N/A	N/A	N/A	0.13

Table 46: R^2 results for step-wise linear regression using the highly correlated normalized difference indices for Riesling from the veraison phenological stage at the canopy 15^o off-nadir view angle

Nutrient	SLR - Correlated NDI				
	R^2	R^2 Adjusted	Criterion	RMSE	Top Bands
Boron	N/A	N/A	N/A	N/A	0.00
Magnesium	0.51	0.49	AIC/BIC/ R^2	403.16 (mg/kg)	0.28
Nitrogen	0.51	0.49	AIC/BIC/ R^2	0.07 (%)	0.18
Phosphorus	0.17	0.14	AIC/BIC/ R^2	320.16 (mg/kg)	0.00
Potassium	N/A	N/A	N/A	N/A	0.00
Zinc	N/A	N/A	N/A	N/A	0.00

Overall, for Cabernet Franc, the step-wise linear regression method for generating a model fit for the nutrient data worked well when using the wavelengths. However, this was only true if the view-angle from which the data were collected for a given nutrient could be chosen by the user. Using the

correlated NDI, on the other hand, did not produce any results superior to those obtained from a standard linear fit approach.

The step-wise linear regression method performed well for the Riesling cultivar when using the complete reflectance spectra as potential input variables, if the user could select the preferred view-angle. Though unlike Cabernet Franc, the canopy 15^{o} off-nadir spectrum had superior performance for the greatest number of nutrients over the two growing seasons. The SLR approach based on correlated indices did not outperform the standard linear fit method, for a number of nutrient and view angle combinations. In fact, in most cases the SLR method produced results that were either the same or inferior to those from the standard linear fit model. The next step was to look at a modification of the spectral data for input to the SLR model, after using the individual wavelengths and the correlated indices as the input variables for the SLR.

5.2.5 Derivative SLR results

The first approach in the "modified input variable" section was based on the 1st derivative of the reflectance spectra as the input variables for SLR. The same three criteria that were used previously were again used for the derivative SLR method. However, it was found that the AIC and BIC criteria could not resolve the SLR for a reasonable number of bands. In this case, reasonable was defined as fewer than 24 unique bands. Only the R^2 criterion was able to calculate a coefficient of determination that resulted in a reasonable number of bands. This band cut-off was decided on in order to ensure robust models and avoid overfitting, and was set at less than 24 as that is the minimum number of samples we had from any particular data set.

Tables 47-49 show the results for the R^2 values for Cabernet Franc during bloom. The immediate thing that stands out from looking at the result tables is that all nutrients for all three view angles had strongly positive R^2 values. In other words, unlike the cases raw wavelengths or correlated NDIs were used, there were no zero R^2 values observed.

It seems, based on the first cultivar-growing season pairing, that using the derivative of the spectrum may allow a user to select which view-angle is optimal for his/her collection method and for the nutrients of interest. For instance, using only the two canopy view-angles we were able to achieved R^2 values between 0.54-0.73, depending on the nutrient in question. This is a distinct improvement on any of the prior results.

Table 47: R^2 results for step-wise linear regression using all 1st derivatives for Cabernet Franc from the bloom phenological stage at the leaf view angle

Nutrient	SLR - Derivative			
	R^2	R^2 Adjusted	Criterion	RMSE
Boron	0.64	0.61	R^2	2.59 (mg/kg)
Magnesium	0.65	0.59	R^2	503.10 (mg/kg)
Nitrogen	0.61	0.57	R^2	0.08 (%)
Phosphorus	0.70	0.66	R^2	1107.75 (mg/kg)
Potassium	0.58	0.53	R^2	5166.26 (mg/kg)
Zinc	0.56	0.51	R^2	6.74 (mg/kg)

Table 48: R^2 results for step-wise linear regression using all 1st derivatives for Cabernet Franc from the bloom phenological stage at the canopy nadir view angle

Nutrient	SLR - Derivative			
	R^2	R^2 Adjusted	Criterion	RMSE
Boron	0.47	0.44	R^2	3.09 (mg/kg)
Magnesium	0.35	0.31	R^2	654.10 (mg/kg)
Nitrogen	0.58	0.53	R^2	0.09 (%)
Phosphorus	0.67	0.62	R^2	1161.80 (mg/kg)
Potassium	0.68	0.65	R^2	4478.60 (mg/kg)
Zinc	0.51	0.46	R^2	7.08 (mg/kg)

Table 49: R^2 results for step-wise linear regression using all 1st derivatives for Cabernet Franc from the bloom phenological stage at the canopy 15° off-nadir view angle

Nutrient	SLR - Derivative			
	R^2	R^2 Adjusted	Criterion	RMSE
Boron	0.54	0.49	R^2	2.96 (mg/kg)
Magnesium	0.73	0.68	R^2	449.50 (mg/kg)
Nitrogen	0.14	0.11	R^2	0.12 (%)
Phosphorus	0.59	0.56	R^2	1264.46 (mg/kg)
Potassium	0.63	0.59	R^2	4846.76 (mg/kg)
Zinc	0.56	0.51	R^2	6.83 (mg/kg)

Results for the veraison data are shown in Tables 50-52 below. Again, we observed good R^2 values across the board for each of the view-angles. The acceptable value for the coefficient of determination is highly subjective, and is selected by the individual researcher. For this research, in order to ease the discussion of performance of the different methods for modeling the nutrients over the seasons and between cultivars, we will again select a level of 0.70. An $R^2 \geq 0.70$ will be considered to have performed well for our purposes. In general, all three view angles will be considered. Therefore if we achieve a R^2 value of 0.10 for one view-angle, but 0.75 for another, the nutrient will still be considered as performing well, since a user theoretically can select the preferred view-angle. However, it should be noted that for many applications, an $R^2 \geq 0.50$ could even be considered adequate, since such a model theoretically explain greater than 50% of the variability in the dependent variable.

Table 50: R^2 results for step-wise linear regression using all 1st derivatives for Cabernet Franc from the veraison phenological stage at the leaf view angle

Nutrient	SLR - Derivative			
	R^2	R^2 Adjusted	Criterion	RMSE
Boron	0.53	0.50	R^2	3.72 (mg/kg)
Magnesium	0.65	0.60	R^2	252.23 (mg/kg)
Nitrogen	0.67	0.64	R^2	0.06 (%)
Phosphorus	0.34	0.29	R^2	600.33 (mg/kg)
Potassium	0.45	0.38	R^2	1793.91 (mg/kg)
Zinc	0.55	0.50	R^2	3.57 (mg/kg)

Table 51: R^2 results for step-wise linear regression using all 1st derivatives for Cabernet Franc from the veraison phenological stage at the canopy nadir view angle

Nutrient	SLR - Derivative			
	R^2	R^2 Adjusted	Criterion	RMSE
Boron	0.65	0.60	R^2	3.34 (mg/kg)
Magnesium	0.63	0.58	R^2	250.39 (mg/kg)
Nitrogen	0.63	0.58	R^2	0.06 (%)
Phosphorus	0.53	0.46	R^2	539.68 (mg/kg)
Potassium	0.74	0.68	R^2	1313.87 (mg/kg)
Zinc	0.76	0.71	R^2	2.22 (mg/kg)

Table 52: R^2 results for step-wise linear regression using all 1st derivatives for Cabernet Franc from the veraison phenological stage at the canopy 15° off-nadir view angle

Nutrient	SLR - Derivative			
	R^2	R^2 Adjusted	Criterion	RMSE
Boron	0.71	0.68	R^2	3.05 (mg/kg)
Magnesium	0.72	0.66	R^2	227.30 (mg/kg)
Nitrogen	0.66	0.61	R^2	0.06 (%)
Phosphorus	0.52	0.46	R^2	529.86 (mg/kg)
Potassium	0.58	0.55	R^2	1516.19 (mg/kg)
Zinc	0.33	0.28	R^2	4.21 (mg/kg)

We observed that both Mg and P performed well for the bloom phonological stage, with the lowest R^2 values coming from B, N and Zn. However, the veraison results had a different outcome: Mg modeling continued to perform well, as did K, which was one of the mid-level R^2 nutrients in bloom. Boron and Zn, on the other hand, the two nutrients with the worst model fits for bloom, were high performers for veraison, with Zn generating the highest R^2 value at 0.76.

The Riesling cultivar R^2 results for bloom, generated for the six nutrients over the three view-angles, are shown in Tables 53-55. The previous Cabernet Franc results showed that nutrients that generated high R^2 values were restricted to a single view-angle. However, the Riesling results show that a number of the nutrients had high results in multiple view angles, thereby allowing more flexibility in field data collection. Furthermore, we observed that between the three view-angles for Riesling bloom phase, all six nutrients performed well, with the highest $R^2 = 0.84$ coming from P. In addition, B, Mg and N all exhibited $R^2 \geq 0.70$ for at least two different view-angles.

Table 53: R^2 results for step-wise linear regression using all 1st derivatives for Riesling from the bloom phenological stage at the leaf view angle

Nutrient	SLR - Derivative			
	R^2	R^2 Adjusted	Criterion	RMSE
Boron	0.75	0.70	R^2	3.35 (mg/kg)
Magnesium	0.78	0.74	R^2	575.55 (mg/kg)
Nitrogen	0.79	0.74	R^2	0.05 (%)
Phosphorus	0.53	0.49	R^2	2514.34 (mg/kg)
Potassium	0.71	0.68	R^2	1960.71 (mg/kg)
Zinc	0.84	0.81	R^2	6.42 (mg/kg)

Table 54: R^2 results for step-wise linear regression using all 1st derivatives for Riesling from the bloom phenological stage at the canopy nadir view angle

Nutrient	SLR - Derivative			
	R^2	R^2 Adjusted	Criterion	RMSE
Boron	0.71	0.66	R^2	3.55 (mg/kg)
Magnesium	0.75	0.71	R^2	600.78 (mg/kg)
Nitrogen	0.66	0.58	R^2	0.06 (%)
Phosphorus	0.84	0.79	R^2	1602.91 (mg/kg)
Potassium	0.34	0.31	R^2	2894.34 (mg/kg)
Zinc	0.63	0.55	R^2	9.80 (mg/kg)

Table 55: R^2 results for step-wise linear regression using all 1st derivatives for Riesling from the bloom phenological stage at the canopy 15° off-nadir view angle

Nutrient	SLR - Derivative			
	R^2	R^2 Adjusted	Criterion	RMSE
Boron	0.46	0.41	R^2	4.70 (mg/kg)
Magnesium	0.48	0.43	R^2	843.69 (mg/kg)
Nitrogen	0.81	0.76	R^2	0.05 (%)
Phosphorus	0.68	0.62	R^2	2180.53 (mg/kg)
Potassium	0.51	0.47	R^2	2543.38 (mg/kg)
Zinc	0.62	0.54	R^2	9.94 (mg/kg)

Tables 56-58 show the Riesling results from veraison; we can observe that the veraison R^2 results have decreased, when compared to those from bloom. The maximum R^2 value (N) was 0.84, which was the same maximum value as obtained for bloom, but the other nutrient R^2 values decreased. Five of the six nutrients performed well with $R^2 \geq 0.70$. Magnesium was the only nutrient not to achieve a $R^2 \geq 0.70$, topping out at 0.63. Also, there were no nutrients that had high R^2 values for multiple view-angles - all the peak R^2 values were achieved using the spectra collected at the canopy nadir view angle.

Table 56: R^2 results for step-wise linear regression using all 1st derivatives for Riesling from the veraison phenological stage at the leaf view angle

Nutrient	SLR - Derivative			
	R^2	R^2 Adjusted	Criterion	RMSE
Boron	0.53	0.46	R^2	3.72 (mg/kg)
Magnesium	0.62	0.58	R^2	252.23 (mg/kg)
Nitrogen	0.67	0.62	R^2	0.06 (%)
Phosphorus	0.65	0.59	R^2	600.33 (mg/kg)
Potassium	0.57	0.49	R^2	1793.91 (mg/kg)
Zinc	0.68	0.63	R^2	3.57 (mg/kg)

Table 57: R^2 results for step-wise linear regression using all 1st derivatives for Riesling from the veraison phenological stage at the canopy nadir view angle

Nutrient	SLR - Derivative			
	R^2	R^2 Adjusted	Criterion	RMSE
Boron	0.81	0.77	R^2	3.34 (mg/kg)
Magnesium	0.63	0.59	R^2	250.39 (mg/kg)
Nitrogen	0.84	0.81	R^2	0.06 (%)
Phosphorus	0.74	0.70	R^2	539.68 (mg/kg)
Potassium	0.72	0.65	R^2	1313.87 (mg/kg)
Zinc	0.70	0.67	R^2	2.22 (mg/kg)

Table 58: R^2 results for step-wise linear regression using all 1st derivatives for Riesling from the veraison phenological stage at the canopy 15° off-nadir view angle

Nutrient	SLR - Derivative			
	R^2	R^2 Adjusted	Criterion	RMSE
Boron	0.62	0.56	R^2	3.05 (mg/kg)
Magnesium	0.57	0.53	R^2	227.30 (mg/kg)
Nitrogen	0.63	0.60	R^2	0.06 (%)
Phosphorus	0.59	0.55	R^2	529.86 (mg/kg)
Potassium	0.16	0.12	R^2	1561.62 (mg/kg)
Zinc	0.59	0.55	R^2	4.21 (mg/kg)

The use of the 1st derivative of the reflectance spectrum as input variables to the step-wise linear regression improved on the R^2 values that were achieved for the six nutrients using either the wavelengths-only or the correlated index approaches. It was possible to achieve $R^2 \geq 0.51$ for all six nutrients during both growing seasons and for both cultivars, with R^2 values typically being greater than 0.70 for most nutrients. This is especially interesting, since results were achieved across most view angles, thus allowing greater flexibility during field data collection. If a user were limited to a single view-angle, the selection of the view-angle could depend on the cultivar and if he/she were focusing on particular nutrients or the complete set. Using the canopy nadir view-angle as an example, the lowest R^2 value between both cultivars and growing seasons was 0.35, i.e., the selection of optimum view-angle comes down to the R^2 model level one is willing to accept.

5.2.6 Continuum Removal SLR results

The final data analysis approach was continuum removal (CR; Kokaly and Clark, 1999), with the specific spectral feature being the red trough region (approximately 600-700nm). It should be noted that no additional wavelength regions were highly correlated to nutrient values; therefore no additional spectral regions were subjected to continuum removal. Tables 59-61 show the CR results for Cabernet Franc collected at bloom. Of note, similar to the raw wavelength and correlated NDI, all three criteria produced usable results and therefore were reported.

We found that P nutrient levels were well modeled using the CR approach, with a R^2 value ranging between 0.72-0.74 across the three view-angles. This was not the case for all the nutrients and similar to what was found when using the wavelengths and correlated NDI, not every nutrient generated a non-zero R^2 value. Similar to the results found for P, B exhibited positive R^2 values across all three view-angles, though at distinctly lower R^2 values. Each of the other four nutrients had a non-zero model fit when considered between the three view-angles (R^2 values ranged between 0.07-0.34).

Table 59: R^2 results for step-wise linear regression using continuum removal for Cabernet Franc from the bloom phenological stage at the leaf view angle

Nutrient	SLR - Continuum Removal			
	R^2	R^2 Adjusted	Criterion	RMSE
Boron	0.32	0.29	AIC/BIC/ R^2	3.46 (mg/kg)
Magnesium	0.25	0.20	AIC/ R^2	703.95 (mg/kg)
Nitrogen	0.34	0.32	AIC/BIC/ R^2	0.10 (%)
Phosphorus	0.73	0.60	AIC	1199.51 (mg/kg)
Potassium	0.00	0.00	BIC/ R^2	7523.44 (mg/kg)
Zinc	0.20	0.18	AIC/BIC/ R^2	8.71 (mg/kg)

Table 60: R^2 results for step-wise linear regression using continuum removal for Cabernet Franc from the bloom phenological stage at the canopy nadir view angle

Nutrient	SLR - Continuum Removal			
	R^2	R^2 Adjusted	Criterion	RMSE
Boron	0.47	0.43	BIC	3.10 (mg/kg)
Magnesium	0.07	0.04	AIC	771.17 (mg/kg)
Nitrogen	0.00	0.00	BIC/ R^2	0.13 (%)
Phosphorus	0.72	0.66	AIC	1100.47 (mg/kg)
Potassium	0.12	0.09	AIC/BIC/ R^2	7177.91 (mg/kg)
Zinc	0.31	0.26	AIC	8.23 (mg/kg)

Table 61: R^2 results for step-wise linear regression using continuum removal for Cabernet Franc from the bloom phenological stage at the canopy 15^o off-nadir view angle

Nutrient	SLR - Continuum Removal			
	R^2	R^2 Adjusted	Criterion	RMSE
Boron	0.35	0.33	AIC/BIC/ R^2	3.39 (mg/kg)
Magnesium	0.00	0.00	AIC/BIC/ R^2	758.03 (mg/kg)
Nitrogen	0.07	0.03	AIC	0.12 (%)
Phosphorus	0.74	0.60	AIC	1206.01 (mg/kg)
Potassium	0.00	0.00	AIC/BIC/ R^2	7557.50 (mg/kg)
Zinc	0.00	0.00	BIC/ R^2	9.76 (mg/kg)

Tables 62-64 below show that the Cabernet Franc veraison CR results were similar to those seen from bloom, in that some of the nutrients resulted in models that generated R^2 values of zero. However, the veraison phonological stage resulted in fewer of such R^2=0 models. The R^2 values that were non-zero across the three view-angles ranged between 0.11-0.85. This peak value is higher

than any achieved through using the derivative analysis SLR approach, although the high values were not as consistent.

Table 62: R^2 results for step-wise linear regression using continuum removal for Cabernet Franc from the veraison phenological stage at the leaf view angle

Nutrient	SLR - Continuum Removal			
	R^2	R^2 Adjusted	Criterion	RMSE
Boron	0.85	0.78	AIC	2.46 (mg/kg)
Magnesium	0.00	0.00	AIC/BIC/ R^2	396.67 (mg/kg)
Nitrogen	0.13	0.10	AIC/BIC	0.09 (%)
Phosphorus	0.09	0.05	AIC	691.39 (mg/kg)
Potassium	0.25	0.20	AIC/BIC/ R^2	2044.10 (mg/kg)
Zinc	0.54	0.44	AIC	3.77 (mg/kg)

Table 63: R^2 results for step-wise linear regression using continuum removal for Cabernet Franc from the veraison phenological stage at the canopy nadir view angle

Nutrient	SLR - Continuum Removal			
	R^2	R^2 Adjusted	Criterion	RMSE
Boron	0.24	0.21	AIC/BIC/ R^2	4.71 (mg/kg)
Magnesium	0.11	0.08	AIC/BIC/ R^2	371.18 (mg/kg)
Nitrogen	0.00	0.00	AIC/BIC/ R^2	0.09 (%)
Phosphorus	0.32	0.24	AIC	640.97 (mg/kg)
Potassium	0.29	0.27	AIC/BIC/ R^2	1987.98 (mg/kg)
Zinc	0.28	0.23	AIC/BIC/ R^2	3.63 (mg/kg)

Table 64: R^2 results for step-wise linear regression using continuum removal for Cabernet Franc from the veraison phenological stage at the canopy 15° off-nadir view angle

Nutrient	SLR - Continuum Removal			
	R^2	R^2 Adjusted	Criterion	RMSE
Boron	0.38	0.36	AIC/BIC/ R^2	4.30 (mg/kg)
Magnesium	0.19	0.13	AIC	364.28 (mg/kg)
Nitrogen	0.15	0.12	BIC/ R^2	0.09 (%)
Phosphorus	0.56	0.49	BIC	514.66 (mg/kg)
Potassium	0.34	0.32	AIC/BIC/ R^2	1917.34 (mg/kg)
Zinc	0.25	0.17	AIC	4.54 (mg/kg)

The continuum removal approach also was applied to Riesling data (Tables 65-67), but the results seem to be poorer across the set of nutrients when compared to Cabernet Franc. The Riesling results peaked at a maximum R^2= 0.60, compared to the value of R^2=0.74 from Cabernet Franc at bloom. Again, as seen with Cabernet Franc, several of the nutrient models for particular view-angles had R^2 values of zero. But as before, it is possible to select a nutrient model with a non-zero R^2 value by choosing the appropriate view-angle.

Table 65: R^2 results for step-wise linear regression using continuum removal for Riesling from the bloom phenological stage at the leaf view angle

Nutrient	SLR - Continuum Removal			
	R^2	R^2 Adjusted	Criterion	RMSE
Boron	0.09	0.05	AIC	5.95 (mg/kg)
Magnesium	0.60	0.54	AIC	761.18 (mg/kg)
Nitrogen	0.60	0.49	AIC	0.07 (%)
Phosphorus	0.37	0.31	AIC/BIC	2913.18 (mg/kg)
Potassium	0.22	0.19	AIC/BIC/ R^2	3131.83 (mg/kg)
Zinc	0.14	0.10	AIC/BIC/ R^2	13.89 (mg/kg)

Table 66: R^2 results for step-wise linear regression using continuum removal for Riesling from the bloom phenological stage at the canopy nadir view angle

Nutrient	SLR - Continuum Removal			
	R^2	R^2 Adjusted	Criterion	RMSE
Boron	0.00	0.00	BIC/ R^2	6.10 (mg/kg)
Magnesium	0.32	0.25	AIC	970.05 (mg/kg)
Nitrogen	0.14	0.10	BIC/ R^2	0.09 (%)
Phosphorus	0.30	0.24	AIC/ R^2	3072.21 (mg/kg)
Potassium	0.27	0.23	AIC/BIC/ R^2	3045.94 (mg/kg)
Zinc	0.33	0.27	AIC/BIC/ R^2	12.50 (mg/kg)

Table 67: R^2 results for step-wise linear regression using continuum removal for Riesling from the bloom phenological stage at the canopy 15° off-nadir view angle

Nutrient	SLR - Continuum Removal			
	R^2	R^2 Adjusted	Criterion	RMSE
Boron	0.10	0.05	AIC	5.93 (mg/kg)
Magnesium	0.25	0.18	AIC/BIC/ R^2	1016.44 (mg/kg)
Nitrogen	0.00	0.00	AIC/BIC/ R^2	0.10 (%)
Phosphorus	0.00	0.00	AIC/BIC/ R^2	3514.37 (mg/kg)
Potassium	0.18	0.14	AIC/BIC/ R^2	3225.50 (mg/kg)
Zinc	0.23	0.19	AIC/BIC/ R^2	13.15 (mg/kg)

We found improved nutrient model fits for the Riesling veraison data (Tables 68-70), when compared to the bloom results for the same cultivar. There was a single nutrient-view angle combination that resulted in a zero R^2 value, while the peak R^2 value increased to 0.81.

Table 68: R^2 results for step-wise linear regression using continuum removal for Riesling from the veraison phenological stage at the leaf view angle

Nutrient	SLR - Continuum Removal			
	R^2	R^2 Adjusted	Criterion	RMSE
Boron	0.16	0.12	AIC/BIC/ R^2	2.46 (mg/kg)
Magnesium	0.49	0.41	AIC/BIC	396.67 (mg/kg)
Nitrogen	0.81	0.77	BIC	0.09 (%)
Phosphorus	0.50	0.46	AIC/BIC/ R^2	691.39 (mg/kg)
Potassium	0.11	0.07	AIC/ R^2	2044.10 (mg/kg)
Zinc	0.43	0.41	AIC/BIC/ R^2	3.77 (mg/kg)

Table 69: R^2 results for step-wise linear regression using continuum removal for Riesling from the veraison phenological stage at the canopy nadir view angle

Nutrient	SLR - Continuum Removal			
	R^2	R^2 Adjusted	Criterion	RMSE
Boron	0.10	0.05	AIC	4.74 (mg/kg)
Magnesium	0.51	0.46	BIC/ R^2	371.18 (mg/kg)
Nitrogen	0.57	0.55	AIC/BIC/ R^2	0.09 (%)
Phosphorus	0.56	0.51	AIC/BIC	640.97 (mg/kg)
Potassium	0.00	0.00	AIC/BIC/ R^2	1987.98 (mg/kg)
Zinc	0.40	0.34	BIC/ R^2	3.63 (mg/kg)

Table 70: R^2 results for step-wise linear regression using continuum removal for Riesling from the veraison phenological stage at the canopy 15^o off-nadir view angle

Nutrient	SLR - Continuum Removal			
	R^2	R^2 Adjusted	Criterion	RMSE
Boron	0.59	0.50	AIC	4.30 (mg/kg)
Magnesium	0.72	0.65	AIC	364.28 (mg/kg)
Nitrogen	0.58	0.56	AIC/BIC	0.09 (%)
Phosphorus	0.67	0.57	BIC	514.66 (mg/kg)
Potassium	0.10	0.05	AIC/BIC/ R^2	1917.34 (mg/kg)
Zinc	0.55	0.49	AIC/BIC/ R^2	4.54 (mg/kg)

A comparison of the performance of the continuum removal method vs. previously discussed methods showed that, while not providing the modeling performance consistency of the derivative method, the continuum removal method provided higher R^2 values for some of the nutrients in specific circumstances.

5.2.7 An overview of the best modeling results for 1nm data

We next attempted to provide a concise summary of the best nutrient modeling results in order to highlight the nutrient-specific modeling approach, results, and very importantly, the wavelengths that were included as independent (driver) variables. Tables 71-79 list the peak values that resulted from the five methods employed to generate a model to best fit the nutrient data: SLR of all wavelengths, SLR of the highly correlated indices, SLR of the 1st derivative of the reflectance spectrum, SLR using continuum removal, and NDI linear fit. The tables below list the following columns broken down by nutrient: the method that provided the peak R^2 value, the values generated, which criterion was used in the SLR, and the wavelengths that were used. This latter aspect is critical – it is indicative of the potential band combinations that a user could employ on a UAV-type platform to map specific nutrients.

Tables 71-73 show the results for Cabernet Franc during bloom, for the three view-angles; it was found that while the 1st derivative is the most selected method (based on performance), using the raw wavelengths and the continuum removal in the SLR also work in several cases. Phosphorous, over all three view-angles is best modeled using either the wavelength-based SLR or the continuum removal SLR. This is an oddity, since for every other nutrient the derivative SLR is the optimal method for at least two out of the three view-angles.

Table 71: Peak R^2 values for 1nm Cabernet Franc nutrient models from the bloom phenological stage at the leaf view angle

Bloom Cabernet Franc				Leaf View		
Nutrient	**Method**	**Rsquared**	**Rsquared Adjusted**	**Criterion**	**RMSE**	**Wavelengths for Peak Value**
Boron	SLR - Derivative	0.64	0.61	R^2	2.59 (mg/kg)	674/763/912
Magnesium	SLR - Derivative	0.65	0.59	R^2	503.10 (mg/kg)	884/888/940/972
Nitrogen	SLR - All Wavelengths	0.68	0.61	AIC	0.08 (%)	420/426/512/657/718
Phosphorus	SLR - Continuum Removal	0.73	0.60	AIC	1199.51 (mg/kg)	651/653/664/669/674/675/677/693/740/749
Potassium	SLR - Derivative	0.58	0.53	R^2	5166.26 (mg/kg)	769/938/972
Zinc	SLR - All Wavelengths	0.58	0.51	AIC	6.71 (mg/kg)	400/405/429/730

Table 72: Peak R^2 values for 1nm Cabernet Franc nutrient models from the bloom phenological stage at the canopy nadir view angle

Bloom Cabernet Franc				Canopy Nadir View		
Nutrient	**Method**	**Rsquared**	**Rsquared Adjusted**	**Criterion**	**RMSE**	**Wavelengths for Peak Value**
Boron	SLR - Correlated NDI	0.51	0.49	AIC/BIC/R^2	2.69 (mg/kg)	702/515
Magnesium	SLR - Derivative	0.35	0.31	R^2	654.10 (mg/kg)	464/849
Nitrogen	SLR - Derivative	0.58	0.53	R^2	0.09 (%)	596/715/969
Phosphorus	SLR - Continuum Removal	0.72	0.66	AIC/BIC/R^2	1100.47 (mg/kg)	560/678/745/746/750
Potassium	SLR - Derivative	0.68	0.65	R^2	4478.60 (mg/kg)	442/625/827
Zinc	SLR - Derivative	0.51	0.46	R^2	7.08 (mg/kg)	839/909/966

Table 73: Peak R^2 values for 1nm Cabernet Franc nutrient models from the bloom phenological stage at the canopy 15° off-nadir view angle

Bloom Cabernet Franc				Canopy 15 Degrees Off-Nadir View		
Nutrient	**Method**	**Rsquared**	**Rsquared Adjusted**	**Criterion**	**RMSE**	**Wavelengths for Peak Value**
Boron	SLR - Derivative	0.54	0.49	R^2	2.96 (mg/kg)	839/844/869
Magnesium	SLR - Derivative	0.73	0.68	R^2	449.50 (mg/kg)	469/476/488/866
Nitrogen	SLR - Derivative	0.14	0.11	R^2	0.12 (%)	950
Phosphorus	SLR - All Wavelengths	0.82	0.78	AIC	898.85 (mg/kg)	442/445/534/540/675/682
Potassium	SLR - Derivative	0.63	0.59	R^2	4845.76 (mg/kg)	881/882/913
Zinc	SLR - Derivative	0.56	0.51	R^2	6.83 (mg/kg)	407/679/980

We also evaluated the model characteristics for each best-performing model; specifically, the linear fit was plotted, along with its residuals (to evaluate residual behavior). To this end Figures 43-45 show the fit and residuals for the three view-angles for Cabernet Franc during bloom. Figure 43, for instance, shows that the data fit is distinctly linear and there exist no systematic patterns in residuals behavior, which could indicate that a non-linear model fit or variable transform should have been used. This was augmented by an examination of the results from the canopy-nadir and canopy 15° off-nadir view angles, where we found that, as was the case with the leaf-view, a linear fit for the data was deemed appropriate.

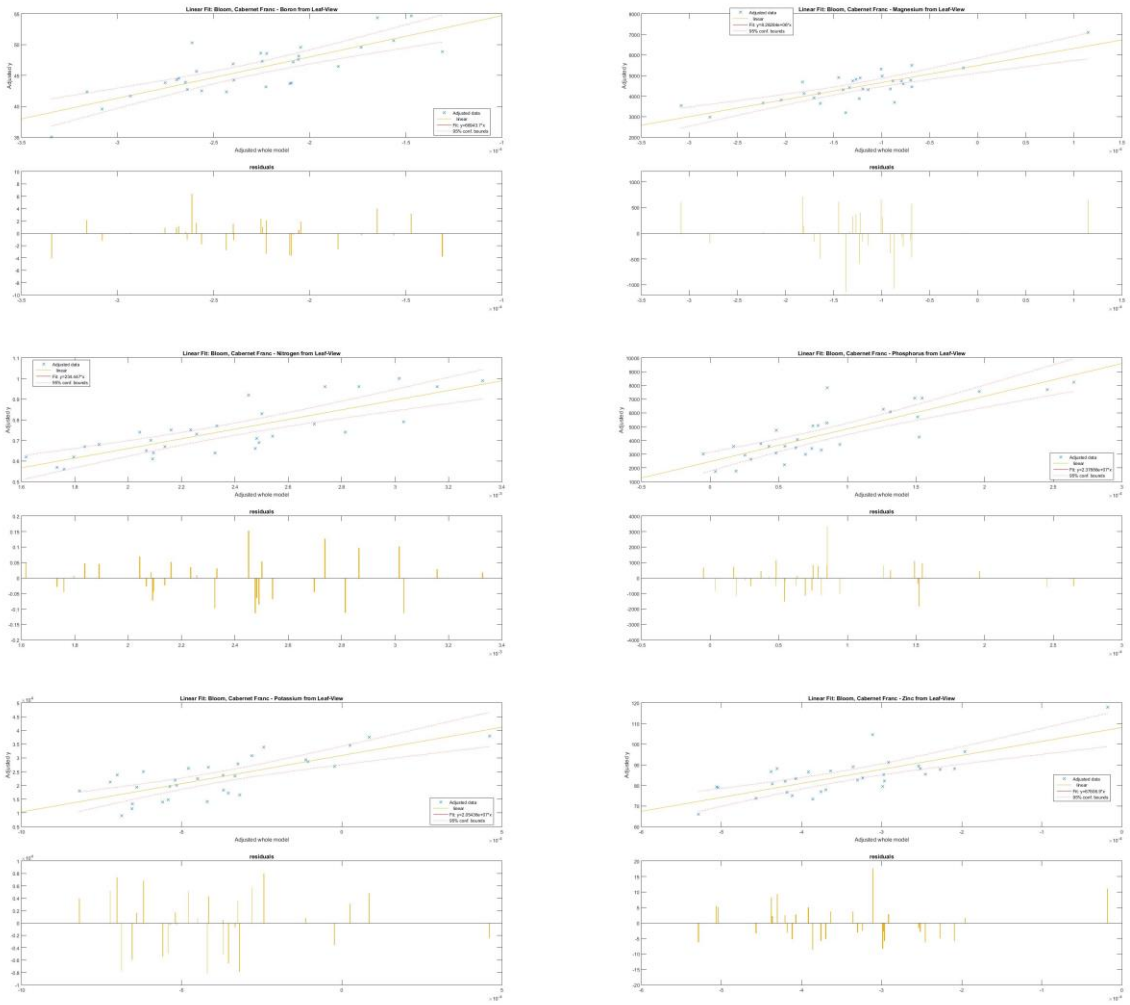

Figure 43: Linear modeling fit for 1nm Cabernet Franc reflectance data collected during bloom phenological stage at the leaf view angle: (a) boron, (b) magnesium, (c) nitrogen, (d) phosphorus, (e) potassium, (f) zinc

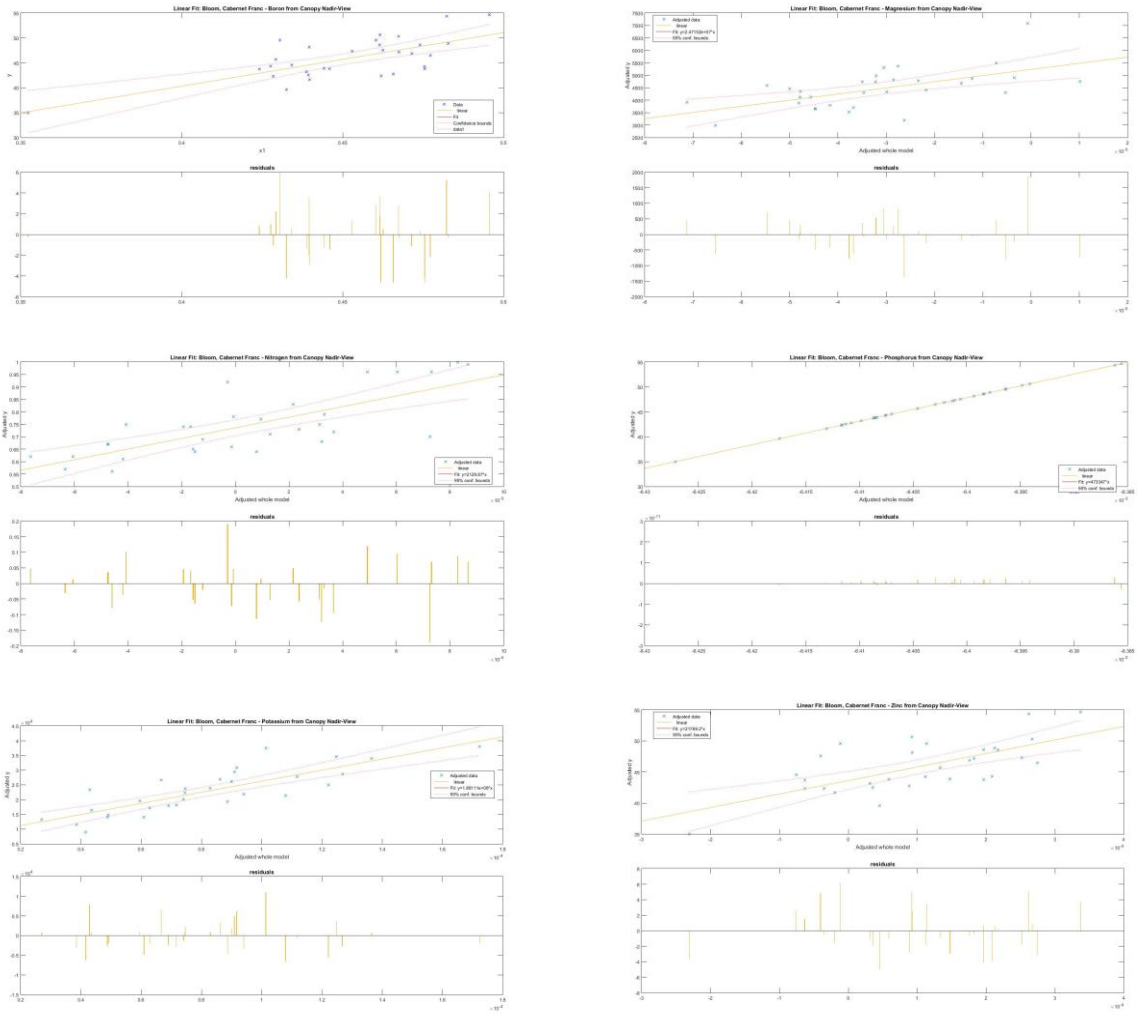

Figure 44: Linear modeling fit for 1nm Cabernet Franc reflectance data collected during bloom phenological stage at the canopy nadir view angle: (a) boron, (b) magnesium, (c) nitrogen, (d) phosphorus, (e) potassium, (f) zinc

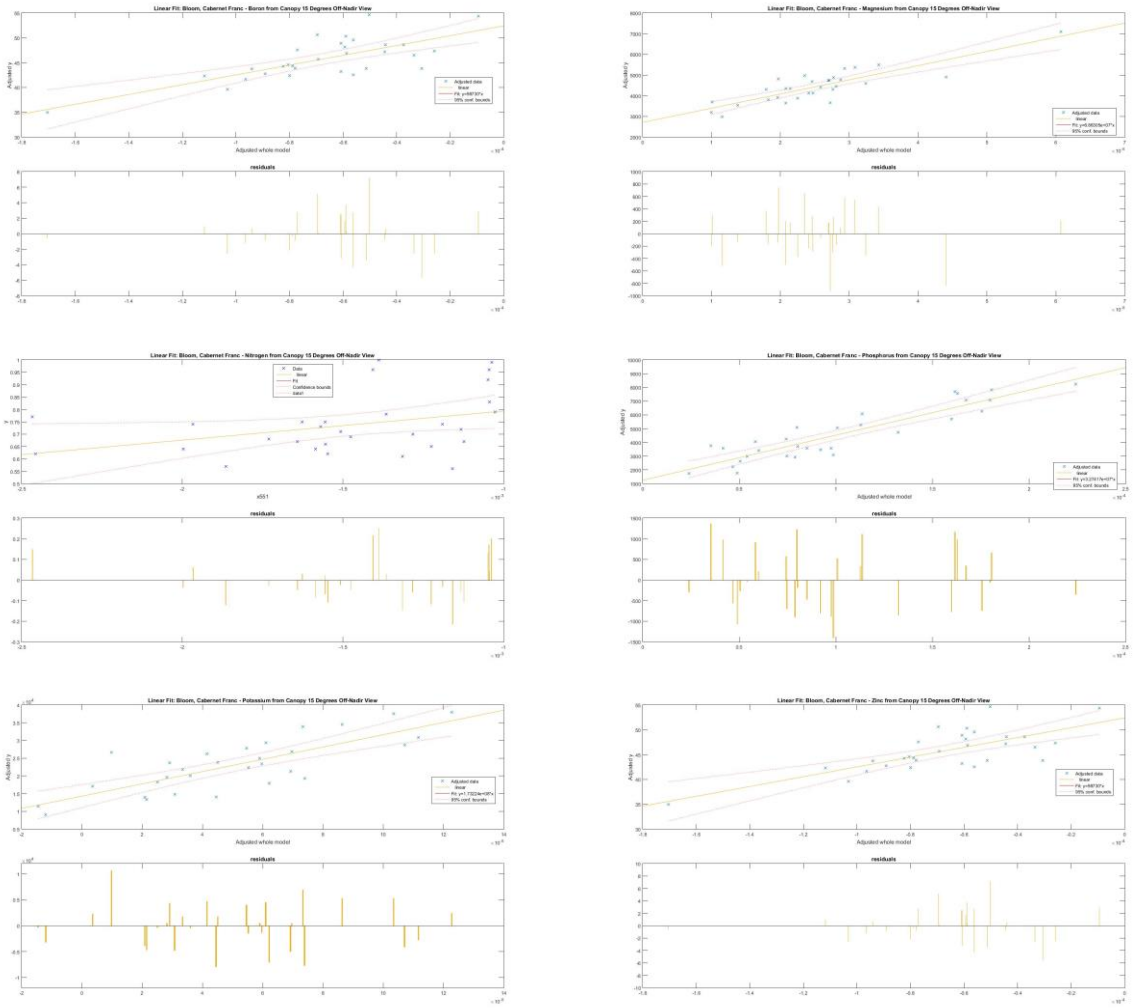

Figure 45: Linear modeling fit for 1nm Cabernet Franc reflectance data collected during bloom phenological stage at the canopy 15^{o} off-nadir view angle: (a) boron, (b) magnesium, (c) nitrogen, (d) phosphorus, (e) potassium, (f) zinc

The results repeat themselves in the case of the Cabernet Franc veraison data (Tables 74-76): Again the derivative SLR dominates as the primary method to produce the strongest model fit. During bloom, both P and Mg had $R^2 \geq 0.70$. With the veraison data, we see that Mg model performance remained high, but P fell out of that range. Boron, K and Zn achieved high R^2 values as well.

Table 74: Peak R^2 values for 1nm Cabernet Franc nutrient models from the veraison phenological stage at the leaf view angle

Veraison Cabernet Franc				Leaf View		
Nutrient	**Method**	**Rsquared**	**Rsquared Adjusted**	**Criterion**	**RMSE**	**Wavelengths for Peak Value**
Boron	SLR - Continuum Removal	0.85	0.78	AIC	2.46 (mg/kg)	560/571/674/677/684/687/693/694/750
Magnesium	SLR - Derivative	0.65	0.60	R^2	252.23 (mg/kg)	786/838/919/979
Nitrogen	SLR - Derivative	0.67	0.64	R^2	0.06 (%)	404/908/990
Phosphorus	SLR - Derivative	0.34	0.29	R^2	600.33 (mg/kg)	967/977
Potassium	SLR - Derivative	0.45	0.38	R^2	1793.91 (mg/kg)	494/627/637
Zinc	SLR - All Wavelengths	0.57	0.48	AIC	3.65 (mg/kg)	425/748/758/760/1000

Table 75: Peak R^2 values for 1nm Cabernet Franc nutrient models from the veraison phenological stage at the canopy nadir view angle

Veraison Cabernet Franc				Canopy Nadir View		
Nutrient	**Method**	**Rsquared**	**Rsquared Adjusted**	**Criterion**	**RMSE**	**Wavelengths for Peak Value**
Boron	SLR - Derivative	0.65	0.60	R^2	3.34 (mg/kg)	910/944/959
Magnesium	SLR - Derivative	0.63	0.58	R^2	250.39 (mg/kg)	832/924/937
Nitrogen	SLR - Derivative	0.63	0.58	R^2	0.06 (%)	403/907/912/920
Phosphorus	SLR - Derivative	0.53	0.46	R^2	539.68 (mg/kg)	403/761/875/886
Potassium	SLR - Derivative	0.74	0.68	R^2	1313.90 (mg/kg)	410/944/945/953/962
Zinc	SLR - Derivative	0.76	0.71	R^2	2.22 (mg/kg)	402/769/885/887/947

Table 76: Peak R^2 values for 1nm Cabernet Franc nutrient models from the veraison phenological stage at the canopy 15^o off-nadir view angle

Veraison Cabernet Franc				Canopy 15 Degrees Off-Nadir View		
Nutrient	**Method**	**Rsquared**	**Rsquared Adjusted**	**Criterion**	**RMSE**	**Wavelengths for Peak Value**
Boron	SLR - All Wavelengths	0.86	0.80	AIC	2.39 (mg/kg)	400/406/407/409/416/423/425/426/427
Magnesium	SLR - Derivative	0.72	0.66	R^2	227.30 (mg/kg)	561/860/870/909/978
Nitrogen	SLR - Derivative	0.66	0.61	R^2	0.06 (%)	408/837/842/930
Phosphorus	SLR - Continuum Removal	0.56	0.49	BIC	514.66 (mg/kg)	670/672/739/748
Potassium	SLR - Derivative	0.58	0.55	R^2	1516.20 (mg/kg)	783/941
Zinc	SLR - Derivative	0.33	0.28	R^2	4.21 (mg/kg)	402/980

Figures 46-48 show the model fits graphically, and we did not find any fits that give us pause regarding the linearity or residual behavior of the data.

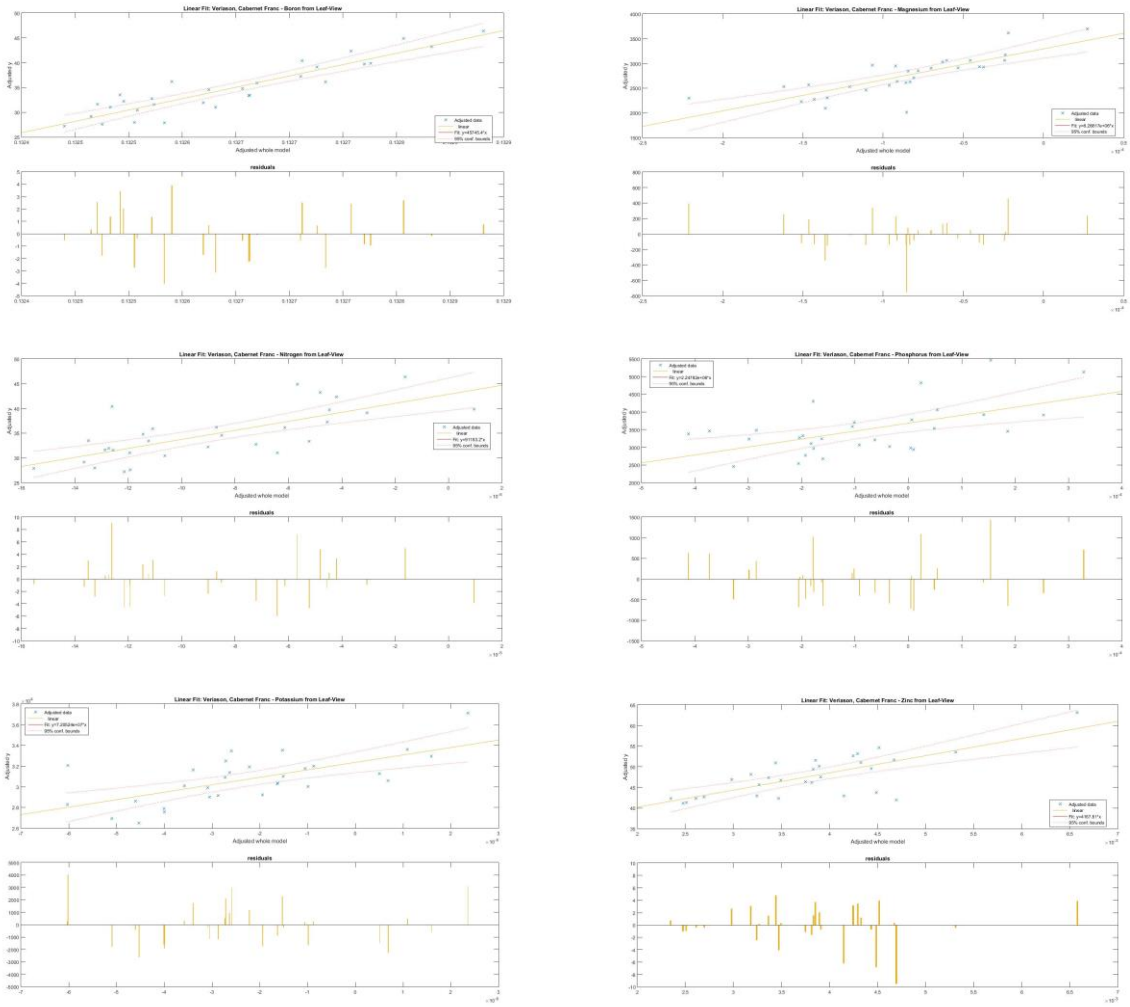

Figure 46: Linear modeling fit for 1nm Cabernet Franc reflectance data collected during veraison phenological stage at the leaf view angle: (a) boron, (b) magnesium, (c) nitrogen, (d) phosphorus, (e) potassium, (f) zinc

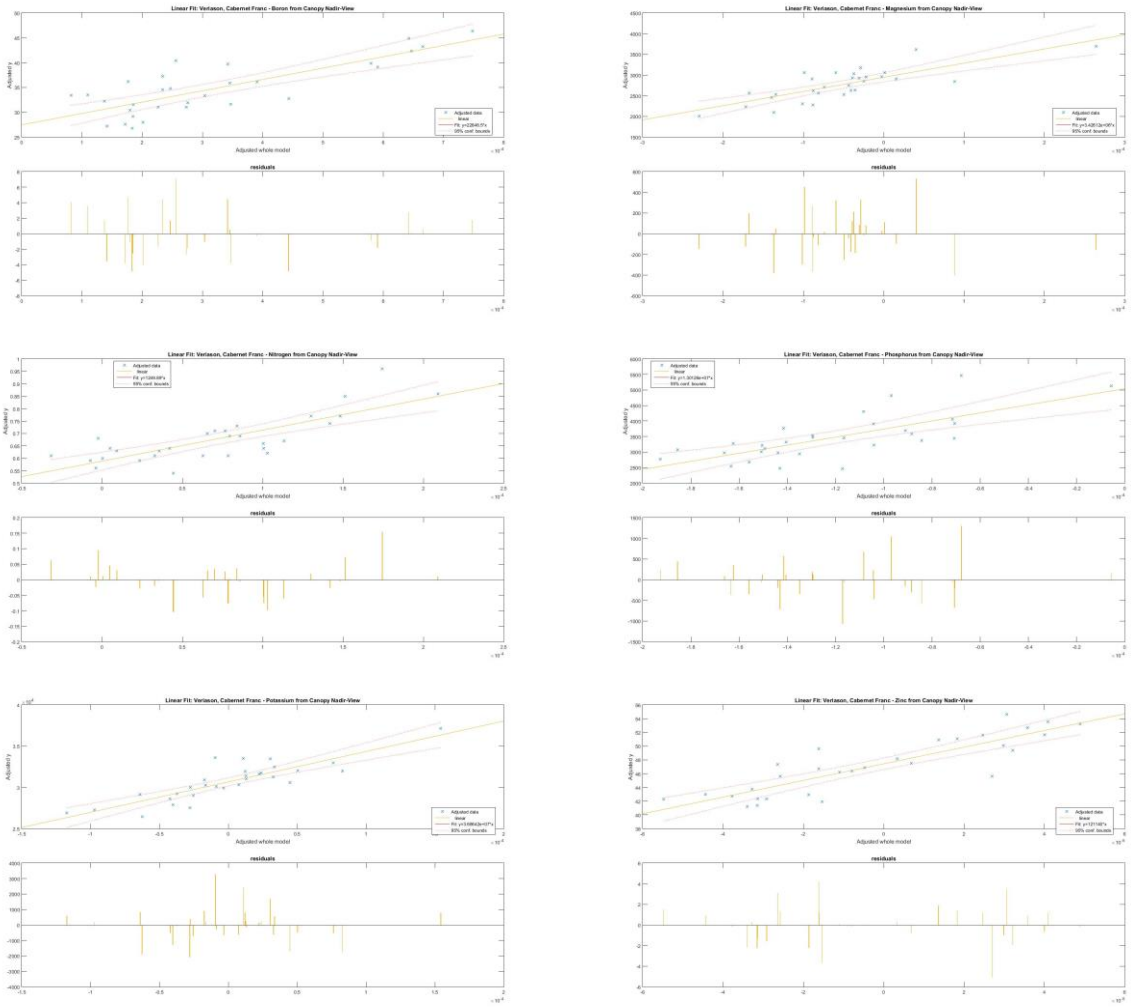

Figure 47: Linear modeling fit for 1nm Cabernet Franc reflectance data collected during veraison phenological stage at the canopy nadir view angle: (a) boron, (b) magnesium, (c) nitrogen, (d) phosphorus, (e) potassium, (f) zinc

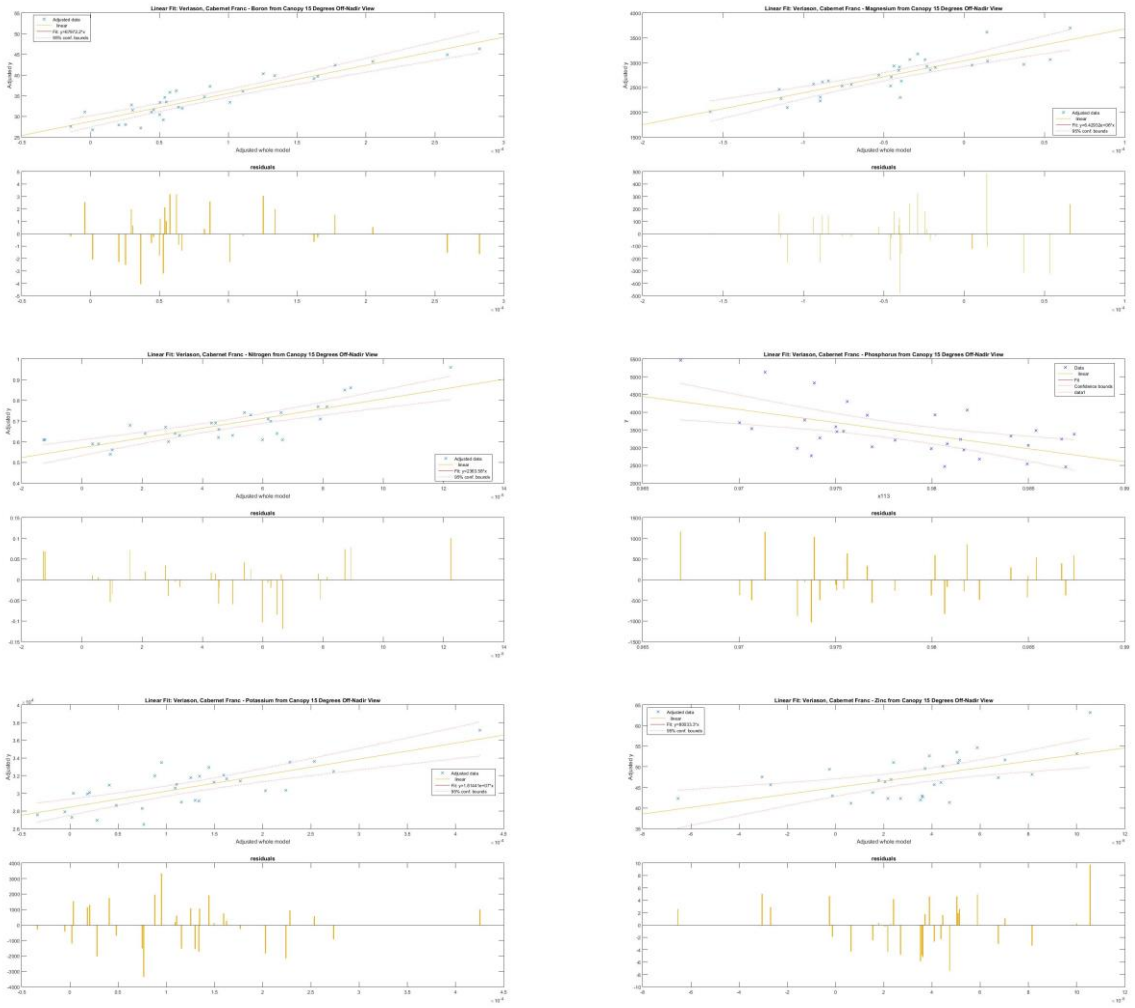

Figure 48: Linear modeling fit for 1nm Cabernet Franc reflectance data collected during veraison phenological stage at the canopy 15^{o} off-nadir view angle: (a) boron, (b) magnesium, (c) nitrogen, (d) phosphorus, (e) potassium, (f) zinc

The next evaluation is concerned with bloom results for Riesling (Tables 77-79), where we observed that the SLR-based method, using 1st derivative spectral data, once again was the predominant method for generating the highest R^2 values. It was also found that the linear fit using the normalized difference index performed the best for K at the canopy nadir view-angle; this was the only instance that the standard linear fit approach, based on normalized difference index data, created the best model fit for one of the nutrients.

Table 77: Peak R^2 values for 1nm Riesling nutrient models from the bloom phenological stage at the leaf view angle

Bloom Riesling				Leaf View		
Nutrient	**Method**	**Rsquared**	**Rsquared Adjusted**	**Criterion**	**RMSE**	**Wavelengths for Peak Value**
Boron	SLR - Derivative	0.75	0.70	R^2	3.35 (mg/kg)	862/944/974/975
Magnesium	SLR - Derivative	0.78	0.74	R^2	575.55 (mg/kg)	405/411/859/937
Nitrogen	SLR - Derivative	0.79	0.74	R^2	0.05 (%)	674/762/868/938
Phosphorus	SLR - Derivative	0.53	0.49	R^2	2514.34 (mg/kg)	938/945
Potassium	SLR - Derivative	0.71	0.68	R^2	1960.71 (mg/kg)	921/975
Zinc	SLR - Derivative	0.84	0.81	R^2	6.42 (mg/kg)	870/951/963/976

Table 78: Peak R^2 values for 1nm Riesling nutrient models from the bloom phenological stage at the canopy nadir view angle

Bloom Riesling				Canopy Nadir View		
Nutrient	**Method**	**Rsquared**	**Rsquared Adjusted**	**Criterion**	**RMSE**	**Wavelengths for Peak Value**
Boron	SLR - Derivative	0.71	0.66	R^2	3.55 (mg/kg)	539/631/817
Magnesium	SLR - Derivative	0.75	0.71	R^2	600.78 (mg/kg)	452/904/936
Nitrogen	SLR - Derivative	0.66	0.58	R^2	0.06 (%)	773/878/936/971
Phosphorus	SLR - Derivative	0.84	0.79	R^2	1602.91 (mg/kg)	778/863/878/936/943
Potassium	NDI Linear Fit	0.51	0.48	N/A	2500.43 (mg/kg)	463/464
Zinc	SLR - Derivative	0.63	0.55	R^2	9.80 (mg/kg)	866/870/900/963

Table 79: Peak R^2 values for 1nm Riesling nutrient models from the bloom phenological stage at the canopy 15^o off-nadir view angl

Bloom Riesling				Canopy 15 Degrees Off-Nadir View		
Nutrient	**Method**	**Rsquared**	**Rsquared Adjusted**	**Criterion**	**RMSE**	**Wavelengths for Peak Value**
Boron	SLR - Derivative	0.46	0.41	R^2	4.70 (mg/kg)	407/773
Magnesium	SLR - All Wavelengths	0.58	0.49	BIC	800.47 (mg/kg)	405/706/834/939
Nitrogen	SLR - Derivative	0.81	0.76	R^2	0.05 (%)	408/479/545/941/948
Phosphorus	SLR - Derivative	0.68	0.62	R^2	2180.53 (mg/kg)	454/467/870/872
Potassium	SLR - All Wavelengths	0.53	0.43	R^2	2636.00 (mg/kg)	400/403/408/416
Zinc	SLR - Derivative	0.62	0.54	R^2	9.94 (mg/kg)	777/848/870/921

e

Regardless of the SLR method employed, the fit was based solely on how high the generated R^2 value was. This outcomes was expected, but must be confirmed to ensure that a non-linear fit would not have been more appropriate for a different SLR data set.

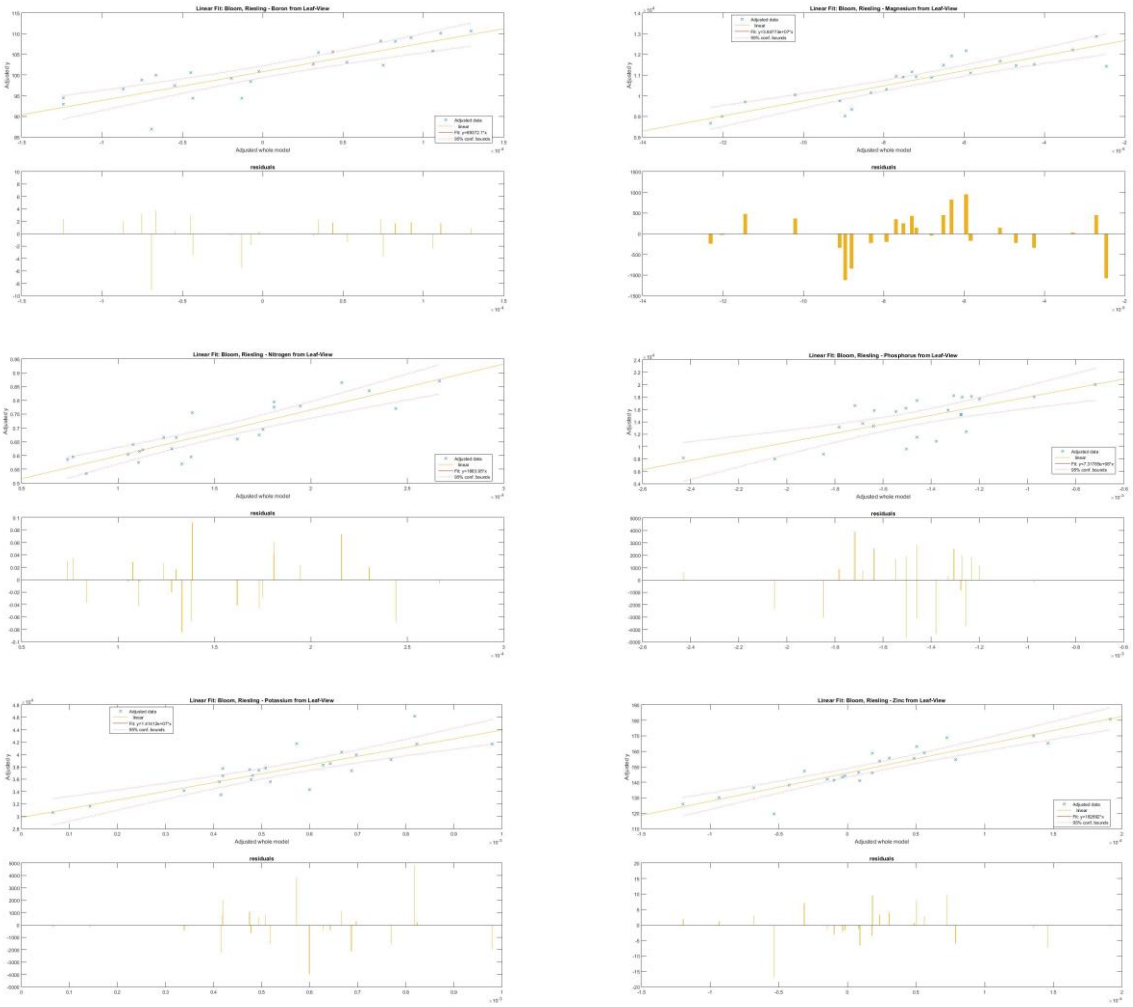

Figure 49: Linear modeling fit for 1nm Riesling reflectance data collected during bloom phenological stage at the leaf view angle: (a) boron, (b) magnesium, (c) nitrogen, (d) phosphorus, (e) potassium, (f) zinc

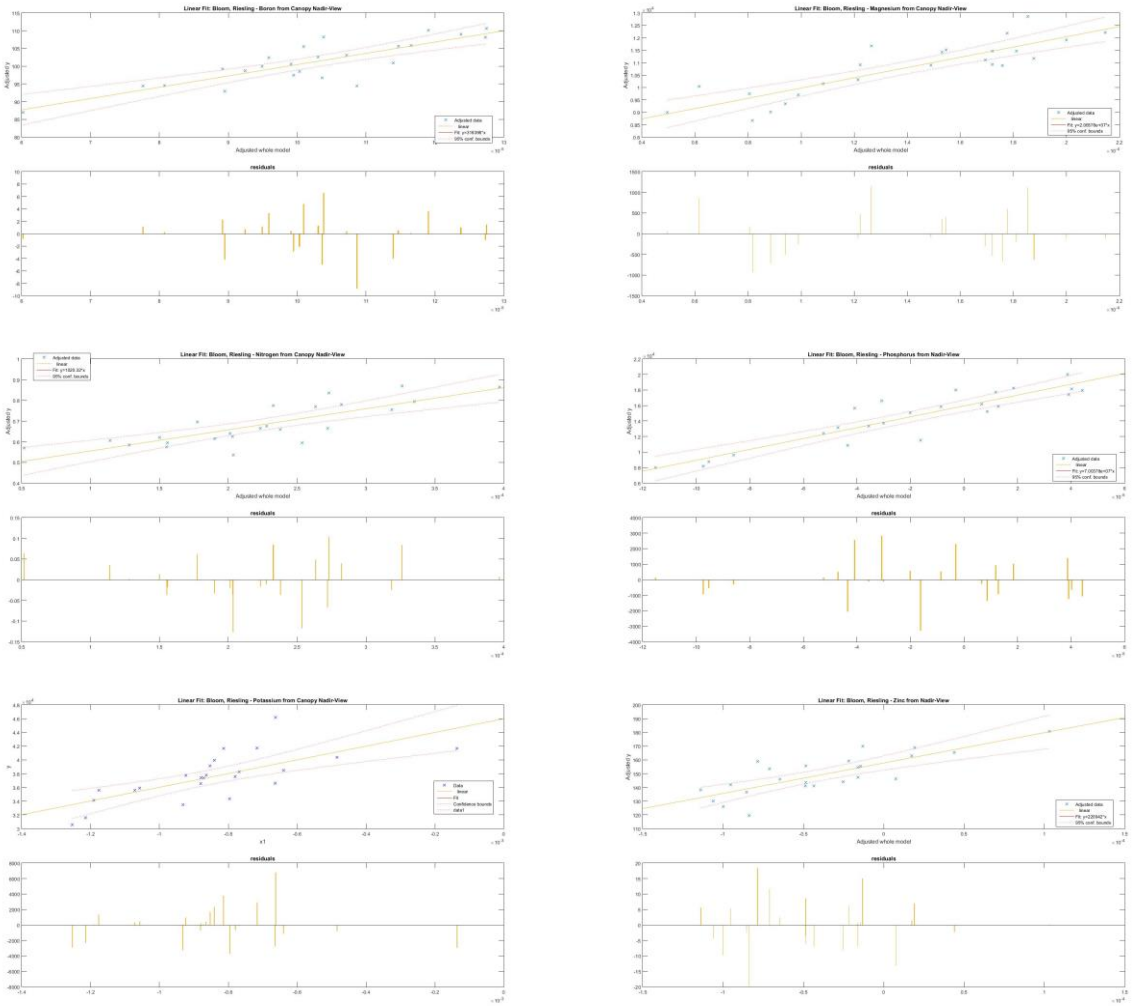

Figure 50: Linear modeling fit for 1nm Riesling reflectance data collected during bloom phenological stage at the canopy nadir view angle: (a) boron, (b) magnesium, (c) nitrogen, (d) phosphorus, (e) potassium, (f) zinc

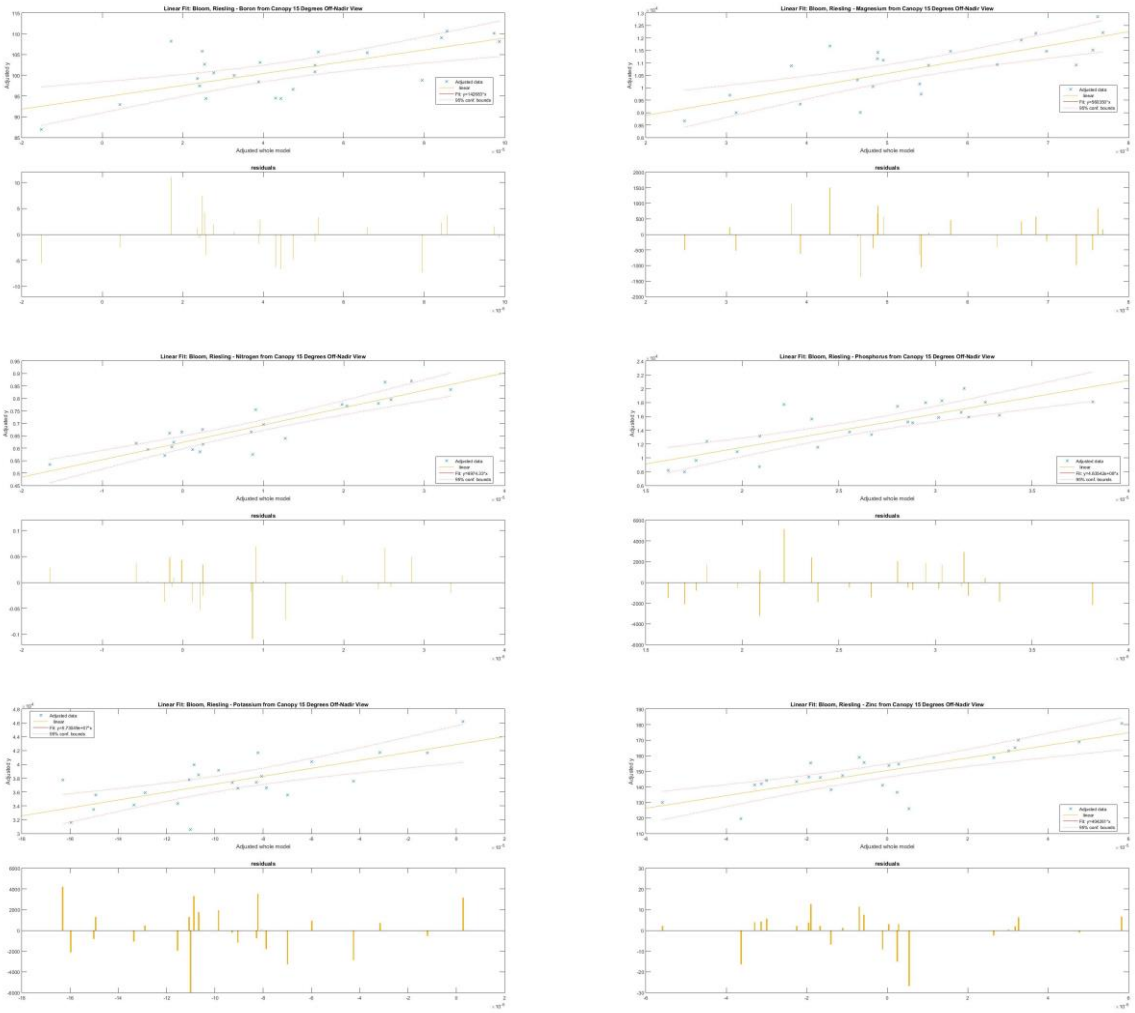

Figure 51: Linear modeling fit for 1nm Riesling reflectance data collected during bloom phenological stage at the canopy 15^{o} off-nadir view angle: (a) boron, (b) magnesium, (c) nitrogen, (d) phosphorus, (e) potassium, (f) zinc

The derivative method again tended to be used the most to generate the peak R^2 values for Riesling during veraison (Tables 80-82). For the canopy 15^{o} off-nadir view, we found that the highest occurrence of other model fit methods being used to generate solid model results - fully half of the nutrient models with peak model fits stemmed from either continuum removal SLR or the wavelength SLR. Unfortunately, there did not appear to be a pattern across the cultivars and growing seasons regarding which nutrients are best fit with a data manipulation method, other than the solid-performing 1st derivative-based models.

Table 80: Peak R^2 values for 1nm Riesling nutrient models from the veraison phenological stage at the leaf view angle

Veraison Riesling				Leaf View		
Nutrient	**Method**	**Rsquared**	**Rsquared Adjusted**	**Criterion**	**RMSE**	**Wavelengths for Peak Value**
Boron	SLR - Derivative	0.53	0.46	R^2	3.72 (mg/kg)	424/627/777
Magnesium	SLR - Derivative	0.62	0.58	R^2	252.23 (mg/kg)	400/975
Nitrogen	SLR - Continuum Removal	0.81	0.77	BIC	0.09 (%)	677/679/723/730
Phosphorus	SLR - Derivative	0.65	0.59	R^2	600.33 (mg/kg)	799/875/945
Potassium	SLR - Derivative	0.57	0.49	R^2	1793.91 (mg/kg)	403/411/428/940
Zinc	SLR - Derivative	0.68	0.63	R^2	3.57 (mg/kg)	420/465/873

Table 81: Peak R^2 values for 1nm Riesling nutrient models from the veraison phenological stage at the canopy nadir view angle

Veraison Riesling				Canopy Nadir View		
Nutrient	**Method**	**Rsquared**	**Rsquared Adjusted**	**Criterion**	**RMSE**	**Wavelengths for Peak Value**
Boron	SLR - Derivative	0.81	0.77	R^2	3.34 (mg/kg)	400/481/564/971
Magnesium	SLR - Derivative	0.63	0.59	R^2	250.39 (mg/kg)	884/921
Nitrogen	SLR - Derivative	0.84	0.81	R^2	0.06 (%)	420/468/758/872
Phosphorus	SLR - Derivative	0.74	0.70	R^2	539.68 (mg/kg)	883/946/959
Potassium	SLR - Derivative	0.72	0.65	R^2	1313.87 (mg/kg)	400/401/950/971
Zinc	SLR - Derivative	0.70	0.67	R^2	2.22 (mg/kg)	865/996

Table 82: Peak R^2 values for 1nm Riesling nutrient models from the veraison phenological stage at the canopy 15^o off-nadir view angle

Veraison Riesling				Canopy 15 Degrees Off-Nadir View		
Nutrient	**Method**	**Rsquared**	**Rsquared Adjusted**	**Criterion**	**RMSE**	**Wavelengths for Peak Value**
Boron	SLR - Derivative	0.62	0.56	R^2	3.05 (mg/kg)	429/448/464
Magnesium	SLR - Continuum Removal	0.72	0.65	aic	364.28 (mg/kg)	560/573/667/674/698
Nitrogen	SLR - Derivative	0.63	0.60	R^2	0.06 (%)	826/883
Phosphorus	SLR - Continuum Removal	0.67	0.57	BIC	514.66 (mg/kg)	658/659/662/679/690
Potassium	SLR - Derivative	0.16	0.12	R^2	1561.62 (mg/kg)	410
Zinc	SLR - All Wavelengths	0.81	0.74	aic	4.98 (mg/kg)	438/443/454/474/475/706

We again observed no issues regarding the model fit, based on visual inspection of Figures 52-54. We are confident that for all data sets and associated nutrient-spectral models, the relationship was in fact linear and that residuals were normally distributed, without any obvious non-modeled trends.

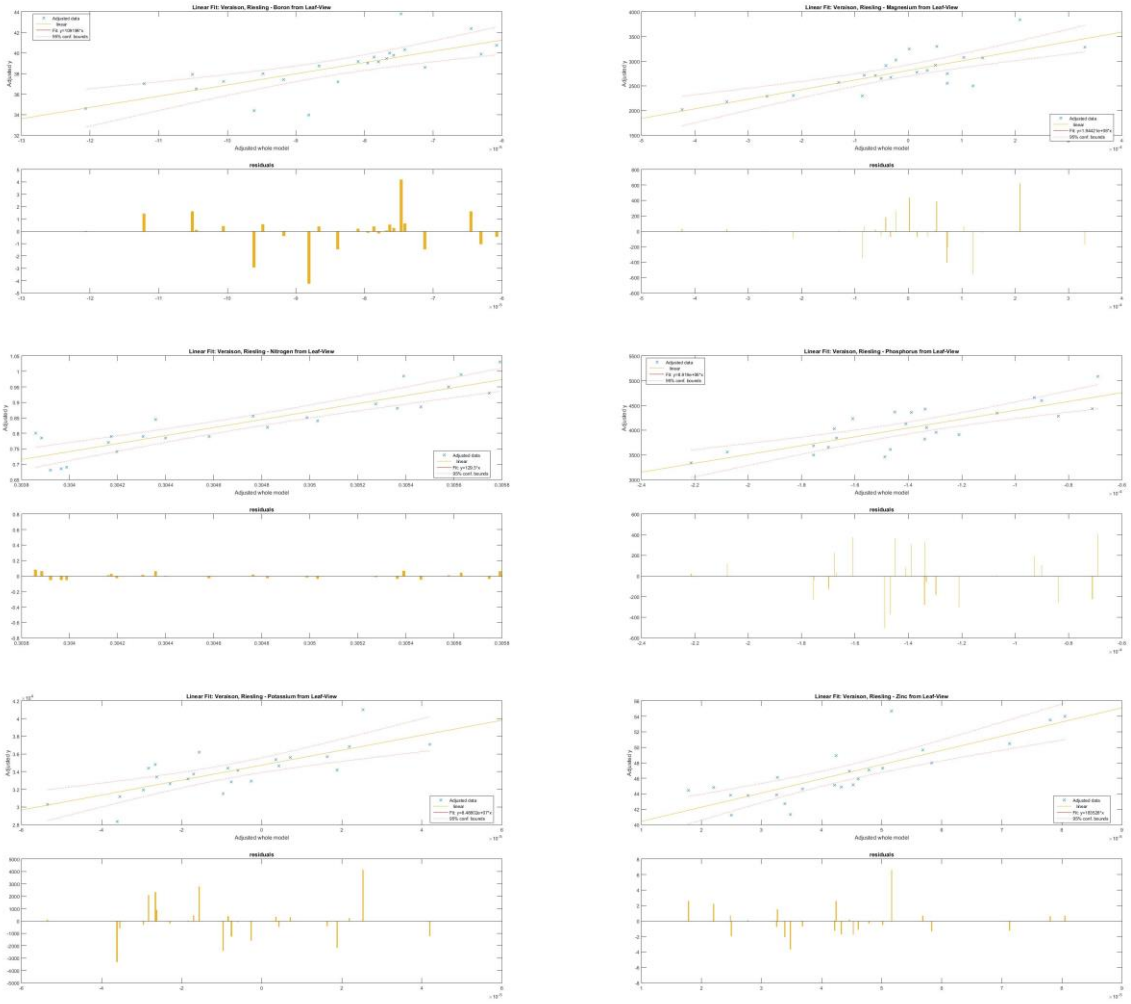

Figure 52: Linear modeling fit for 1nm Riesling reflectance data collected during veraison phenological stage at the leaf view angle: (a) Boron, (b) Magnesium, (c) Nitrogen, (d) Phosphorus, (e) Potassium, (f) Zinc

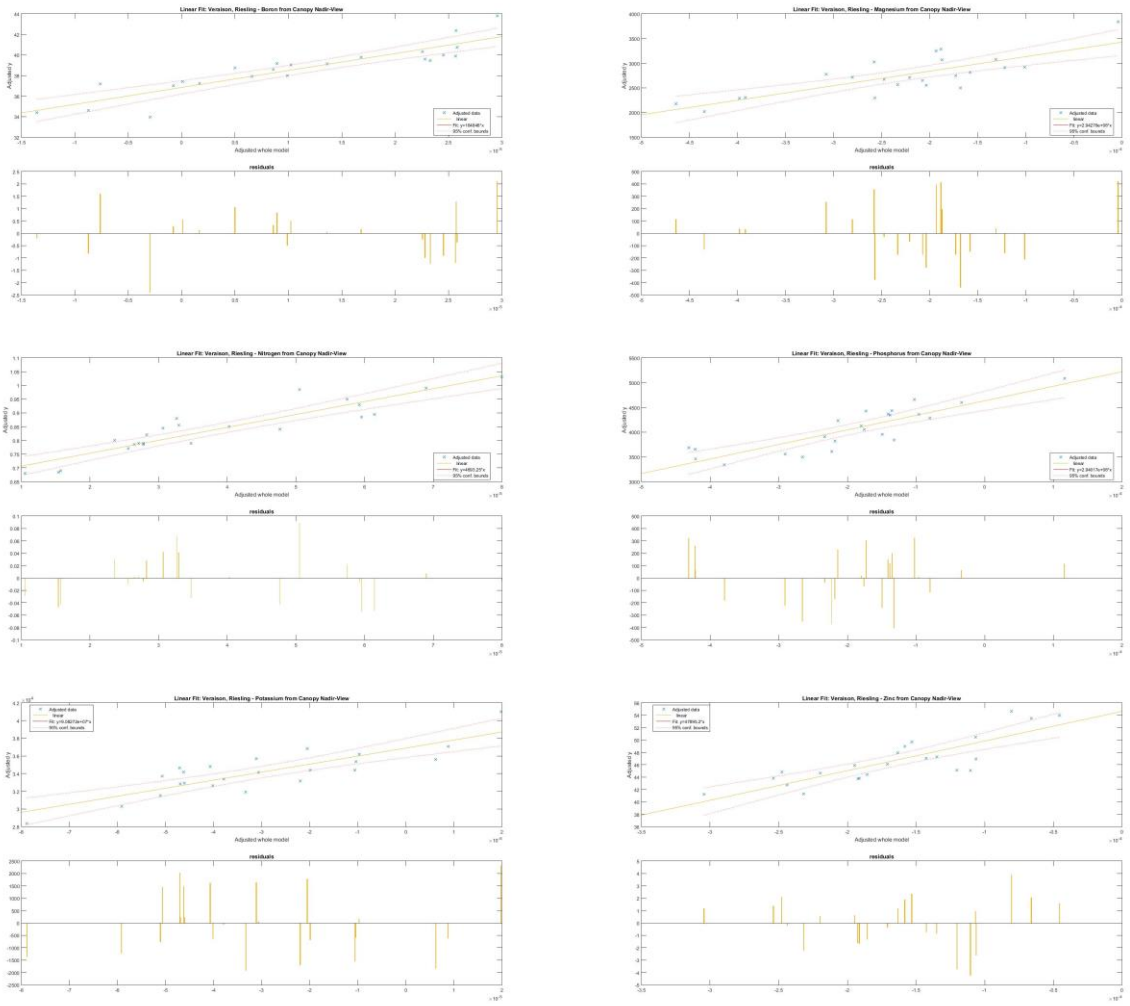

Figure 53: Linear modeling fit for 1nm Riesling reflectance data collected during veraison phenological stage at the canopy nadir view angle: (a) Boron, (b) Magnesium, (c) Nitrogen, (d) Phosphorus, (e) Potassium, (f) Zinc

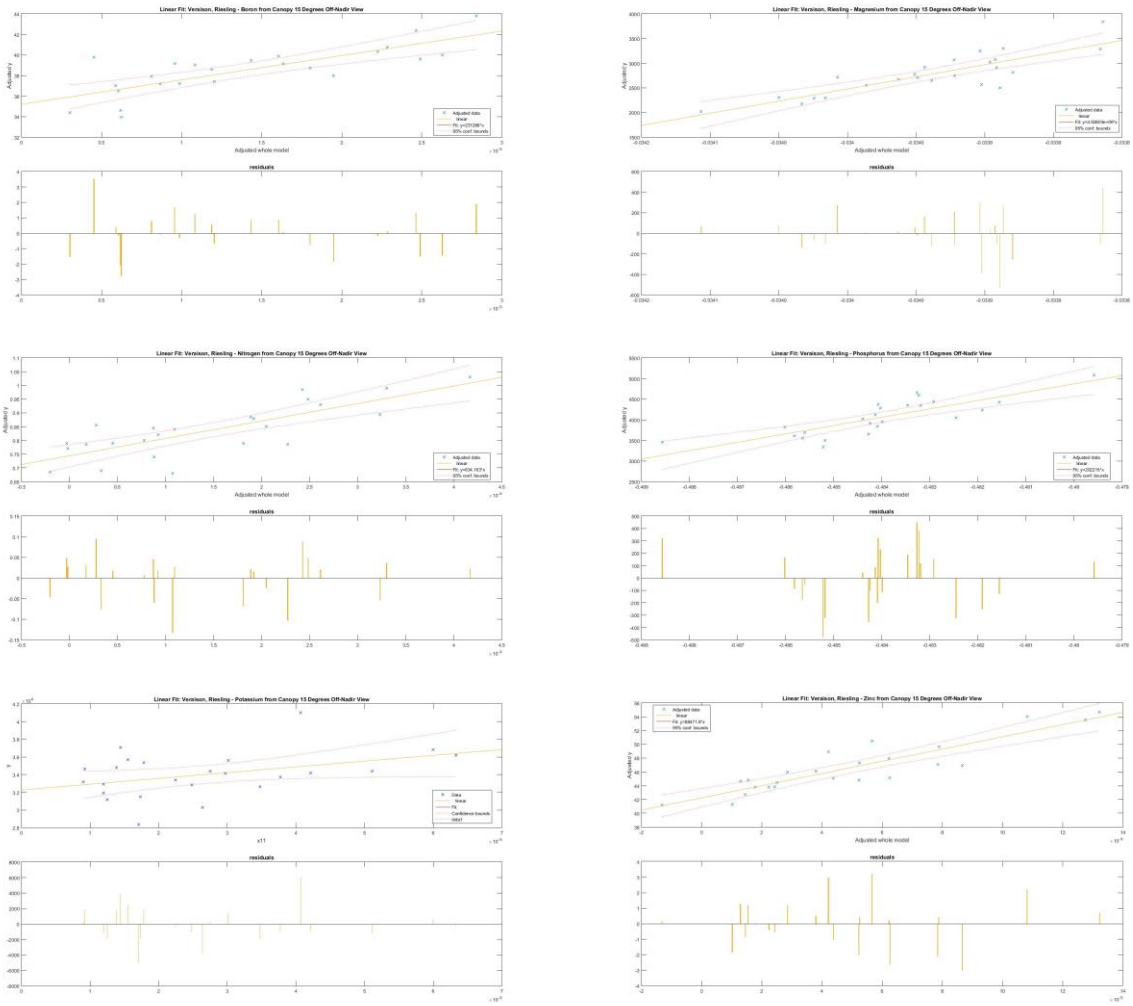

Figure 54: Linear modeling fit for 1nm Riesling reflectance data collected during veraison phenological stage at the canopy 15° off-nadir view angle: (a) Boron, (b) Magnesium, (c) Nitrogen, (d) Phosphorus, (e) Potassium, (f) Zinc

We concluded that of the 72 peak model results: 55 were generated by the derivative SLR, seven by continuum removal SLR, eights by the wavelength SLR, and one each by the correlated NDI and NDI linear fit approaches. The continuum removal SLR results were based on between four and ten wavelength bands, averaging six wavelengths/bands over the set. The wavelength SLR results were created using between four and nine wavelength bands, averaging five (rounded from 5.38 to eliminate the "partial" band). The correlated NDI SLR result and the NDI linear fit results were each made up of two bands. The derivative SLR results were generated from between one and five wavelength bands, averaging three bands (3.24 unrounded). Although the wavelength bands used by the derivative method were actually a combination of two separate wavelengths, i.e., the derivative method required between two and ten wavelengths, averaging six wavelengths in order

to produce a full set of peak results, it was still encouraging that a relatively limited set of bands could be identified for future, potentially operational nutrient modeling. While this average number of wavelengths tied for highest among the methods employed, the 1st derivative method also resulted in the highest R^2 values over the full set of nutrients, and therefore should be the method of choice if only one method was required.

The next analysis step involved identifying the wavelengths necessary for generating the best model fit for the nutrient data; specifically, we were interested in where these wavelengths were located, and how they vary between the nutrients, cultivars, and growing seasons. We therefore recorded the number of times that the wavelengths appeared in the case of the peak R^2 model values for the six nutrients (Tables 71-82 above). These wavelengths then were grouped into 10nm bins for ease of viewing and plotted based on the different criteria mentioned above (cultivar, growing season, and nutrient). This effort resulted in plots that show which regions of the visible and NIR spectrum performed best for each given criteria. Note, for all the plots below, an approximate trend line for the grape vine reflectance spectra has been added for improved visual interpretation relative to the various parts of the EMR spectrum. This trend line is approximate, as it has been taken from a single data sample from Cabernet Franc during bloom and it therefore does not change with cultivar or season.

Figure 55 shows the breakdown of important wavelengths, plotted for the combined cultivars with Cabernet Franc in blue and Riesling in red. We see that the majority of useful wavelengths were located either in the blue and (low) green regions, or in the near-infrared regions of the spectrum. There are a total of 255 bands shown here, with 132 coming from Cabernet Franc and 123 from Riesling.

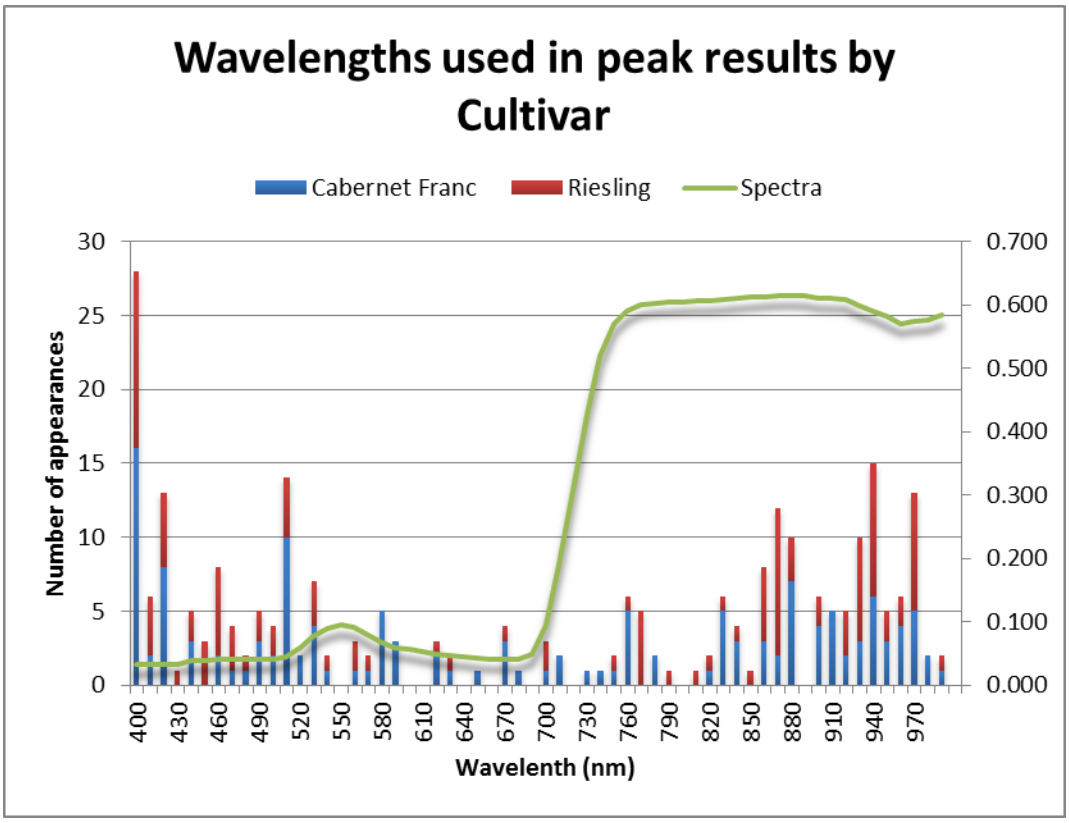

Figure 55: Wavelengths used in linear modeling for 1nm peak results, cultivars combined

In breaking out the results by cultivar, it can easily be seen from the side-by-side comparison that of the two cultivars, Riesling exhibited a higher concentration of wavelengths in the NIR range, 860-980nm, and in the blue range. Cabernet Franc, while having a large number of wavelengths in the 400-410nm range, similar to Riesling, was spread more evenly over the blue and the NIR, as well as some representation in the green spectral region. It also exhibited more wavelengths in the red and red edge region, when compared to results for the Riesling cultivar.

Figure 57 shows the same list of wavelengths as seen in Figure 55, but this time the blue bands are those wavelengths that were used to generate the peak values from bloom, and the red from veraison. The wavelengths used only for bloom are shown below in Figure 58, broken down by cultivar; of the 130 bands that make up Figure 57, 67 are from Cabernet Franc and 63 from Riesling analyses.

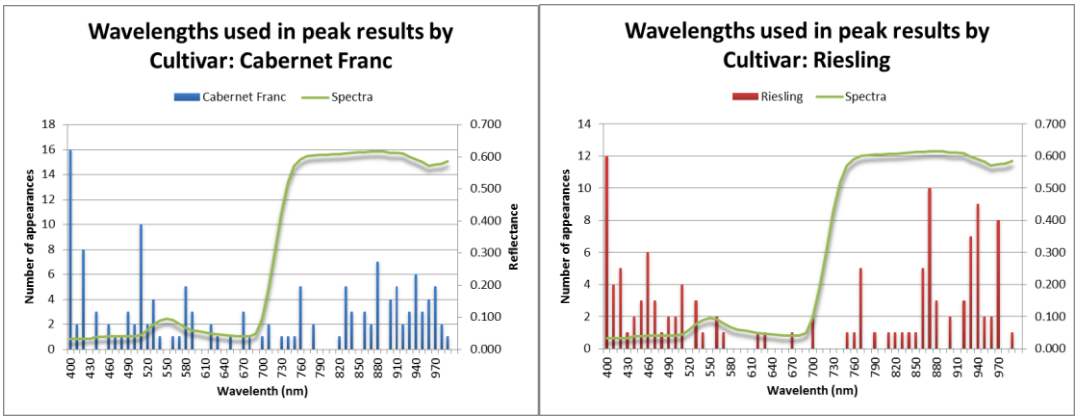

Figure 56: Wavelengths used in linear modeling for 1nm peak results by cultivar: (a) Cabernet Franc, (b) Riesling

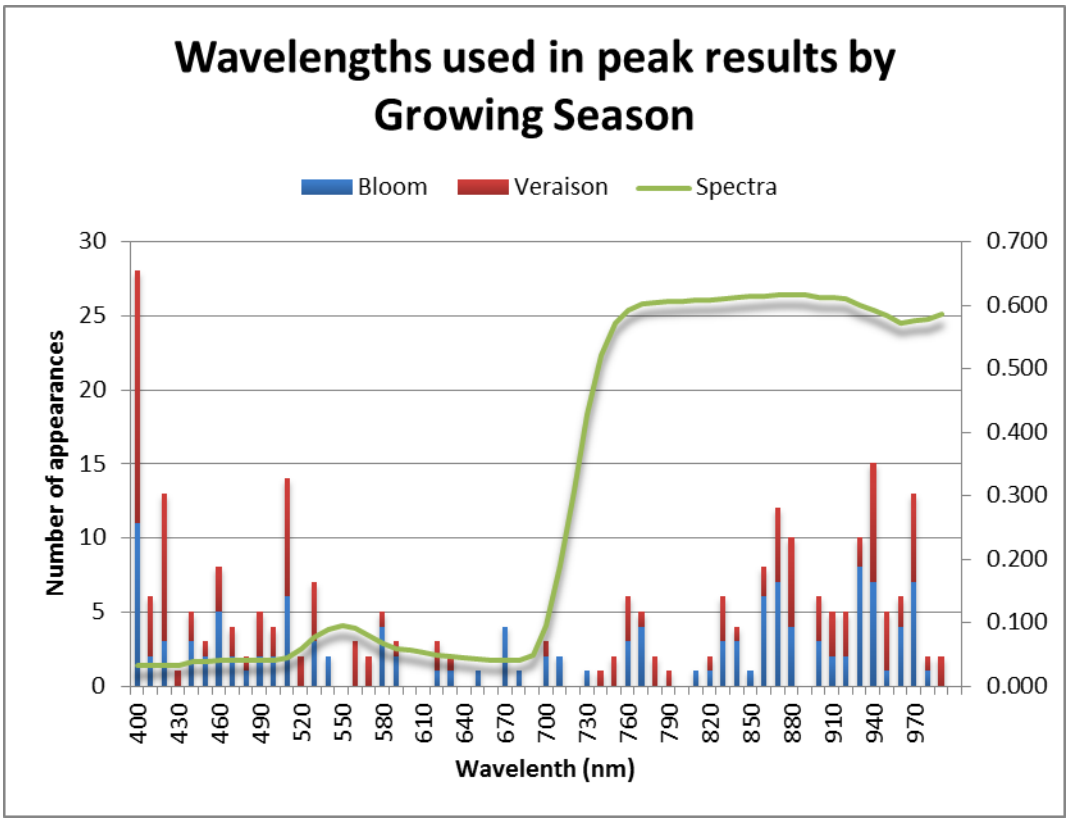

Figure 57: Wavelengths used in linear modeling for 1nm peak results, growing seasons combined

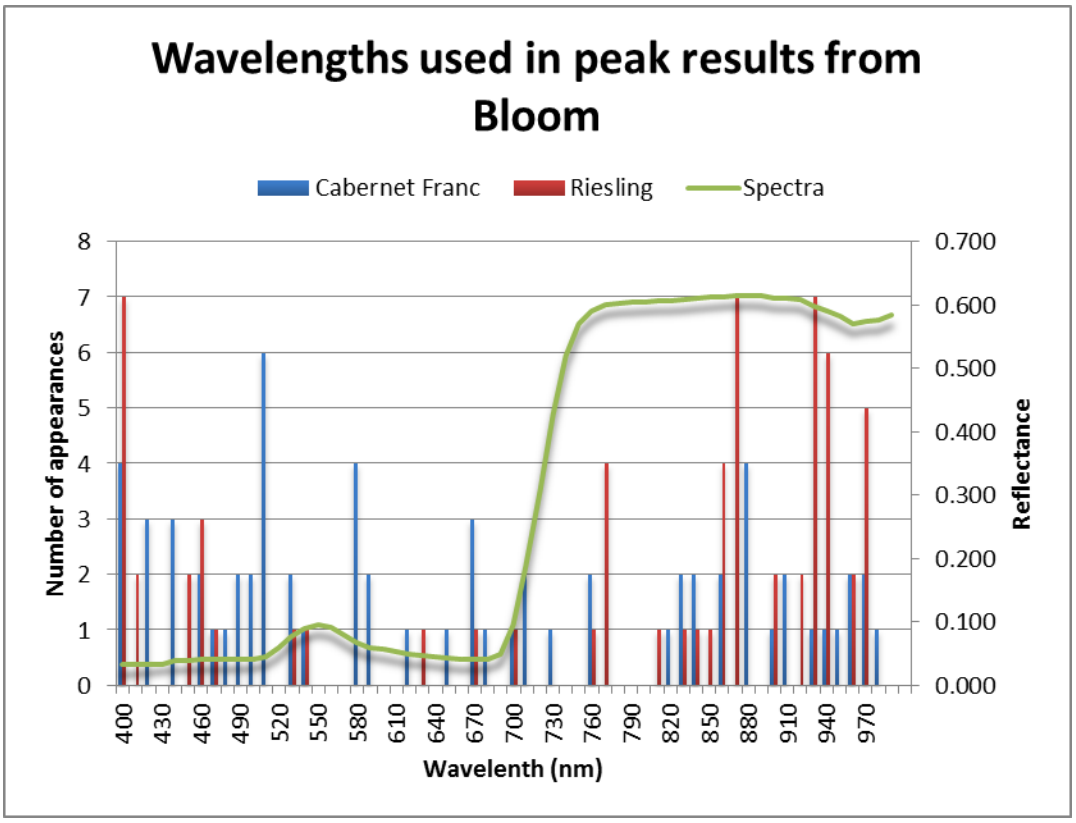

Figure 58: Wavelengths used in linear modeling for 1nm peak results, bloom combined

Furthermore, when comparing the two cultivars during bloom (Figure 59), Cabernet Franc exhibited wavelengths similar to those seen for this cultivar over both growing seasons, i.e., more representation in the blue and NIR, but spread across the complete silicon range. Riesling on the other hand, was heavily weighted towards the NIR region of the silicon spectrum during bloom.

In the case of veraison (Figure 60), the number of wavelengths in the NIR appears to be reduced, when compared to those observed for bloom. This was observed along with a reduction in the number of bands required to form the peak models, i.e., a slight reduction from 130 bands to 125 bands.

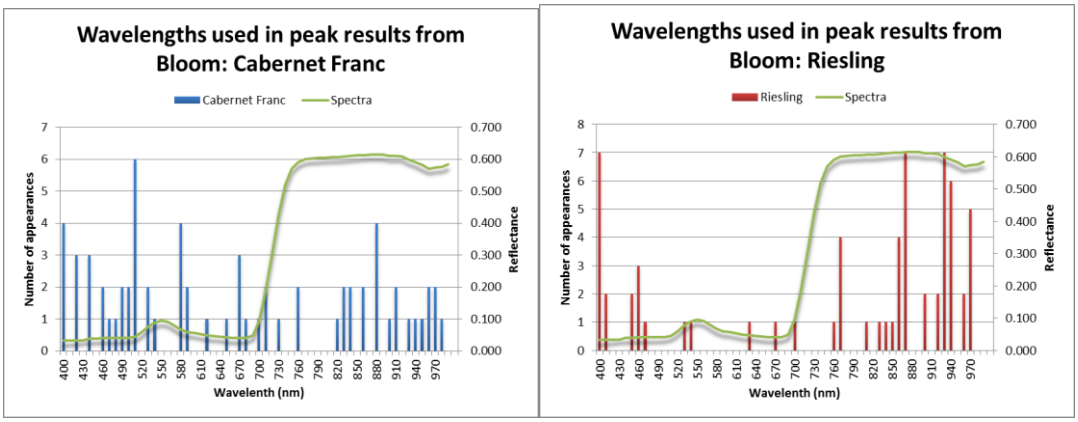

Figure 59: Wavelengths used in linear modeling for 1nm peak results from bloom: (a) Cabernet Franc, (b) Riesling

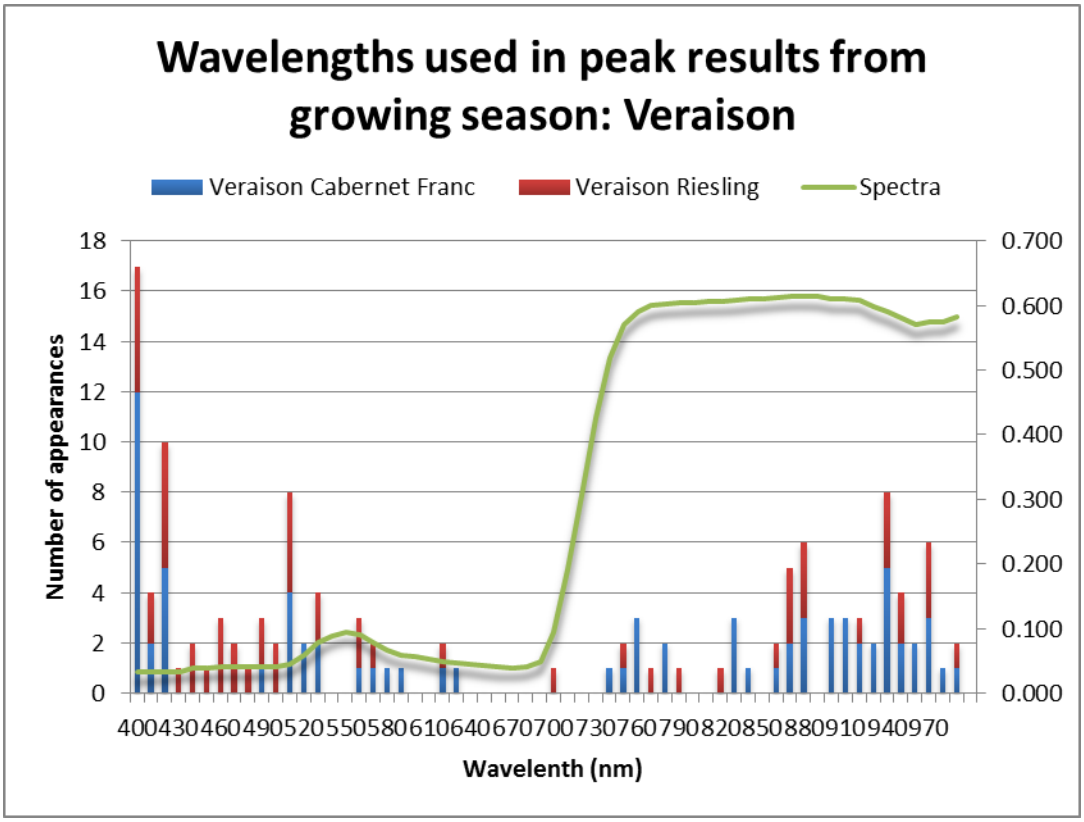

Figure 60: Wavelengths used in linear modeling for 1nm peak results, veraison combined

The 65 wavelengths used in modeling by Cabernet Franc nutrient relationships during veraison were much less distributed across the complete spectrum. Instead we found that they were clumped in three regions: the low 400nm range in blue, across the green part of the spectrum, and spread across the NIR. Interestingly, none of the wavelengths were located in the red or on the red edge. Riesling modeling was based on 60 bands from predominantly in the NIR and some blue

during bloom, to being heavily in the blue, with some wavelengths coming from the high 800/900nm ranges during veraison.

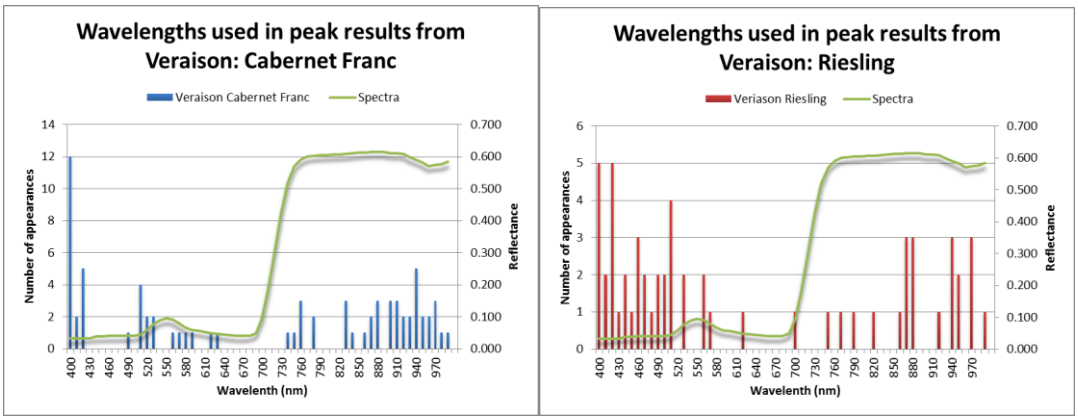

Figure 61: Wavelengths used in linear modeling for 1nm peak results from veraison: (a) Cabernet Franc, (b) Riesling

Breaking down the wavelengths used by the six nutrients we have the combined result in Figure 62 below.

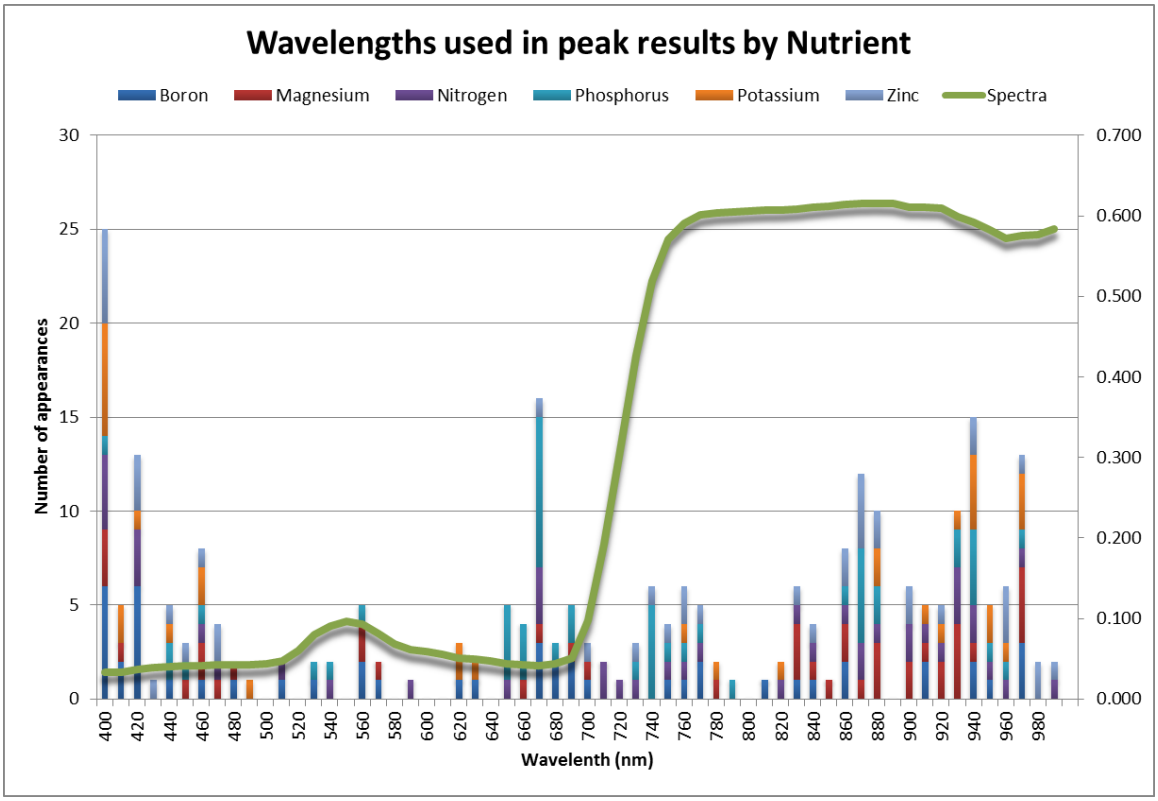

Figure 62: Wavelengths used in linear modeling for 1nm peak results, nutrients combined

In an examination of B first, we found that the 12 peak model values use 48 bands. These wavelengths were spread over the whole silicon spectrum, but the largest concentrations were located in the low blue and low green wavelength regions. Demir and Serindag (2006), based on their work with grapes and associated B concentrations, found that the maximum absorption for B in grapes was located at 412nm. Our results corroborated the findings from that study, where large concentrations of wavelengths being used for modeling B were located in and around this 412nm region.

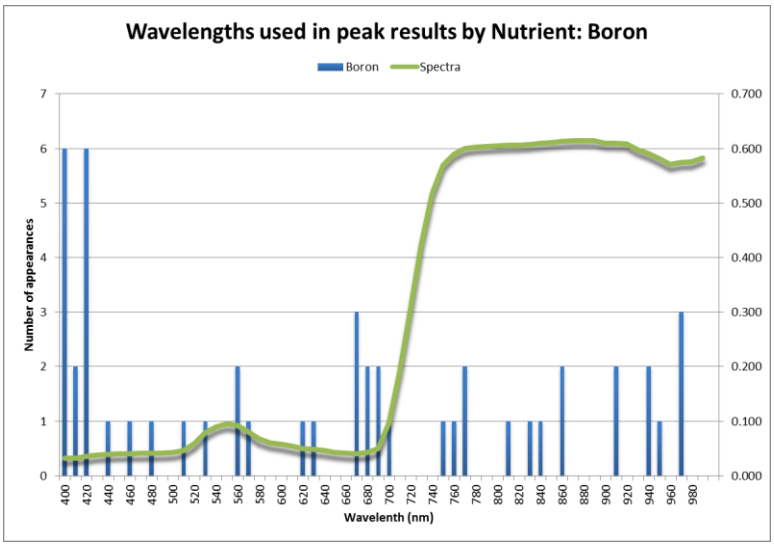

Figure 63: Wavelengths used in linear modeling for 1nm peak results, nutrients boron

Magnesium nutrient modeling used only 42 bands and the bands were more clumped, in contrast to the 48 bands that B modeling required. The majority of the bands fell in the NIR above 830nm, while the remainder, excluding two bands in the lower NIR and red edge, were all in the green and blue spectral regions. These observations for Mg agreed with what was seen in the heat maps produced from the highly correlated indices. High correlation areas were created by a combination of wavelengths in the blue to green and wavelengths in the NIR, combined with blue-green, or between two NIR bands.

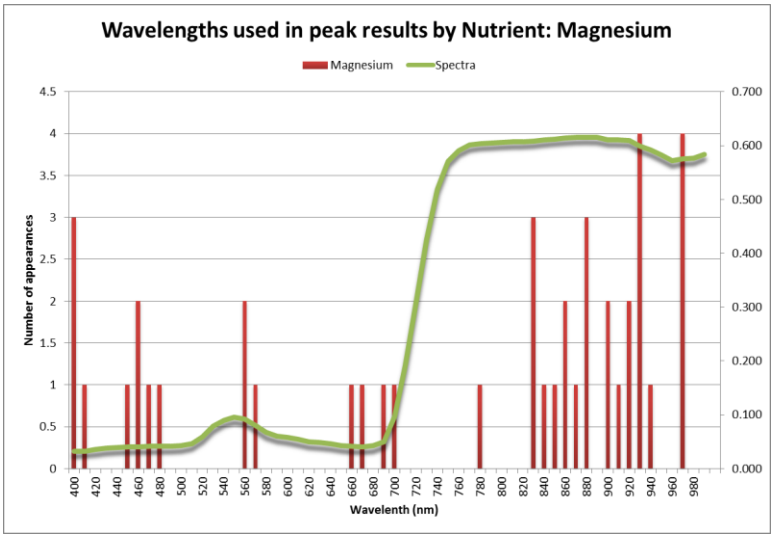

Figure 64: Wavelengths used in linear modeling for 1nm peak results, nutrients magnesium

Figure 65 shows the 43 bands used for N modeling, which like B were spread across the silicon spectrum, while the higher concentrations occurred in the low blue and high NIR. Elvidge and Chen (1995) used narrow spectral bands from the reflectance spectra collected from rooted pinyon pine canopy and found that the most pronounced chlorophyll absorption feature was located at 674nm. Although this study did not focus on pinyon trees, we acknowledge that chlorophyll has a close relationship to N content (Hunt Jr *et al.,* 2013). One of the wavelengths used by our methods for the model fit for N was indeed 674nm, agreeing with the previous research cited here. The main physiological reason that live vegetation has a red edge feature, is that chlorophyll causes a rise in the NIR part of the spectrum, along with increased NIR backscatter due to intercellular spaces in leaves. It stands to reason than that, since the N content is closely related to the chlorophyll content of a plant, a model fit for N would require a number of wavelengths from the NIR region of the spectrum (Eismann 2012).

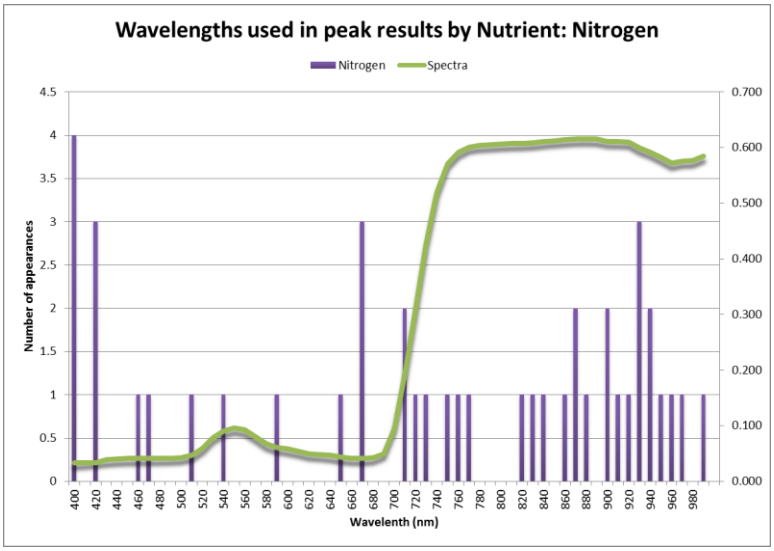

Figure 65: Wavelengths used in linear modeling for 1nm peak results, nutrients nitrogen

Figure 66 shows that it took 53 wavelengths/bands to generate the peak P R^2 values. While a number of the bands were located in the NIR region, the largest group of bands was situated in the green region of the spectrum. The distribution of bands used for the P modeling agrees with the spectral regions that exhibited high correlations with the indices from the two cultivars.

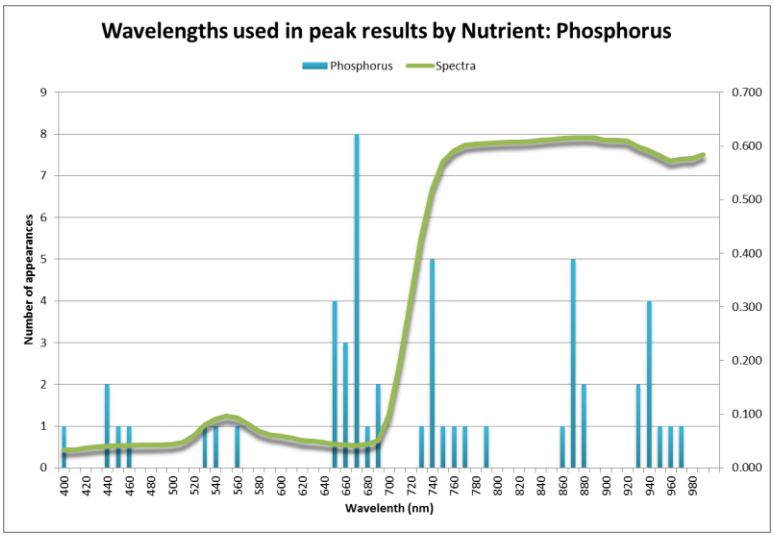

Figure 66: Wavelengths used in linear modeling for 1nm peak results, nutrients phosphorus

The K results (Figure 67) were formed using the smallest number of bands, i.e., only 34. Similar to what we have seen before, these mostly were located in the NIR and blue regions of the spectrum. Smart *et al.* (2007) discusses the symptoms of K deficiency in their work. They found that signs of

this were found at 495nm and 625nm. It is worth noting that, while the majority of the samples were within the nutrient range or above (Wolfe, 2008), a few of the samples did have lower levels of K then the sufficiency range listed. This could account for the inclusion of wavelengths around 495nm and 625nm in K-specific modeling results.

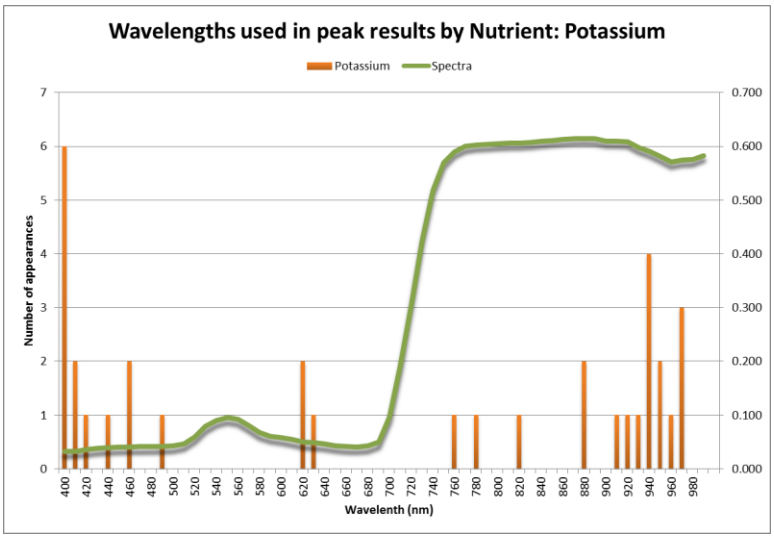

Figure 67: Wavelengths used in linear modeling for 1nm peak results, nutrients potassium

Finally, Zn used 44 bands to achieve the peak model results. These bands were concentrated across the NIR and blue regions of the spectrum. A couple bands were identified in the red trough or the start of the red edge, but none of the bands were located in red or green spectral regions. The wavelength distribution furthermore agreed well with the heat maps: From the Riesling heat map we found a small area of high correlation formed by the combination of blue bands. Also, the peak correlation values were generated for the two cultivars by a pair of bands in the 870nm range, which corresponds to Figure 68.

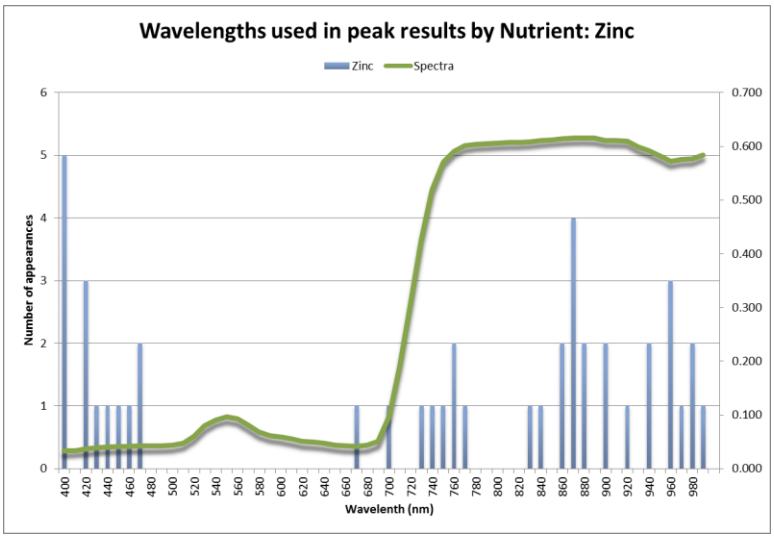

Figure 68: Wavelengths used in linear modeling for 1nm peak results, nutrients zinc

We concluded that, based on our examination of the distribution of the wavelengths for the nutrients of interest, the wavelengths used in the models to fit the nutrient data generally conform to the wavelengths used in the correlation heat maps. We furthermore observed that the wavelengths used in the nutrient models generally conformed to the wavelengths used in the correlation heat maps. In addition, regions of interest for particular nutrients matched with those from other studies conducted on the same nutrients, which provided evidence that our nutrient data and models were robust selections.

5.3 Results and discussion – 10nm data

The analysis of the 10nm proceeded in the same order as the 1nm data. A more abbreviated version of the 10nm data results will be presented, since the 1nm data were fully described and explained above in a step-by-step process, showing all the results that were achieved. A summary of the results will be discussed, with a focus on the level of the model fit and the differences seen between the 10nm and 1nm results.

The first step was to test the correlation of the NDI indices. In the case of the Cabernet Franc cultivar during bloom only, B viewed at canopy-nadir surpassed the CC≥0.70 threshold. For the veraison data, however, it was found that none of the nutrient-view angle combinations met the threshold level, while for the Riesling cultivar during bloom, only one nutrient-view angle combination exceeded the threshold (Mg viewed at the leaf level). However, there were a significant number of wavelength combinations that generated a CC value that exceeded the 0.70

threshold for veraison. These were Mg, viewed at canopy-nadir and canopy 15° off-nadir, N at all three view angles, and P, viewed at canopy-nadir and canopy 15° off-nadir. For the various nutrient-view angles that correlated highly over the cultivars and growing seasons, the correlation coefficients ranged between 0.71-0.79.

The heat maps for the high correlations were plotted in the same manner as for the 1nm data, in order to see which combination of wavelength bands formed the peak and highly correlated values. An example of the heat maps is seen in Figure 69 below, for Cabernet Franc during bloom, depicting the results for B when viewed at canopy-nadir. A comparison with the heat map from the 1nm data reveals that the shape of the correlations matches, though the peak values differ. For the 1nm data, the peak value was generated by two wavelengths in the mid 400nm range, while for the 10nm data, the peak was formed by bands at 704nm and 521nm.

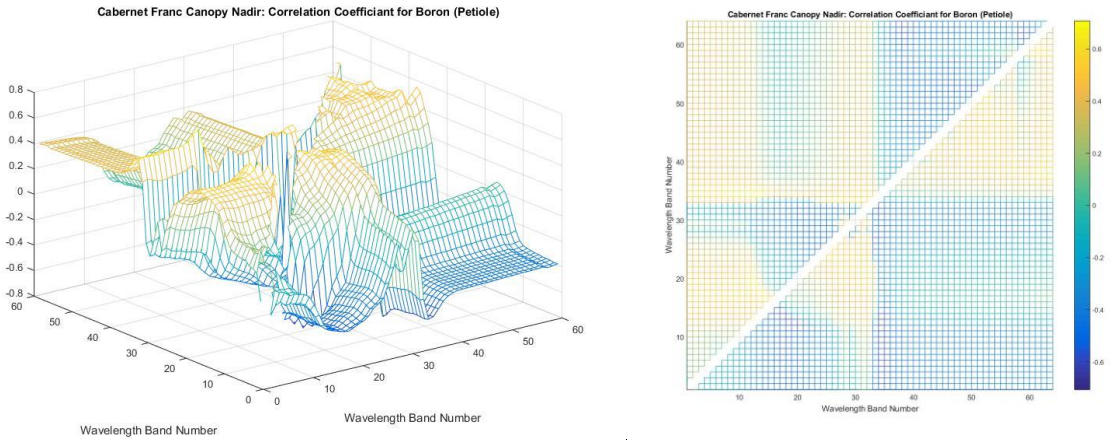

Figure 69: 10nm Bloom Cabernet Franc boron canopy nadir: (a) 3-D view, (b) 2-D view

We found that, for the 10nm data collected from the Riesling cultivar during bloom, the correlation heat map for Mg (viewed at leaf level) matched the heat map for the 1nm data. However, unlike the Cabernet Franc B results, the wavelengths generating the peak value for Mg modeling matched as well. This was a unique result among the heat maps. In all the cases, the shape of the correlations matched between the 1nm and 10nm data. In all nine nutrient-view angle combinations from the 10nm data with high correlations, this is the only one in which the peak values aligned.

The *linear fit* for each of the nutrient-view angle combinations that achieved a high correlation next was evaluated. Unlike the 1nm data, where the input to the linear fit was restricted to the indices that correlated highly, for the 10nm data there were only 4,096 possible indices, so all indices were used in the linear fit. From these combinations, R^2 values ranged between 0.50 - 0.63. We then ran a

step-wise linear regression using the 64 wavelength bands as input variables. The results showed R^2 values for the models ranging between 0.10-0.75. Similar to the 1nm data, only two to four nutrients from each view achieved non-zero results, and all of these non-zero results came from the use of the AIC criterion.

Running the *SLR on the correlated NDI* for the 10nm data turned out to generate less effective models for the nutrient data than were created using the linear fit. The R^2 values for the correlated NDI SLR ranged between 0-0.54, where the linear fit was between 0.50-0.63.

The 1st derivatives then were used as the input variables to the SLR, which resulted in all three criteria producing results without using an excessive number of wavelengths, as was seen when using the AIC and BIC criterion for the 1nm data. The peak fits were generated from a mixture of all three criteria. For Cabernet Franc, the SLR produced non-zero results for all six nutrients during both growing seasons. The values ranged from 0.09-0.95; however, in order to generate the peak value of 0.95, it required 15 separate derivative values as model input. For Riesling, two cases resulted in zero model fits, namely Zn at canopy 15^{o} off-nadir from bloom and B at canopy nadir view angle during veraison; other than these two cases, the remainder varied between 0.08-0.73.

Finally, continuum removal in the SLR approach yielded similar results to the 1nm effort, i.e., for most view angles, between the two cultivars and growing seasons, a mixture of non-zero and zero model fits were generated. The peak model fit came from N when based on the veraison Riesling data (leaf-view). This combination also performed well for the 1nm data.

A table for the peak model fit values was generated for each cultivar and growing season combination, as was the case for the 1nm data. A comparison between the 1nm and 10nm peak results in Tables 83-85 shows that, for all nutrients in the 10nm data that used a method other than derivative SLR to generate the peak model, the 1nm data also used a method other than the derivative SLR. The methods did not match in all cases, but for those nutrients it was discovered that at those specific view angles for Cabernet Franc during bloom, the 1st derivative approach did not model the nutrients the best.

Table 83: Peak R^2 values for 10nm Cabernet Franc nutrient models from the bloom phenological stage at the leaf view angle

Bloom Cabernet Franc				Leaf View		
Nutrient	**Method**	**Rsquared**	**Rsquared Adjusted**	**Criterion**	**RMSE**	**Wavelengths for Peak Value**
Boron	SLR - Derivative	0.71	0.57	AIC	2.71 (mg/kg)	424/560/674/753/811/879/898/927/937/966
Magnesium	SLR - Derivative	0.49	0.41	AIC/BIC	603.96 (mg/kg)	472/840/937/976
Nitrogen	SLR - Correlated Wavelengths	0.61	0.57	AIC/BIC	0.08 (%)	414/521/714
Phosphorus	SLR - Derivative	0.71	0.61	AIC	1844.47 (mg/kg)	405/472/560/792/850/947/966/976
Potassium	SLR - Derivative	0.67	0.58	BIC	4860.42 (mg/kg)	472/492/840/869/937/976
Zinc	SLR - Derivative	0.62	0.54	AIC/BIC	6.52 (mg/kg)	792/840/879/937/947

Table 84: Peak R^2 values for 10nm Cabernet Franc nutrient models from the bloom phenological stage at the canopy nadir view angle

Bloom Cabernet Franc				Canopy Nadir View		
Nutrient	**Method**	**Rsquared**	**Rsquared Adjusted**	**Criterion**	**RMSE**	**Wavelengths for Peak Value**
Boron	SLR - Correlated Wavelengths	0.62	0.54	AIC	2.79 (mg/kg)	531/541/714/937/956
Magnesium	SLR - Derivative	0.26	0.21	AIC	700.96 (mg/kg)	743/850
Nitrogen	SLR - Derivative	0.93	0.89	BIC	0.04 (%)	511/580/589/599/638/658/665/674/704/840/869/918
Phosphorus	SLR - Derivative	0.79	0.72	BIC	990.17 (mg/kg)	414/434/609/840/927/937/956
Potassium	SLR - Derivative	0.65	0.60	BIC	4775.23 (mg/kg)	589/840/937/956
Zinc	SLR - Derivative	0.56	0.45	AIC	7.14 (mg/kg)	434/762/821/840/889/976

Table 85: Peak R^2 values for 10nm Cabernet Franc nutrient models from the bloom phenological stage at the canopy 15^o off-nadir view angle

Bloom Cabernet Franc				Canopy 15 Degrees Off-Nadir View		
Nutrient	**Method**	**Rsquared**	**Rsquared Adjusted**	**Criterion**	**RMSE**	**Wavelengths for Peak Value**
Boron	SLR - Derivative	0.73	0.61	AIC	2.59 (mg/kg)	472/772/821/850/908/918/927/937/956
Magnesium	SLR - Derivative	0.43	0.39	BIC/R^2	625.35 (mg/kg)	453/472
Nitrogen	SLR - Derivative	0.32	0.21	AIC	0.11 (%)	628/889/898/956
Phosphorus	SLR - Correlated Wavelengths	0.75	0.65	AIC	1126.76 (mg/kg)	404/424/434/472/531/541/684/723
Potassium	SLR - Derivative	0.57	0.48	BIC	5469.40 (mg/kg)	648/668/860/869/927
Zinc	SLR - Derivative	0.62	0.54	BIC	6.64 (mg/kg)	619/674/889/947/956

It furthermore was observed that for the Cabernet Franc data from veraison, based on 10nm spectral bands, only B modeling at the canopy nadir view-angle used a model other than the derivative SLR. For the 1nm data, a larger number of nutrient-view angle combinations used a method other than the derivative SLR, but in a similar fashion to the 10nm data, the derivative method was the most common. A qualitative comparison between the two spectral resolutions used, showed that the 1nm data generally had better model fits; however, in the cases where the 1nm data generated poorer model fits, the 10nm data also resulted in lower model performance.

Table 86: Peak R^2 values for 10nm Cabernet Franc nutrient models from the veraison phenological stage at the leaf view angle

Veraison Cabernet Franc				Leaf View		
Nutrient	**Method**	**Rsquared**	**Rsquared Adjusted**	**Criterion**	**RMSE**	**Wavelengths for Peak Value**
Boron	SLR - Derivative	0.95	0.90	AIC	1.66 (mg/kg)	414/463/541/560/658/753/762/772/792/821/898/908/918/956/966
Magnesium	SLR - Derivative	0.84	0.77	BIC	188.49 (mg/kg)	531/541/811/831/860/879/889/927
Nitrogen	SLR - Derivative	0.54	0.46	AIC	0.07 (%)	658/850/869/966
Phosphorus	SLR - Derivative	0.34	0.30	AIC	596.24 (mg/kg)	472/956
Potassium	SLR - Derivative	0.32	0.27	AIC/BIC/R^2	1941.37 (mg/kg)	658/908
Zinc	SLR - Derivative	0.75	0.66	AIC	2.96 (mg/kg)	414/463/472/723/733/743/753/927

Table 87: Peak R^2 values for 10nm Cabernet Franc nutrient models from the veraison phenological stage at the canopy nadir view angle

Veraison Cabernet Franc				Canopy Nadir View		
Nutrient	**Method**	**Rsquared**	**Rsquared Adjusted**	**Criterion**	**RMSE**	**Wavelengths for Peak Value**
Boron	SLR - Continuum Removal	0.71	0.58	AIC	3.44 (mg/kg)	560/655/665/684/704/714/733/743/753
Magnesium	SLR - Derivative	0.39	0.33	AIC/BIC/R^2	318.47 (mg/kg)	414/589/956
Nitrogen	SLR - Derivative	0.10	0.07	AIC/R^2	0.09 (%)	831
Phosphorus	SLR - Derivative	0.29	0.21	AIC	653.46 (mg/kg)	762/879/908
Potassium	SLR - Derivative	0.35	0.27	R^2	1984.51 (mg/kg)	414/723/850
Zinc	SLR - Derivative	0.35	0.28	AIC	3.50 (mg/kg)	443/840/860

Table 88: Peak R^2 values for 10nm Cabernet Franc nutrient models from the veraison phenological stage at the canopy 15° off-nadir view angle

Veraison Cabernet Franc				Canopy 15 Degrees Off-Nadir View		
Nutrient	**Method**	**Rsquared**	**Rsquared Adjusted**	**Criterion**	**RMSE**	**Wavelengths for Peak Value**
Boron	SLR - Derivative	0.73	0.67	AIC	3.06 (mg/kg)	463/472/674/782/811
Magnesium	SLR - Derivative	0.56	0.45	AIC	290.32 (mg/kg)	550/908/918/937/976/985
Nitrogen	SLR - Derivative	0.34	0.26	AIC	0.08 (%)	550/762/956
Phosphorus	SLR - Derivative	0.39	0.32	BIC/R^2	595.90 (mg/kg)	658/976/985
Potassium	SLR - Derivative	0.71	0.66	AIC	1360.50 (mg/kg)	405/860/879/956/976
Zinc	SLR - Derivative	0.09	0.05	AIC	4.84 (mg/kg)	762

Tables 89-91 show results for Riesling during bloom. There was no evident pattern regarding which methods produced the best model fit between the 1nm and 10nm data. In terms of the peak R^2 values achieved, the 10nm data was mostly inferior, with only one or two nutrients (and no consistency in which nutrients) per view-angle in the 10nm data generating a superior model fit.

Table 89: Peak R^2 values for 10nm Riesling nutrient models from the bloom phenological stage at the leaf view angle

Bloom Riesling				Leaf View		
Nutrient	**Method**	**Rsquared**	**Rsquared Adjusted**	**Criterion**	**RMSE**	**Wavelengths for Peak Value**
Boron	SLR - Derivative	0.45	0.37	BIC/R^2	4.85 (mg/kg)	762/927/985
Magnesium	NDI Linear Fit	0.60	0.58	N/A	1110.06 (mg/kg)	638/697
Nitrogen	SLR - Correlated Wavelengths	0.47	0.39	R^2	0.08 (%)	414/733
Phosphorus	SLR - Correlated Wavelengths	0.60	0.51	AIC	2454.66 (mg/kg)	405/918/927/947
Potassium	SLR - Derivative	0.48	0.43	BIC/R^2	2626.64 (mg/kg)	918/937
Zinc	SLR - Derivative	0.41	0.33	AIC	12.01 (mg/kg)	850/879/947

Table 90: Peak R^2 values for 10nm Riesling nutrient models from the bloom phenological stage at the canopy nadir view angle

Bloom Riesling				Canopy Nadir View		
Nutrient	**Method**	**Rsquared**	**Rsquared Adjusted**	**Criterion**	**RMSE**	**Wavelengths for Peak Value**
Boron	SLR - Derivative	0.30	0.27	BIC/R^2	5.23 (mg/kg)	762
Magnesium	SLR - Continuum Removal	0.26	0.19	AIC/BIC/R^2	1010.28 (mg/kg)	570/684
Nitrogen	SLR - Continuum Removal	0.65	0.52	AIC	0.07 (%)	570/580/599/619/665/743
Phosphorus	SLR - Derivative	0.23	0.20	BIC/R^2	3144.64 (mg/kg)	772
Potassium	SLR - Derivative	0.73	0.66	BIC	2038.20 (mg/kg)	531/589/638/658/956
Zinc	SLR - Derivative	0.22	0.15	AIC	13.50 (mg/kg)	550/850

Table 91: Peak R^2 values for 10nm Riesling nutrient models from the bloom phenological stage at the canopy 15° off-nadir view angle

Bloom Riesling				Canopy 15 Degrees Off-Nadir View		
Nutrient	**Method**	**Rsquared**	**Rsquared Adjusted**	**Criterion**	**RMSE**	**Wavelengths for Peak Value**
Boron	SLR - Derivative	0.70	0.57	AIC	4.01 (mg/kg)	414/733/743/821/840/927/947
Magnesium	SLR - Derivative	0.73	0.62	AIC	693.06 (mg/kg)	424/723/782/879/908/918/966
Nitrogen	SLR - Derivative	0.33	0.27	AIC/BIC/R^2	0.09 (%)	743/947
Phosphorus	SLR - Derivative	0.17	0.13	BIC/R^2	3278.20 (mg/kg)	443
Potassium	SLR - Derivative	0.33	0.26	AIC/BIC/R^2	2976.99 (mg/kg)	472/674
Zinc	SLR	0.00	0.00	AIC/BIC/R^2	14.61 (mg/kg)	N/A

Finally, when comparing the model fits for the veraison Riesling data (Table 92-94) it was found that, while the 1nm data was best modeled via the derivative method, the 10nm data used a larger combination of methods to generate the best model fits. With the exception of Mg at canopy-nadir and P at canopy-nadir from the 10nm data, the 1nm data produced better model fits in all cases.

Table 92: Peak R^2 values for 10nm Riesling nutrient models from the veraison phenological stage at the leaf view angle

Veraison Riesling				Leaf View		
Nutrient	**Method**	**Rsquared**	**Rsquared Adjusted**	**Criterion**	**RMSE**	**Wavelengths for Peak Value**
Boron	SLR - Derivative	0.43	0.30	AIC	1.94 (mg/kg)	443/628/840/966
Magnesium	SLR - Derivative	0.38	0.35	BIC/R^2	336.2 (mg/kg)	966
Nitrogen	SLR - Continuum Removal	0.74	0.68	AIC	0.05 (%)	648/665/684/723
Phosphorus	SLR - Derivative	0.51	0.44	AIC/BIC	329.19 (mg/kg)	414/792/869
Potassium	SLR	0.00	0.00	AIC/BIC/R^2	2250.47 (mg/kg)	N/A
Zinc	SLR - Continuum Removal	0.51	0.41	AIC	2.85 (mg/kg)	684/714/723/753

Table 93: Peak R^2 values for 10nm Riesling nutrient models from the veraison phenological stage at the canopy nadir view angle

Veraison Riesling				Canopy Nadir View		
Nutrient	**Method**	**Rsquared**	**Rsquared Adjusted**	**Criterion**	**RMSE**	**Wavelengths for Peak Value**
Boron	SLR	0.00	0.00	AIC/BIC/R^2	2.34 (mg/kg)	N/A
Magnesium	SLR - Derivative	0.73	0.63	AIC	249.59 (mg/kg)	541/743/762/956/985
Nitrogen	NDI Linear Fit	0.63	0.61	N/A	0.093 (%)	684/704
Phosphorus	SLR - Derivative	0.75	0.67	AIC/BIC	256.84 (mg/kg)	405/414/714/782/898
Potassium	SLR - Derivative	0.11	0.07	AIC/R^2	2441.46 (mg/kg)	762
Zinc	SLR - Derivative	0.61	0.54	AIC/BIC/R^2	2.55 (mg/kg)	821/918/976

Table 94: Peak R^2 values for 10nm Riesling nutrient models from the veraison phenological stage at the canopy 15° off-nadir view angle

Veraison Riesling				Canopy 15 Degrees Off-Nadir View		
Nutrient	**Method**	**Rsquared**	**Rsquared Adjusted**	**Criterion**	**RMSE**	**Wavelengths for Peak Value**
Boron	SLR - Derivative	0.48	0.41	R^2	1.79 (mg/kg)	424/463/589/609
Magnesium	SLR - Derivative	0.72	0.64	BIC	248.41 (mg/kg)	414/560/655/743/898
Nitrogen	SLR - Continuum Removal	0.61	0.57	AIC	0.06 (%)	570/580
Phosphorus	NDI Linear Fit	0.54	0.52	N/A	413.11 (mg/kg)	511/463
Potassium	SLR - Continuum Removal	0.09	0.05	AIC	2486.29 (mg/kg)	694
Zinc	SLR - All Wavelengths	0.71	0.63	AIC	2.25 (mg/kg)	443/453/472/511/704

Figure 70 shows the linear fits for the six nutrients from Cabernet Franc during veraison. It is evident from the residuals that there was no systematic form or trend to the residuals, implying that the linear fit was appropriate. The results from the other three cultivars and growing season combinations yielded similar results.

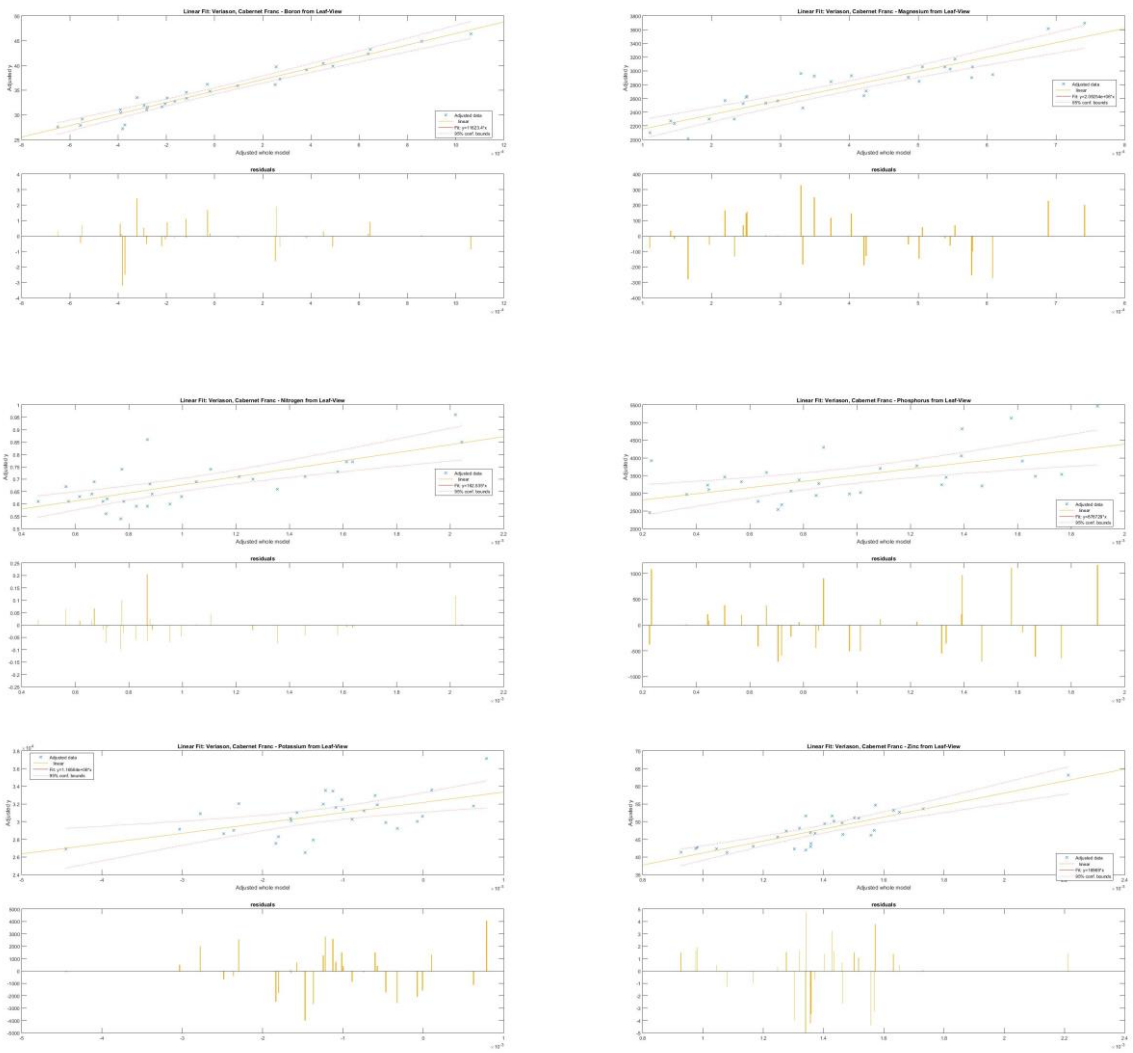

Figure 70: Linear modeling fit for 10nm Cabernet Franc reflectance data collected during the veraison phonological stage at the leaf view angle: (a) Boron, (b) Magnesium, (c) Nitrogen, (d) Phosphorus, (e) Potassium, (f) Zinc

In the same fashion as with the 1nm data, the wavelength bands that were used to generate the peak values were recorded and the distribution over the spectrum was plotted for each of the nutrients. Figure 71 shows the combined wavelength bands that were used in the formation of the peak models for the six nutrients for 10nm data. The peak modeling results for the nutrients used wavelength bands from across the spectrum, as was the case for the 1nm data. Each of the six nutrients are shown separately below in order to evaluate how they compare against the 1nm data in terms of wavelength selection for specific models.

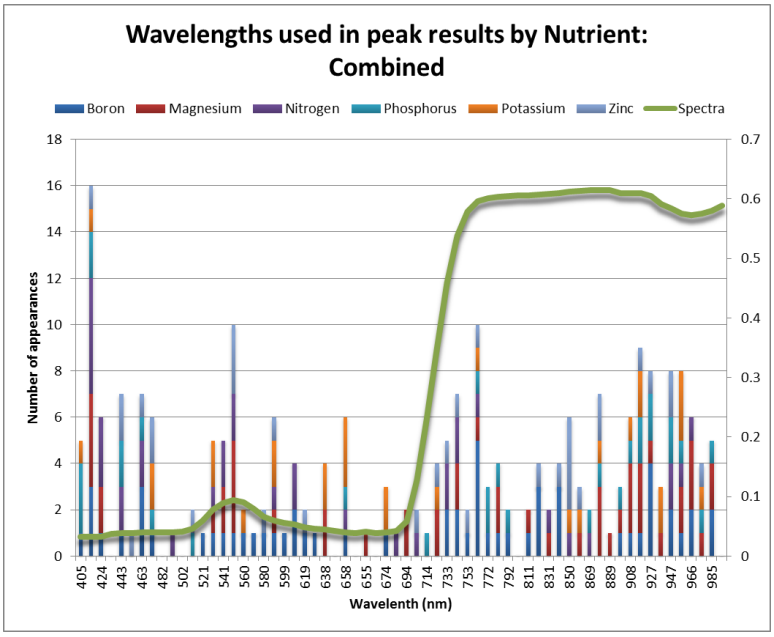

Figure 71: Wavelengths used in linear modeling for 10nm peak results, nutrients combined

Figure 72 shows the wavelengths used for B, which used 59 bands to form the peak models, compared to the 48 bands used by the 1nm data. Compared to the 1nm data, the 10nm data used more bands in the NIR region of the spectrum. Also, while the 1nm data contained a large number of bands in the low blue and low green wavelengths, the 10nm data pulled more strongly from across the whole green spectrum, as well as in the low blue.

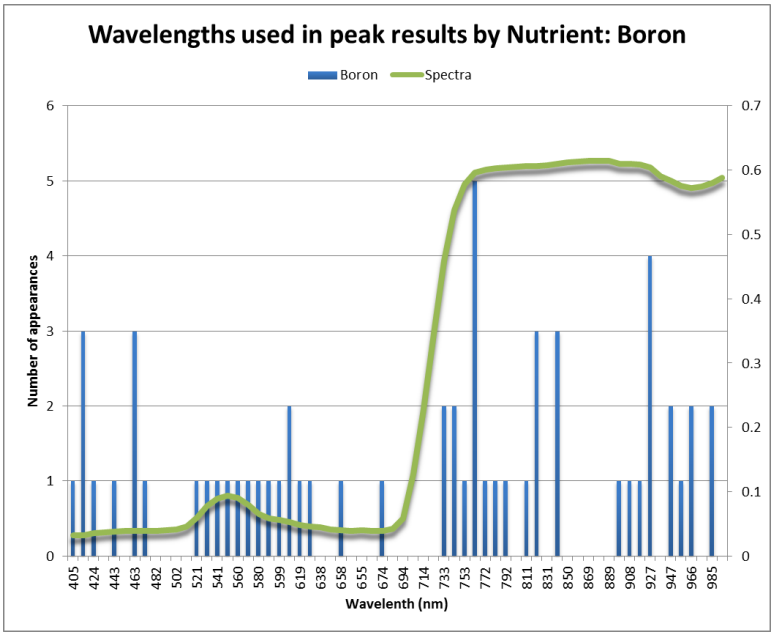

Figure 72: Wavelengths used in linear modeling for 10nm peak results, boron

The results for Mg are shown in Figure 73; Mg modeling used 50 bands, compared to the 42 bands used in the case of modeling based on 1nm data. The spread of the 10nm Mg bands was similar to that of the 1nm bands, albeit slightly shifted. Similar to the 1nm data, there was a high concentration of upper NIR bands, but unlike the 1nm data, we observed that more bands on the red edge and one in the upper blue region have shifted into the low green in the case of the 10nm data.

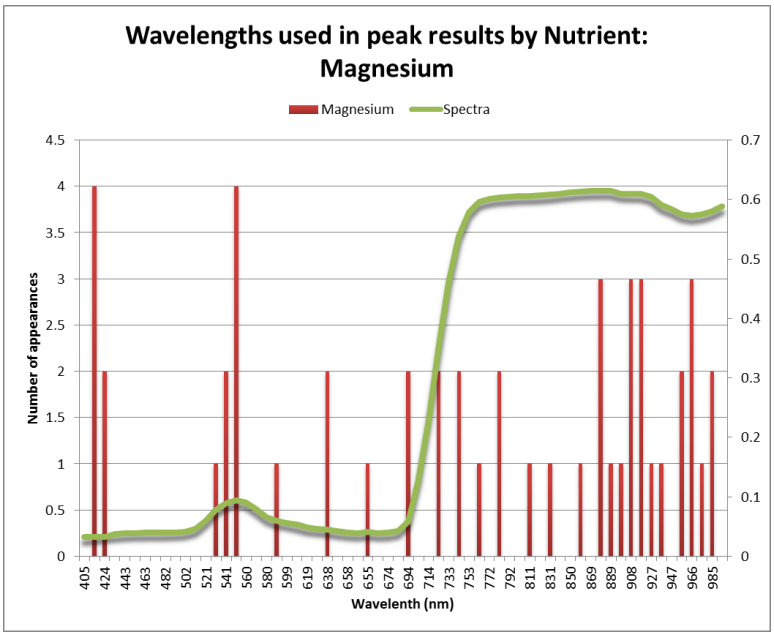

Figure 73: Wavelengths used in linear modeling for 10nm peak results, magnesium

The distribution of the bands used by the 10nm-based N modeling was similar to that from the 1nm data (Figure 74); bands were selected from across the complete silicon spectrum. The 10nm data used fewer bands than the 1nm data (36 and 43 bands, respectively) and the reduction in bands came from the NIR range, a region in which the 10nm data were not as strongly represented.

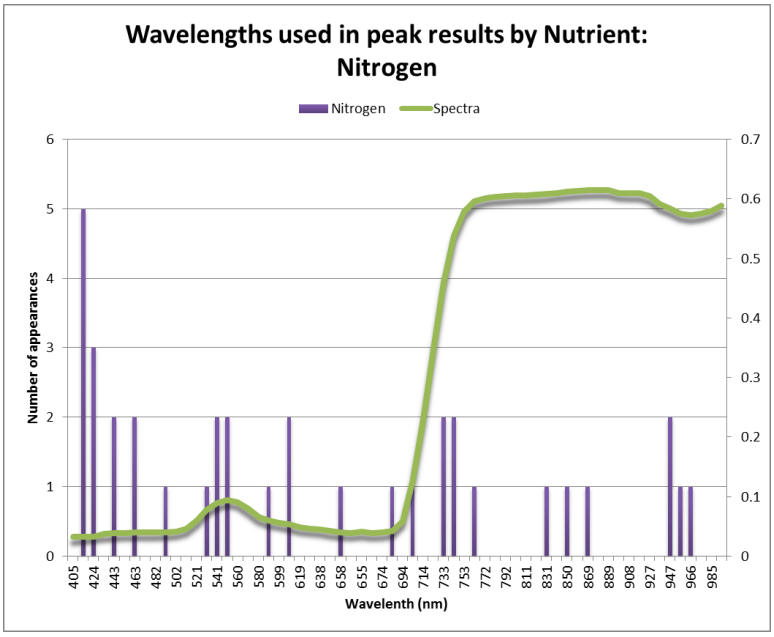

Figure 74: Wavelengths used in linear modeling for 10nm peak results, nitrogen

The wavelengths used to model P are in Figure 75; the 10nm data used only 30 bands for the model fits, compared to the 53 bands that were used for the 1nm data. From the 10nm band placement, we can see that it was based on more bands in the NIR range, while the 1nm data were better represented in the green spectral region.

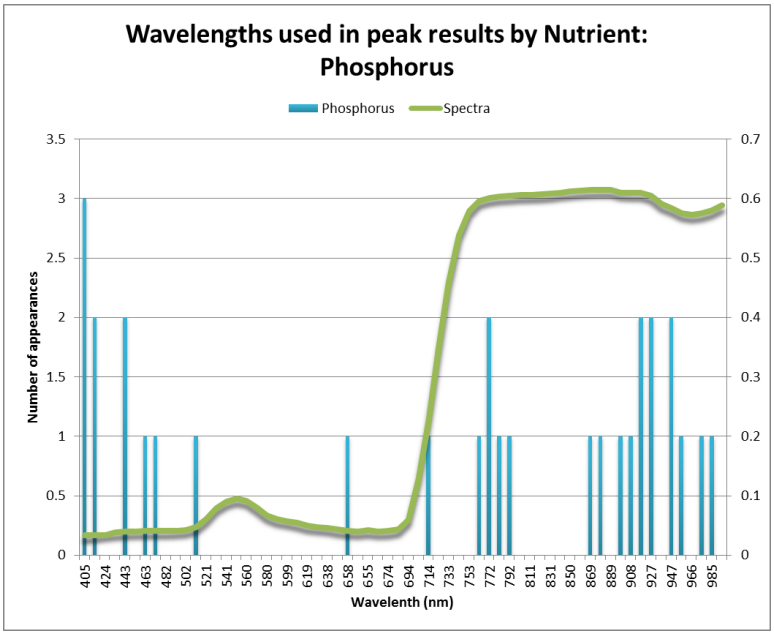

Figure 75: Wavelengths used in linear modeling for 10nm peak results, phosphorus

In the case of K, the 10nm modeling extracted 30 wavelength bands, instead of the 34 bands used to model the 1nm nutrients. The 10nm results show that the bands used were distributed across the visible spectrum, significantly more so than for the 1nm data. Both data sets used a number of bands in the 900nm region of the EMR spectrum.

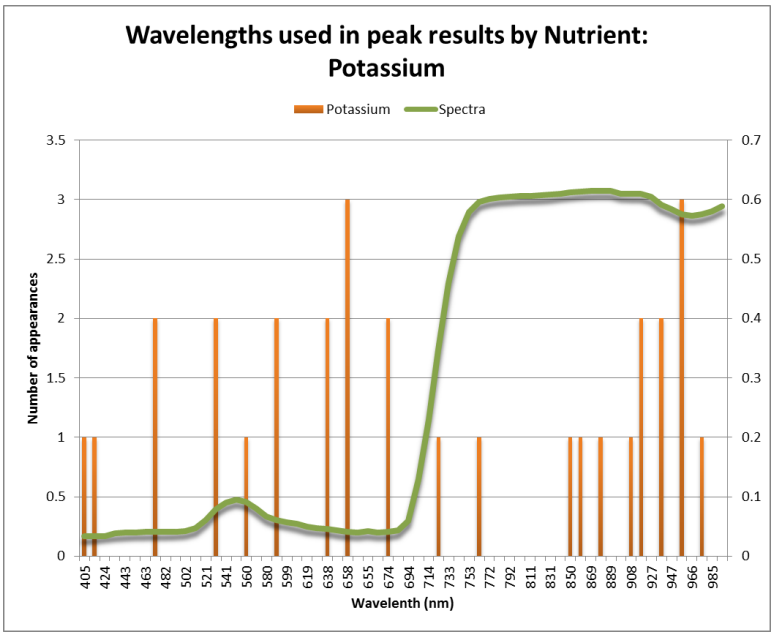

Figure 76: Wavelengths used in linear modeling for 10nm peak results, potassium

Finally, the Z modeling results are shown in Figure 77. Both 10nm and 1nm modeling approaches had a similar NIR region representation. However, in the visible range, the 10nm modeling employed more bands in the green spectral region, while the 1nm modeling used no green bands, and was more concentrated in the blue EMR region.

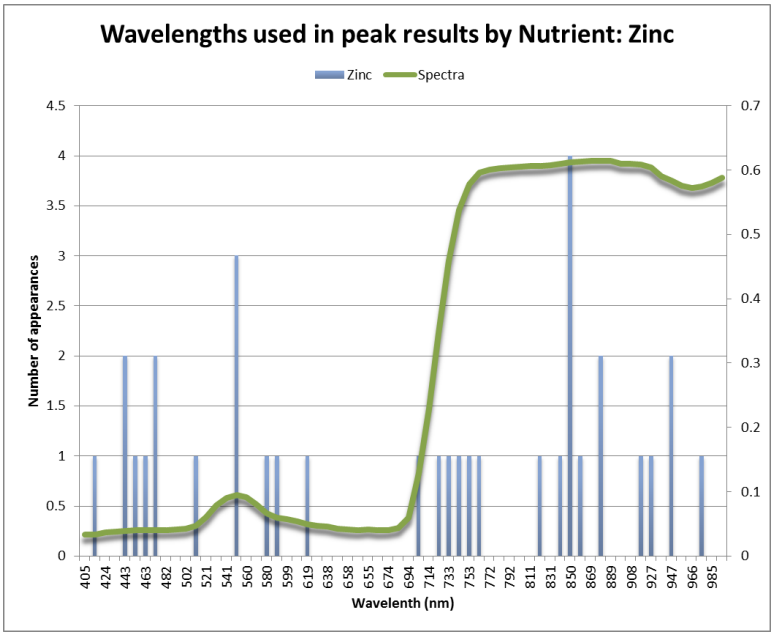

Figure 77: Wavelengths used in linear modeling for 10nm peak results, zinc

6.0 Conclusions

There are a number of important conclusions that can be drawn from our analysis of i) nutrient levels at the petiole and leaf levels, for ii) Riesling and Cabernet Franc grape cultivars, across iii) bloom and veraison phenological stages, with spectral data collected at iv) leaf, canopy-nadir, and canopy 15° off nadir view angles, for v) for the silicon range (400-1000nm). Although clear trends were not always obvious, it was found that:

- Little agreement regarding the nutrient concentration of the plant existed between the leaf and petiole nutrient analyses;
- The petiole nutrient analysis was in closer agreement with the expected concentration of nutrients for wine grapes grown in Eastern North America;
- Both the normalized difference index (NDI) and ratio index approaches yielded similar results to two decimal places;
- For both the 1nm and 10nm resampled spectral reflectance data, there was a greater correlation between the NDI and the nutrient content for the Riesling reflectance spectra compared to the NDI for Cabernet Franc reflectance spectra;
- At both 1nm and 10nm resampled spectral resolutions there were similarities in the shape of nutrient-spectra correlation heat maps for a nutrient between different cultivars and growing season;
- For the 1nm data, only the 1st derivative analysis method generated a model fit for each of the nutrients in all view-angles, while for both resolutions, it was the most common method to generate the peak model fits;
- A 1nm spectral resolution resulted in better overall model performance in terms nutrient concentration predictive ability then the 10nm spectral resolution; and
- The distribution of the wavelengths used in our models to fit the nutrient data concurred with previous research.

Specifically, from the five methods that were employed as part of this research it was found that, while all five methods produced model fits for one or more nutrients over the span of cultivars and growing seasons, the three predominant methods for achieving the best model fits were i) SLR using the wavelengths, ii) using continuum removal, or iii) using the 1st derivative of the reflectance spectrum as the input/independent variables. Among these three methods, only the 1st derivative approach, when applied to the 1nm data, was found to produce solid model fits for all six nutrients for both cultivars over the span of the growing period.

One could argue that we would need to limit the analysis to data from the two canopy view-angles, given the potential extension of results to UAV-based platforms, i.e., canopy-specific imagery. In this context and for a 1nm spectral resolution, a comparison between the two canopy view-angles (nadir and 15° off-nadir; Tables 71-82) showed that: the peak R^2 values ranged between 0.35-0.84 for canopy nadir and required between two and ten wavelengths per nutrient to generate any of the models; For the canopy 15^o off-nadir view-angle at 1nm spectral resolution, the peak R^2 values ranged between 0.14-0.86 and again required between two and ten wavelengths to generate the complete set of nutrient models, similar to the results for canopy nadir viewing. A comparison of the average R^2 values over the complete set showed that the canopy nadir view-angle exhibited an average R^2 value of 0.66, while the canopy 15^o off-nadir view-angle yielded an average R^2 value of 0.60. For the 10nm spectral resolution (Tables 83-94) we found that for the canopy-nadir view angle the peak R^2 values ranged between 0-0.93 and employed between 2-24 wavelength bands. The results for the canopy 15^o off-nadir view-angle at 10nm showed that peak R^2 values ranged from 0-0.71 and used between 1-18 wavelength bands. Therefore, we determined that the canopy nadir view-angle is the superior view angle from which to sample the grape blocks at both spectral resolutions.

However, when choosing between the two spectral resolutions we found that, although the 10nm resolution can result in a better model fit in one or two nutrient and view angle cases, this comes at the price of requiring almost double the wavelengths sampled in order to fit the model. When considering all six nutrients, the 1nm spectral resolution provided an overall better modeling of the nutrient data with fewer required bands.

It became clear that in order to achieve optimized model fits for the nutrient data, the use of multiple data models is recommended. However, if only one approach is preferred, we would recommend the use of 1nm, 1^{st} derivative spectral data – this data set consistently produced the best modeling results across the set of nutrients, for the two cultivars, and during both growing seasons. Finally, in examining the feasibility of sampling the data with a UAV, and depending on the required nutrients to be modeled, for a specific cultivar and phenological stage, it was established that between two and ten separate wavelengths needed to be sampled. In most cases, this will require multiple passes over the block for a single nutrient and while this result did not satisfy our quest of being able to select a set of ≤6 wavelengths for typical UAV-based cameras, this research demonstrated that this only a somewhat unrealistic goal. Technology likely will advance to a level where UAV platforms either can accommodate several multispectral cameras, or camera

technology will advance to enable image collection for ≥10 bands per pass. In the meantime, a nutrient modeling solution that requires up to 10 wavelengths per nutrient could be accomplished through the use of interchangeable spectral filters and multiple passes over a field, i.e., a collection strategy that spans a couple of hours to a day. The data could then be output in a matter of minutes from the time that it is downloaded. This would yield same-day nutrient concentration assessment for the field, allowing prompt, pro-active crop management for improved health and yield of the vines.

6.3 Next steps

There are several different aspects of the study that further could be explored as part of future research. The data used in our analysis were from a single year's field season. We therefore recommend that samples be obtained from the vineyard/field in subsequent years in order to verify and strengthen the modeling results. Other computational techniques based on multivariate analysis, e.g., partial least squares or principal component analysis, are suggested in order to build a more holistic and robust model for the various nutrients. Furthermore, the manner in which we analyzed the data ignored the different ground treatments, as well as weather variability during the collection stages. An analysis of how the different ground treatments affect the modeling could help to generate models that are extensible across different fields or weather conditions. Although white reference samples were used to minimize the effects of changing weather conditions, i.e., data were converted to reflectance, additional work could focus on trying to mitigate the effects of small illumination changes that occur in the time between when the reference sample and the target sample are collected – this could contribute to further mode optimization. Finally only 1nm and 10nm wavelength bands were analyzed; we thus recommend that other spectral resolutions, such as 2nm or 5nm, also be tested to further evaluate the impact of spectral resolution on nutrient model performance. As an extension of such an analysis, one could also limit the proximity of selected 1nm bands to facilitate system design – this should be done prior to field-testing of any of the models towards developing a truly operational sensor that is designed to be sensitive to specific nutrient absorption features.

References

Adams, M.L., Philpot, W.D., Norvell, W.A., "Yellowness index: An application of spectral second derivatives to estimate chlorosis of leaves in stressed vegetation", International Journal of Remote Sensing, 20:18, 3665-3675 (1999)

Anderson, G., van Aardt, J., Bajorski, P. and Heuvel, J.V., "Detection of wine grape nutrient levels using visible and near infrared 1nm spectral resolution remote sensing", *SPIE Commercial+ Scientific Sensing and Imaging* (pp. 98660H-98660H). International Society for Optics and Photonics. (2016)

AVIRIS Calibration Data, http://aviris.jpl.nasa.gov/data/index.html

Business Wire, http://www.businesswire.com/news/home/20120521005960/en/Research-Markets-Wine-2012-Global-Industry-Almanac

Calkins, K.G., "Measuring Correlation", 4 August 2005, https://www.andrews.edu/~calkins/math/edrm611/edrm05.htm (2016)

Christensen, P., "Nutrient level comparisons of leaf petioles and blades in twenty-six grape cultivars over three years (1979 through 1981)", American Journal of Enology and Viticulture, 35, 124-133 (1984)

Ciavarella, S., Batten, G.D., "Measuring potassium in plant tissues using near infrared spectroscopy", Journal of Near Infrared Spectroscopy, Volume 6 Issue A, 63-66 (1998)

Cho, M.A., Skidmore, A.K., "A new technique for extracting the red edge position from hyperspectral data: The linear extrapolation method", Remote Sensing of Environment, 101, 181-193 (2006)

Claudio, H.C., Cheng, Y., Fuentes, D.A., Gamon, J.A., Luo, H., Oechal, W., Qiu, H.L., Rahman, A.F., Sims, D.A., "Monitoring drought effect on vegetation water content and fluxes in chaparral with the 970nm water band index", Remote Sensing of Environment, 103, 304-311 (2006)

Cornell Nutrient Analysis Laboratory (2016), http://cnal.cals.cornell.edu/forms/pdfs/CNAL_Form_%20P.pdf

Cozzolino, D., Cynkar, W.U., Shah, N., Dambergs, R.G., Smith, P.A., "A brief introduction to multivariate methods in grape and wine analysis", International Journal of Wine Research, 1, 123-130 (2009)

da Silva Junior, M.C., de Assis de Carvalho Pinto, R., Marcal de Queiroz, D., Alves, E.A., Gracia, L.M.N., Gil, J.G., "Correlation between vegetation indices and nitrogen leaf content and dry matter production in Brachiaria decumbens", Image Analysis for Agricultural Products and Processes, 69, 14-150 (2006)

Demetriades-Shah, T.H., Steven, M.D., Clark, J.A., "High resolution derivative spectra in remote sensing", Remote Sensing of Environment, Vol. 33, Issue 1, 55-64 (1990)

Demir, B.S., Serindag, O., "Determination of Boron in grape (Vitis vinifera) by Azomethine H spectrophotometric method", Eurasian Journal of Analytical Chemistry, Vol. 1, No. 1 (2006)

Dr. Justine Vanden Heuvel, conversation (June 2016)

Eismann, M.T., [Hyperspectral Remote Sensing], SPIE Press, Bellingham, Washington, 458 (2012)

Elvidge, C.D., Chen, Z., "Comparison of broad-band and narrow-band red and near-infrared vegetation indices", Remote Sensing Environment, 54, 38-45 (1995)

Fernandez-Novales, J., Lopex, M.I., Sanchex, M.T., Morales, J., "Shortwave-near infrared spectroscopy for determination of reducing sugar content during grape ripening, winemaking, and aging of white and red wines", Food Research International, 42, 285-291 (2008)

Gil-Perex, B., Zarco-Tejada, P.J., Correa-Guimaraes, A., Relea-Gangas, E., Navas-Gracia, L.M., Hernandex-Navarro, S., Sanz-Requena, J.F., Berjon, A., Martin-Gil, J., "Remote sensing detection of nutrient uptake in vineyards using narrow-band hyperspectral imagery", Vitis, 49(4), 167-173 (2010)

Gitelson, A.A., Merzlyak, M.N., "Remote estimation of chlorophyll content in higher plant leaves", International Journal of Remote Sensing, 18, 2691-2697 (1997).

Grossman, Y.L., Ustin, S.L., Jacquemoud, S., Sanderson, E.W., Schmuck, G., Verdebout, J., "Critique of stepwise multiple linear regression for the extraction of leaf biochemistry information from leaf reflectance data", Remote Sensing Environment, 56, 182-193 (1996)

Hamamatsu Optical Sensors, (2016), http://www.hamamatsu.com/us/en/community/optical_sensors/sipm/physics_of_mppc/index.html

Herrera, J., Guesalaga, A., Agosin, E., "Shortwave-near infrared spectroscopy for non-destructive determination of maturity of wine grapes", Measurement Science and Technology, 14, 689-697 (2003)

Herrmann, I., Karnieli, A., Bonfil, D.J., Cohen, Y., Alchanatis, V., "SWIR-based spectral indices for assessing nitrogen content in potato fields", International Journal of Remote Sensing, Vol. 31, No. 19, 5127-5143 (2010)

Horler, D. N. H., Dockray, M., Barber, J., "The red edge of plant reflectance", *International Journal of Remote Sensing*, 4, 273-288. (1983)

Hunt Jr, E.R., Doraiswamy, P.C., McMurtrey, J.E., Daughtry, C.S.T., Perry, E.M., Akhmedov, B., "A visible band index for remote sensing leaf chlorophyll content at the canopy scale", International Journal of Applied Earth Observation and Geoinformation, 21, 103-112 (2013)

Janecek, M., "Reflectivity spectra for commonly used reflectors", IEEE Transactions on Nuclear Science, Vol. 59, NO. 3 (2012)

Klein, I., Strime, M., Fanberstein, L, Mani, Y., "Irrigation and fertigation effects on phosphorus and potassium nutrition of wine grapes", Vitis, 39, 55-62 (2000)

Kokaly, R.F., Clark, R.N., "Spectroscopic determination of leaf biochemistry using band-depth analysis of adsorption features and stepwise multiple linear regression", Remote Sensing of Environment, 67, 276-287 (1999)

Larrain, M., Guesalaga, A.R., Agosin, E., "A multipurpose portable instrument for determining ripeness in wine grapes using NIR spectroscopy", IEEE Transaction on Instrumentation and Measurement, Vol. 57, No. 2 (2008)

Li, F., Mistele, B., Hu, Y., Chen, X., Schmidhalter, U., "Reflectance estimation of canopy nitrogen content in winter wheat using optimized hyperspectral indices and partial least squares regression", European Journal of Agronomy, 52, 198-209 (2014)

Louhaichi, M., Borman, M. M., Johnson, D. E., "Spatially located platform and aerial photography for documentation of grazing impacts on wheat', Geocarto International, 16, 65-70 (2001)

The MathWorks, Inc., MATLAB Documentation 'corrcoef' (2016), http://www.mathworks.com/help/matlab/ref/corrcoef.html (2016)

Pohl, P., "What do metal tell us about wine", Trends in Analytical Chemistry, Vol. 26, No. 9 (2007)

Romero, I., Garcia-Escudero, E., Martin, I., "Effects of Leaf Position on Blade and Petiole Mineral Nutrient Concentration of Tempranillo Grapevine (*Vitis vinifera* L.)", American Journal of Enology and Viticulture, 61, 544-550 (2010)

Romero, I., Garcia-Escudero, E., Martin, I., "Leaf Blade versus Petiole Analysis for Nutritional Diagnosis of *Vitis vinifera* L. cv. Tempranillo", American Journal of Enology and Viticulture, 64, 50-64 (2012)

Sauvage, L., Frank, D., Stearne, J., Millikan, M.B., "Trace metal studies of selected white wines: and alternative approach", Analytica Chimica Acta, 458, 223-230 (2002)

Serrano, L., Gonzalez-Flor, C., Gorchs, G., "Assessing vineyard water status using the reflectance based Water Index", Agriculture, Ecosystems and Environment, 139, 490-499 (2010)

Schott, J.R., [Remote Sensing The Image Chain Approach], Oxford University Press, Oxford, New York, (2007)

Shao,Y., He, Y., "Nitrogen, phosphorus, and potassium prediction in soils, using infrared spectroscopy", Soil Research, 49(2), 166-172 (2010)

Smart, D.R., Whiting, M.L., Stockert, C., "Remote sensing of grape K deficiency symptoms using leaf level hyperspectral reflectance", Western Nutrient Management Conference, Vol. 7 (2007)

Spectra Vista Corporation, Field Portable Spectroradiometers (2016), http://www.spectravista.com/ground.html (2016)

Taylor, R., "Interpretation of the Correlation Coefficient: A basic review", Journal of Diagnostic Medical Sonography, 1, 35-39 (1990)

Thenkabail, P.S., Smith, R.B., De Pauw, E., "Hyperspectral vegetation indices and their relationships with agricultural crop characteristics", Remote Sensing Environment, 71, 158-182 (1999)

Vogelmann, J.E., Rock, B.N., & Moss, D.M., "Red edge spectral measurements from sugar maple leaves" International Journal of Remote Sensing, 14, 1563-1575 (1993).

Wolf, T. K., [Wine Grape Production Guide for Eastern North America], Plant and Life Sciences Publishing, Ithaca, New York, 141-142 (2008)